Lehrstuhl für Elektrische Antriebssysteme und
Leistungselektronik
Univ.-Prof. Dr.-Ing. Ralph Kennel

Model-based Design and Integration of the Power Network in More Electric Aircraft

Yang Ji

Vollständiger Abdruck der von der Fakultät für Elektrotechnik und Informationstechnik der Technischen Universität München zur Erlangung des akademischen Grades eines

Doktor-Ingenieurs (Dr.-Ing.)

genehmigten Dissertation.

Vorsitzender:	Univ.-Prof. Dr.-rer.nat. Thomas Hamacher
Prüfer der Dissertation:	
1.	Univ.-Prof. Dr.-Ing. Ralph Kennel
2.	Prof. Barrie Mecrow, Ph.D.
3.	Hon.-Prof. Dr.-Ing. Martin Otter

Die Dissertation wurde am 26.01.2016 bei der Technischen Universität München eingereicht und durch die Fakultät für Elektrotechnik und Informationstechnik am 22.03.2016 angenommen.

Vorwort

Die vorliegende Arbeit entstand während meiner Tätigkeit am Institut für Systemdynamik und Regelungstechnik im Deutschen Zentrum für Luft-und Raumfahrt e.V. (DLR). Dem Leiter des Instituts, Herrn Dr. Johann Bals, danke ich für die Möglichkeit, die Arbeit in seinem Institut durchzuführen und den gewährten zeitlichen Freiraum zur Ausarbeitung der Dissertation.

Herrn Prof. Dr. -Ing. Raphl Kennel danke ich für die Übernahme des Erstgutachtens, sowie für die zahlreichen wissenschaftlichen Veranstaltungen bei seinem Lehrstuhl. Herrn Prof. Barrie Mecrow danke ich für die Übernahme des Zweitgutachtens.

Bei Herrn Prof. Dr. -Ing. Martin Otter möchte ich mich in ganz besonderer Weise für seine stetige Unterstützung bei meiner täglichen Arbeit im DLR, sowie meiner Promotion bedanken.

Mein Dank gilt allen Kolleginnen und Kollegen für das sehr gute Arbeitsklima im Institut. Herrn Martin Kuhn als meinem Zimmerkollege, danke ich für die enge Zusammenarbeit bei Projekten und vielen wissenschaftlichen Diskussionen, die zu meiner Dissertation viel beigetragen haben. Herrn Dr. Andreas Pfeiffer danke ich für seinen Beitrag zum Thema optimierungs-basierte Steady State Analyse. Bei dem ehemaligen Kollege, Herrn Prof. Dr. -Ing. Simon Hecker bedanke ich mich für die ausführliche Erklärung zur Theorie der Robusten Regelung. Herrn Dr. Andreas Varga danke ich für die hilfreichen Diskussionen und Vorschläge zum Thema Fehler-Analyse.

Oberpfaffenhofen, 2016
Yang Ji

to Yuping and Meizhen

Abstract

The development of the future More Electric Aircraft (MEA) systems is a challenging task: the system integration is becoming a central topic. In all phases of the system development process, the respective subsystems within the MEA will be treated in a highly integrated manner to achieve optimum efficiency and performance at aircraft and system level. Concerning the electric power network in the MEA, advanced design and analysis methods based on mathematical models are required to face the potential issues accompanying the design process. This thesis presents the recently developed methodologies relying on modeling and simulation techniques to solve the issues arising when designing the future MEA, with respects to system stability, power quality, failure analysis and virtual testing activities.

Contents

List of Figures

List of Tables

Acronyms

AC	Alternate Current
AEA	All Electric Aircraft
API	Application Programming Interface
ATRU	Auto-transformer Rectifier Unit
ATU	Auto-transformer Unit
CSJU	Clean Sky Joint Undertaking
CWT	Continuous Wavelet Transform
DAE	Differential Algebraic Equation
DC	Direct Current
DCAM	DC Averaged Model
DCCU	DC/DC Converter Unit
DWT	Discrete Wavelet Transform
EMA	Electromechanical Actuator
EU	European Union
FEM	Finite Element Method
FHAM	First Harmonic Averaged Model
FMI	Functional Mock-up Interface
FPGA	Field-programmable Gate Array
GCU	Generator Control Unit
HVDC	High Voltage Direct Current
JTI	Joint Technology Initiative
LFR	Linear Fractional Representation
LTI	Linear Time Invariant
MEA	MEA
MOPS	Multi-Objective Parameter Synthesis
MRA	Multi-resolution Analysis
PMSM	Permanent Magnetic Synchronous Machine
PSO	Particle Swarm Optimization
PWM	Pulse Width Modulation
QSS	Quantized State System
RMS	Root Mean Square
SG	Synchronous Generator
SRG	Switched Reluctance Generator
VFG	Variable Frequency Generator

1. Introduction

1.1. More Electric Aircraft

The air transport industry is paying a lot of attention to growing public concern on air pollution, noise and climate change. Although today air transport only produces 2 percent of man-made CO2 emissions, this is expected to increase to 3 percent by 2050. Besides the environmental aspect, in the competitive world of airline economics, where low-cost carriers are driving down profit margins on airline seat-miles, techniques to reduce the direct operating costs of aircraft are in great demand. In an effort to meet this demand, the aircraft manufacturing industry is placing greater emphasis on the use of technology, which can influence maintenance costs and fuel usage. To achieve lower costs, the industry has three technology options: optimize the aircraft equipment systems and engines; optimize the system of systems (the aircraft as a whole); and optimize the solutions that enable the aircraft to fulfill its required functions [71].

Aiming at the global energy optimization of an aircraft, the MEA concept gains traction in the aeronautical industry. Electric equipment is replacing hydraulic, pneumatic and mechanical equipment in the domains of propulsion, control and auxiliary systems (see Fig. 1.1). Compared with the conventional power distribution network, the MEA architecture will demonstrate significant weight reduction, reduced maintenance requirements and increased reliability and also increased passenger comfort. The MEA concept is based on utilizing electric power to drive aircraft subsystems which historically have been driven by a combination of hydraulic, electric, pneumatic and mechanical power transfer systems. The increasing use of electric power is seen as the direction of technological opportunity for aircraft power systems based on rapidly evolving technology advancements in power electronics, fault tolerant electrical power distribution systems and electric-driven primary flight control actuator systems [96].

Since 2006, several European Union (EU) supported projects have been established with the purpose to study and develop corresponding technologies emphasizing electric systems for successfully applying the MEA concept. The power optimized aircraft (POA) is an EU project designed to address the optimization of aircraft equipments, engines and system of systems. The four-year effort, scheduled to run until 2006, is a technology platform within the EU's fifth framework program on research and development. With a budget of about 100 million Euro, the POA was jointly funded by the EU and a 46-company consortium. After the successful completion of the POA project, the MOET (more open electrical technologies) project[4] has been initialized to establish a new industrial standard for the design of the elec-

trical system of commercial aircrafts, applicable for the business and regional aircraft and rotor-craft as well. MOET has enhanced aircraft design and use by working on power source rationalization and electrical power flexibility. This new standard has strengthened the competitiveness of the European aeronautical industry, reduced aircraft emissions and improved operational aircraft capacity. To create this new standard, MOET has launched significant changes in power management, which up to now are not possible due to technological limits. It built these changes based upon the solid foundations of previous European research, especially POA. MOET has established and reinforced competence across the aircraft industry and supply chains by developing key technologies based on extensive European expertise. MOET is comprised of 46 companies (13 being SMEs) and 15 Research Centers or Universities from 14 European countries. The project was coordinated by AIRBUS France. This integrated project was partially funded by the EU, through FP6 and the Framework of the Aeronautics Industry R&D Objectives. The ongoing EC project Clean Sky is the most ambitious aeronautical research program ever launched in Europe. Its mission is to develop breakthrough technologies to significantly increase the environmental performances of airplanes and air transport, resulting in less noisy and more fuel efficient aircraft, hence bringing a key contribution to achieve the Single European Sky environmental objectives. The Clean Sky JTI (Joint Technology Initiative) was born in 2008 and represents a unique Public-Private Partnership between the European Commission and the industry. It is managed by the Clean Sky Joint Undertaking (CSJU) until 31 December 2016.

The main focus of demonstration in Clean Sky is the validation and maturation of the technologies and sub-architectures, not just in a MEA, but moving to an All Electric Aircraft (AEA)[1]. Thus, Clean Sky intends to demonstrate:

- Proven large-scale ground-based architectural integration of electrical generation, distribution and loads, and of thermal management.

- Proven large-scale ground-based architectural integration of thermal management technologies. Where maturity is shown, these will be integrated with the electrical equipment systems.

- Flight proven electrical equipment systems, including environmental conditioning and protection.

- Flight proven technologies and sub-systems for thermal exchange and management, including liquid loops and heat exchangers.

- Flight proven technologies, architectures and concepts for power generation and distribution.

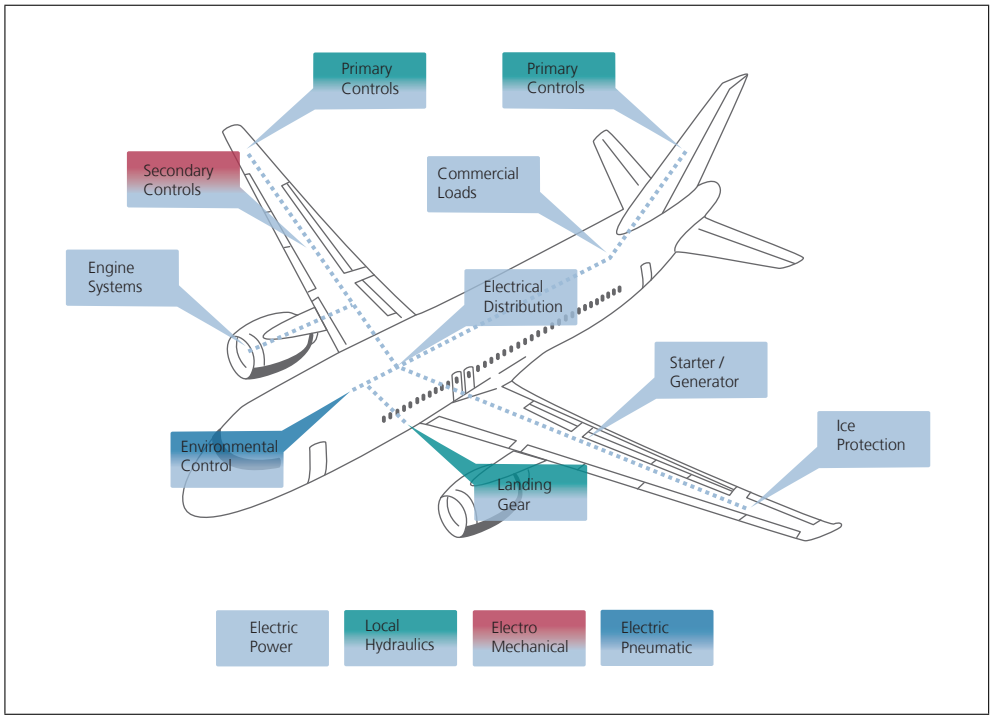

Figure 1.1.: The map of power distribution in the MEA

1.2. Design process for development of aircraft energy systems

The design process for the development of aircraft energy systems consists of 4 major phases:

Concept phase: During the concept phase a two-fold iterative optimization is performed on the aircraft manufacturer side. This includes the aircraft concept and global energy system architecture optimization. Methods and tools for the tasks during the concept phase have been investigated [102], with which an optimal architecture of electrical energy system can be achieved.

System specification phase: In this phase, a frozen energy system concept is provided by the aircraft manufacturer. Additionally, more detailed aircraft data about structure, cabin, flight physics, engine and electrical power generation are available. The selected system suppliers conduct full concept definition where all the requirements and risks are understood. The aircraft manufacturer's requirements is transformed to the level of equipment suppliers by the system suppliers. Stability studies and failure analysis of the aircraft electrical network are typical activities during the system specification phase.

System development and validation phase: In this phase preliminary and detailed design of the equipment takes place. Verification and validation for artifacts are done, which are produced during this phase.

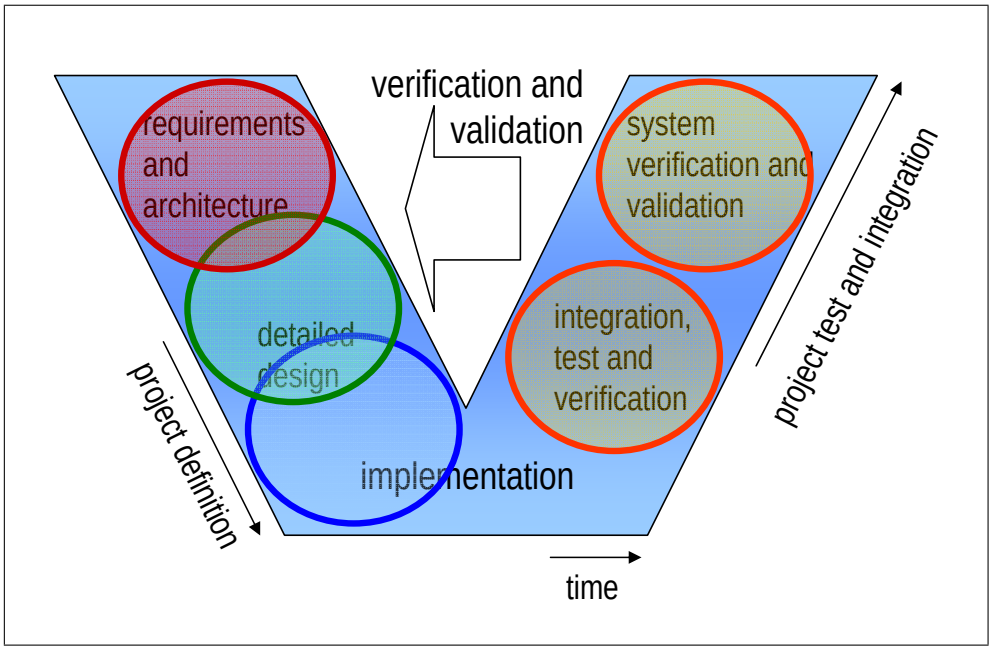

Figure 1.2.: The diagram of design process for the development of the aircraft energy system

System verification phase: The typical tasks of aircraft manufacturer in this phase are: monitor supplier system development by verification of system performance and functions, integrate systems in physical and functional aircraft, verify integrated systems and validate simulation models versus test results. The objective in the system verification phase is to demonstrate the maturity of the systems in a realistic environment. The virtual integration platform for energy systems allows to address the integration issues prior to their physical integration on the test rigs and also extend test coverage. Power quality investigation of the integrated network will be of the interest in this phase.

The main activities associated to all design phases can be visualized by one V diagram, which is depicted by Fig. 1.2.

1.3. Challenges

The development of the future MEA systems is a challenging task: the system integration is becoming a central topic. In all phases of the system development process, the respective subsystems within the MEA will be treated in a highly integrated manner to achieve an optimum efficiency and performance at the aircraft and systems level. Concerning the electric network in the future MEA, advanced design and analysis methods based on mathematical models are required to face the potential issues accompanying the MEA. For this purpose, the use of advanced modeling and simulation technologies is a key success factor. Four major issues regarding the electric network in the MEA are addressed in this thesis. The first issue

is about electric network stability. The electric network tends to instability because the system load can change swiftly and without warning due to a large range of duty cycles and unpredictable spikes. Power quality analysis is another issue. The power quality assessment of the electric power distribution level is generally of great interest to the MEA. The provisions of voltages and system design have to ensure that power loads successfully utilize electric energy without interference or interruption. Moreover, power quality is also usually necessary when checking network stability, since the system has to keep the system variables of interest within desired limits. Those limits in time or frequency domain may be defined for steady state and transient state operation. The third issue to deal with in this thesis is health monitoring of an electric network. Unlike hydraulic and mechanical transfer systems, faults on electric distribution systems can even occur much faster. On-time detection of faults and long term prognosis of health status become a very important and challenging work. Finally, the virtual testing of aircraft power systems is discussed. Due to the increased complexity of the aircraft power system, automatic virtual testing for the integrated system is becoming indispensable and quite challenging.

1.4. State-of-the-art in design and analysis of aircraft power network

Different traditional methods exist to handle the previously mentioned challenges in the development of the future MEA systems. Concerning the modeling activity, a multi-level approach has been applied for aircraft electrical systems design [67]. Till today, the models with different accuracies widely being accepted and used for design and analysis of aircraft power network can be classified into architectural, functional and behavioral level.

To the stability study of electrical power network, the Middlebrook criterion [83] is the mostly accepted method, which examines small signal stability of averaged (=non switching) models. Only the input impedance of the load subsystem and the output impedance of the source subsystem and their Bode diagrams are needed [83]. But the Middlebrook criterion is restrictive and not appropriate for design and optimization goals [14]. The analytic calculation of the input/output impedances may be extensive while there is no information on the sensitivity of the impedances to parameter variations available for a hardware measurement approach [26]. As a result, electric on-board systems are increasingly analyzed by another method for small signal stability. The Modal Analysis gives proof of stability via the region of the eigenvalues and uses participation factors and eigenvalue sensitivities [14, 38, 68] to retrieve dependencies between system modes and elements of the state matrix of a linear time invariant system. The LTI representation needed is calculated by numerical linearization of the system at an equilibrium point. It is easy to see that nonlinear impacts on the steady state condition cannot be regarded with the Modal Analysis approach. For example, the system load has a nonlinear influence and must be treated as constant at linearization which limits the validity of the model to a

special loading case. Additionally, the Modal Analysis approach is not appropriate for finding the critical component which is most fragile to destabilize the system. The drawbacks of Modal Analysis can be avoided with Monte Carlo simulation [107] or µ-analysis [65].

Nowadays, the power quality study can be seen as an extended task of stability study, since industrial standards, e.g. [87] usually define the stability criterion by power quality indicators, such as power frequency spectrum or total distortions. To conduct the power quality analysis, the steady-state voltage and current waveforms of the aircraft power network is a prerequisite. The conventional brute force simulation to yield the steady-state waveforms of a large scale system containing high frequency switching components is very expensive and suffering from numerical instabilities. Existing methods to efficiently solve the steady-state analysis problem can be principally divided into two groups. The methods in the first group such as the harmonic balance based approach [8] integrated in SimulationX or the Quasi-Newton based approach [79] provided by PLECS [5], try to compute the steady-state waveforms with possibly minimum simulation iterations. In another group, the original topological models including high frequency switching components are transformed into the accurate approximated ones without switching effect by generalized averaging technique [98] or discrete wavelet decomposition [73], to improve the speed of the simulation.

Current fault diagnosis techniques for the aircraft electric system are hardware redundancy based fault diagnosis and signal processing based fault diagnosis. The central idea of the hardware redundancy based fault diagnosis consists in the reconstruction of the process components using redundant hardware components. A fault in the process component is regarded as occurred, once the output of the process component differs from one of its redundant components. Signal-based methods, e.g. Fourier or wavelet transform, also provide other possibilities to perform the fault detection and isolation. With the rash development of the new mathematical tool, i.e. wavelet transform [80], a great amount of studies have been done in different fields for fault detection. Some attempts have also been made in power electronics [116, 94]. The implementation of wavelet transform for the post processing of Modelica simulation data has been seen, for example, in a study of vehicle steering, where wavelet transform was carried out in the software MATLAB[1] for calculating power spectra [17].

Regarding the virtual testing of aircraft power network for system verification and validation, the Saber simulator[2] [25] and EASY5[3] [33] are standard tools used by current aircraft manufacturers.

[1]MATLAB is a registered trademarks of the Mathworks Inc.
[2]Saber is a registered trademark of Synopsys Inc.
[3]EASY5 is a trademark of MSC Software

1.5. Contributions

Today, the aircraft industry utilizes a multi-level approach for the design of the aircraft system:

Level 1 Architectural models consist of algebraic equations and are used for steady-state power consumption calculations, e.g. to analyze the power budget.

Level 2 Functional models are derived from behavioral models by time averaging of high frequency periodical switching waveforms. A functional model reflects only low frequency behavior of the original system excluding switching ripples. The functional models are typically used for control design, stability study and transient performance analysis.

Level 3 Behavioral models are based on equations derived from the subsystem structure and electrical circuit. The behavioral models reflect both low and high frequency dynamics including switching effects serving to perform power quality simulation and analysis

This thesis deals with the models in level 2 and 3. Especially, the model details on level 2 are extended, so that analysis methods for Linear Time Invariant (LTI) systems can be utilized in situations previously analyzed only by time consuming nonlinear simulations of level 3 models. In this thesis, new modeling and simulation methods and tools for the different tasks of the design process of the electric network in the MEA are presented. Concretely, it is shown that the lift technique traditionally used for periodic systems is suitable to conduct a generalized averaged model from a topological model of a wide class of power electric systems. Using the derived generalized averaged model, it becomes possible to acquire the improved LTI description in level 2 models including high frequency effects in the original power electric system. This can significantly ease the work to deal with the previously mentioned issues concerning the electric network of the MEA. Various specific model based methods for the network stability, health monitoring and power quality analysis have been developed during the work on this thesis. For the stability analysis, comprehensive comparisons among traditional small signal based stability approaches such as Modal analysis, Middlebrook criteria and the recently proposed robust μ analysis approach are performed. Moreover, the simulation based anti-optimization approach has been applied to conduct large signal stability studies, which are required for the stability assessment specified by industrial standards.

Reviewing the considerable development of fault diagnosis techniques and many successful applications attached to them in the last time, power systems seem to be a real hard challenge for the available fault diagnosis techniques. With the help of more accurate modeling of power systems and embedded microprocessors in digital controllers of power distribution systems within the MEA, an unprecedented affordable opportunity can be provided for health monitoring and fault diagnosis using model based fault diagnosis techniques. In this thesis, the multi-model based health monitoring and fault detection for the power system in the MEA are demonstrated.

The power quality assessment is an important task within the large scale virtual test in the validation and verification design phase of the aircraft development. The virtual testing allows to quickly check the overall performance, discover any problem on the hardware and extrapolate results with real hardware tests. One big issue is the steady-state analysis of an integrated power electric system before conducting power quality analysis e.g. Fourier analysis. The conventional brute force simulation to yield the steady-state waveforms of a complex power system with a large amount of switchers is very expensive and is suffering from numerical instabilities. In this thesis, a new optimization based method to compute the steady-state waveforms is introduced. The convergence performance of the steady-state computation is significantly improved by utilizing starting values calculated from simulations of a set of generalized averaged models of the original power systems.

In the last part of the thesis, the Modelica based modeling, simulation and test approaches have been proved as a promising technique for performing the virtual verification and validation activities within the MEA design process, by means of various test cases.

1.6. Outline

At the beginning of the thesis the MEA concept, its major challenges, goals and objectives as well as the main contributions of the thesis are outlined. The unified harmonic state-space description of power electric systems is addressed in chapter 2. Here the multi-level modeling concept and the generalized averaged model derived by the lift techniques are explained in detail. The harmonic state-space description plays a central role in the following chapters regarding stability, health monitoring and power quality issues. Chapter 3 deals with the stability issue of the electric network in MEA. Both small signal and large signal stability studies are considered. Traditional small signal methods such as modal analysis and impedance based method, e.g. Middlebrook criterion, are extended by a robust μ sensitivity approach, which allows to find the most critical components regarding stability in a system. The simulation based anti-optimization approach and generalized averaged models are used to perform large signal stability studies taking the industrial stability definition and harmonic effects into account. The issue of power quality analysis is addressed in chapter 4. This chapter begins with a brief introduction of virtual integration tests of the aircraft design to figure out the importance and problems in the present virtual test activity. Afterwards, the improved optimization based steady-state analysis and multi-level power quality analysis are represented. In chapter 5, a multi-model detection based approach for health monitoring and fault detection is proposed. The capability of Modelica based modeling and simulation approaches to be a proven technique for undertaking the virtual verification and validation tests are described in chapter 6. In the appendix of the thesis auxiliary material developed within this Ph.D. work are enclosed:

- The Modelica based design platform for switched reluctance drives

- The Modelica aircraft power system library

2. Modeling of the MEA

By incorporating even more proper mathematical models into the total aircraft design process, significant improvements in terms of development time and cost are expected. However, there are various challenges when modeling the aircraft components and systems, particularly for the power systems in the MEA, e.g. due to the high frequency switching components. There is always a tradeoff between the model accuracy and the computational burden of simulations. Some new subsystems and components will appear in the MEA with increased power demand. Among them are Auto-Transformer Rectifier Units (ATRU), Electromechanical Actuators (EMA), Variable Frequency Generators (VFG). For different purposes of design tasks, the MEA electric power network should be modeled with different accuracy levels. Furthermore, advanced simulation techniques are demanded for fast and stable simulation of the power system models.

2.1. Multi-level modeling technique of power systems

A model-based design is a mathematical and visual method to address problems associated with complex control, signal processing and communication systems. It is used in many motion control, industrial equipment, aerospace, and automotive applications. The model-based design provides an efficient approach to establish a common framework for communication throughout the design process while supporting the development cycle. The model-based design paradigm is significantly different from the traditional design methodology. Rather than using complex structures and extensive software code, designers can use model-based design to define models with advanced functional characteristics using continuous-time and discrete-time building blocks. These built models used with simulation tools can lead to rapid prototyping, software testing, and verification. Not only is the testing and verification process enhanced, but also, in some cases, hardware-in-the-loop simulation can be used with the new design paradigm to test dynamic effects on the system more quickly and much more efficiently than with traditional design methodology. The main steps in the model-based design approach are:

1. Plant modeling: Plant modeling can be data-driven or first principles based. Data-driven plant modeling uses techniques such as system identification. With system identification, the plant model is identified by acquiring and processing raw data from a real-world system and choosing a mathematical algorithm with which a mathematical model can be identified. Various kinds of analysis and simulations can be performed using the identified model before it is used to design a model-based controller. First principles based modeling is based on

creating a block diagram model that implements known differential-algebraic equations governing the plant dynamics.

2. Controller analysis and synthesis: The mathematical model conceived in step 1 is used to identify dynamic characteristics of the plant model. A controller can be synthesized based on these characteristics.

3. Offline simulation and real-time simulation: The time response of the dynamic system to complex, time-varying inputs is investigated. This is done by simulating a simple LTI or a non-linear model of the plant with the controller. Simulation allows specification, requirements, and modeling errors to be found immediately, rather than later in the design effort. Real-time simulation can be done by automatically generating code for the controller developed in step 2. This code can be deployed to a special real-time prototyping computer that can run the code and control the operation of the plant. If a plant prototype is not available, or testing on the prototype is dangerous or expensive, the code can be automatically generated from the plant model. This code can be deployed to the special real-time computer that can be connected to the target processor with running controller code. Thus a controller can be tested in real-time against a real-time plant model.

4. Deployment: Ideally this is done via automatic code generation from the controller developed in step 2. It is unlikely that the controller will work on the actual system as well as it did in simulation, so an iterative debugging process is carried out by analyzing results on the actual target and updating the controller model. Model based design tools allow all these iterative steps to be performed in a unified visual environment.

There are mainly two modeling approaches for dynamic systems. The first one is a so-called block diagram approach. Using block diagrams, a system is described in terms of quantities that are known and quantities that are unknown. A block diagram consists of components e.g. blocks, which use the known quantities to compute the unknown quantities. This modeling approach is very suitable for the design of control systems. A very famous simulation tool which adopts this modeling approach is used by Simulink[1]. Unlike the block diagram programming approach, describing system or component behavior by means of energy conservation laws is referred to as acausal modeling. Using acausal formulations, there is no explicit specification of system inputs and outputs. Instead, the constitutive equations of components are combined with conservation equations to determine the overall system of equations to be solved. The tools using acausal formulations such as Saber and Modelica[2] language inherently have those benefits like object-oriented, better re-usability and multi-physic domain.

For the industrial design, evaluation and certification process, it is not always useful to take models of highest detail, as it may not improve the overall accuracy

[1]Simulink is a registered trademark of The MathWorks, Inc.
[2]Modelica is a registered trademark of the Modelica Association

but will slow down the simulation drastically. Concerning the design process of the MEA, appropriate models with different complexity have to be built to fulfill the requirements of various tasks and applications.

The essential parts in power systems are generators, power transformers and electric loads. Depending on the types of components to be modeled, there is a slight difference on the definition of multi-level models. Concerning the switching components, such as AC/DC rectifier and DC/AC power inverter in power systems, the functional model eliminates the switching effects in the topological model (behavioral model) by averaging system dynamic states. For the modeling of electric machines in generators or electric loads, all sinusoidal variables in the behavioral level will be transformed into DQ [90] coordinate system to build the functional model.

2.1.1. Conventional multi-level modeling techniques

Depending on the desired evaluation of an electrical network (power consumption, network stability, network quality), system simulations with models of different levels of accuracy are much better suited. The simulation time of the simplest, architectural level of an integration model is usually 2 to 3 orders of magnitude faster than the most complicated behavioral integration level of the model. The following model levels are common in aircraft electrical development process till now

- Level 1: Architectural level steady-state power consumption. Usually, algebraic equations describing the energy balance between ports without dynamic response. The typical use is power budget.
- Level 2: Functional level steady-state power consumption and mean-value transient behavior (e.g. inrush current, consumption dynamics with regard to input voltage transients). Switching is not included. The typical use are network logic studies and network stability studies.
- Level 3: Behavioral level representing actual wave forms including switching and high frequency injection behavior. The typical use is network power quality studies.
- Level 4: Design level models of highest detail, may contain FEM data. The typical use is system development by the component suppliers.

Design level models just apply to component design and are not integrated into a network. While the architectural layer is defined to contain only static energy balance equations and the behavioral models are close to the hardware level, the definition of the functional models is not as straightforward. These models have to be applicable for linearization technique, towards stability investigations with methods of control theory for LTI systems. For DC systems, the functional level models usually have to be deduced from the complex topological models by averaging the switching models on a time interval and further order reduction techniques. For AC systems such as most AC electrical machines, the time variant characteristics of the

sinusoidal alternating currents prevent a time invariant steady state condition and hence linearization. Therefore, it is proposed to use an equivalent representation which expresses a rotating electric machine in a static rotor fixed system. For an airplane multi-phase power transmission system the following components need to be treated:

- Power source: The generators supply sinusoidal voltage at net frequency. Calculation of voltage and current is usually performed in a rotor-fixed system (synchronous machine), which is called DQ0 system. Alternatively, the Root Mean Square (RMS) values can also be considered when deriving functional models for AC systems. This results in a so-called RMS functional model.
- Loads: For symmetrical resistive, inductive and capacitive loads as well as synchronous motors current/voltage relations are fixed to net frequency.
- Other loads: Switches, diodes, unsymmetrical loads, time variant loads do not have simple steady-state dependencies upon net frequency. Limitations for level-triggered switching devices may be circumvented by state space time averaged models. Especially for self commutating rectifiers there is a need to calculate the mean output voltage/current, averaged on a commutation interval.

2.1.2. Extended multi-level modeling

Modeling of power systems at the functional level is a standard approach to deal with typical design activities at system level, such as stability studies and failure analysis in the current aircraft industry [50, 65]. In order to achieve more reliable analysis results and to make the design process more efficient, the conventional functional model for power systems shall be extended.

Since the conventional functional model only considers the DC part of all system variables by ignoring all harmonic performance, it can deliver very conservative analysis result for design tasks, which are based on small signal analysis. Some examples can be stability studies and health monitoring system design. If the functional model can be extended by adding some harmonic parts in the systems, the modeling accuracy can be significantly increased. Moreover, since the high frequency contents with selectable accuracy is already considered in the extended functional model, the power quality studies could be directly performed by this kind of models without intensive simulation of the behavioral level model[3].

Lift technique for power electronic systems

The lift technique [114] is conventionally used for solving periodic issues. The equivalent technique can also be used in switching power electronic systems. The basic idea is to present the original signal $x(\tau)$ on the interval $\tau \in [t-T, t]$ by the Fourier series [98]:

[3]This section is an extended and improved version of [58]

$$x(\tau) = \sum_{k=-\infty}^{\infty} \langle x \rangle_k(t) e^{ik\omega\tau} \tag{2.1}$$

where $\omega = 2\pi/T$ and T is typically the shortest constant time interval of the switching components in the system. The kth time varying complex Fourier coefficient can be obtained by

$$\langle x \rangle_k(t) = \frac{1}{T} \int_{t-T}^{t} x(\tau) e^{-ik\omega\tau} d\tau \tag{2.2}$$

In spite of the quite detailed explanations with examples to the generalized averaging technique in literature e.g. [78**?**], the readers could be easily led into the misunderstanding, that it is extremely complicated to establish the harmonic state space differential equations in terms of the time varying Fourier coefficients $\langle x \rangle_k(t)$ for power electronic systems. The reason is a missing unified state space representation which permits one to automatically apply the generalized averaging technique. It is well known, that a wide class of power electronic systems e.g. DC/DC, DC/AC converters with a fixed switching time constant can be regarded as linear time periodic (LTP) systems:

$$\begin{aligned} \dot{x} &= A(t)x + B(t)u \\ y &= C(t)x + D(t)u \end{aligned} \tag{2.3}$$

where A, B, C, D are piecewise periodic matrices:

$$\begin{aligned} A(t+T) &= A(t), \qquad B(t+T) = B(t), \\ C(t+T) &= C(t), \qquad D(t+T) = D(t). \end{aligned}$$

The harmonic state space representation for LTP systems has been introduced in [114], which is also feasible to describe a wide class of power electronic systems. The harmonic state space representations of LTP systems is derived by feeding a complex exponentially modulated periodic (EMP) signal

$$u(t) = \sum_{m=-\infty}^{\infty} u_m e^{(s+im\omega)t} \tag{2.4}$$

with $s \in \mathbb{C}$ to a LTP system in Eq. 2.3. The state response of the LTP system is also an EMP signal as

$$x(t) = \sum_{m=-\infty}^{\infty} x_m e^{(s+im\omega)t} \tag{2.5}$$

and the output can be described as linear combination of the state values such as

$$y(t) = \sum_{m=-\infty}^{\infty} y_m e^{(s+im\omega)t}. \tag{2.6}$$

Substituting Eq. 2.4, Eq. 2.5 and Eq. 2.6 into Eq. 2.3 and replacing the piecewise periodic matrices $A(t)$, $B(t)$, $C(t)$, $D(t)$ by their Fourier series using Eq. 2.1 and

Eq. 2.2, yields the following LTI harmonic state space representation of LTP systems in Laplace domain for $n \in \mathbb{Z}$ (for a proof see pp. 76-81 in [114]):

$$\begin{aligned}(s + in\omega)x_n &= \sum_{m=-\infty}^{\infty} A_{n-m}x_m + \sum_{m=-\infty}^{\infty} B_{n-m}u_m \\ y_n &= \sum_{m=-\infty}^{\infty} C_{n-m}x_m + \sum_{m=-\infty}^{\infty} D_{n-m}u_m \end{aligned} \tag{2.7}$$

The x_n is the nth time varying complex Fourier coefficient vector relating to the nth harmonic of the state vector. Analogously, u_m is the mth harmonic of $u(t)$. A_{n-m} is obtained from the Fourier expansion of the system matrix $A(t)$, the same for B_{n-m}, C_{n-m}, and D_{n-m}. Defining a Toeplitz form matrix $\mathcal{A}_k$ in terms of the Fourier series coefficient matrix of the system matrix $A(t)$ such as

$$\mathcal{A}_k = \begin{bmatrix} A_0 & \cdots & A_{-k} & \cdots & A_{-2k} \\ \vdots & \ddots & \vdots & \ddots & \vdots \\ A_k & \cdots & A_0 & \cdots & A_{-k} \\ \vdots & \ddots & \vdots & \ddots & \vdots \\ A_{2k} & \cdots & A_k & \cdots & A_0 \end{bmatrix}$$

where

$$A_k = \frac{1}{T}\int_{t-T}^{t} A(\tau)e^{-ik\omega\tau}d\tau \tag{2.8}$$

A_{-k} is the complex conjugate of A_k. There are similar expressions for $B(t)$, $C(t)$ and $D(t)$ with corresponding Toeplitz matrices, $\mathcal{B}_k$, $\mathcal{C}_k$ and $\mathcal{D}_k$, a compact harmonic state space representation of an approximated LTP system by $k \geq 0$ harmonics can be written as

$$\begin{aligned} s\mathcal{X}_k &= (\mathcal{A}_k - \mathcal{N}_k)\mathcal{X}_k + \mathcal{B}_k\mathcal{U}_k \\ \mathcal{Y}_k &= \mathcal{C}_k\mathcal{X}_k + \mathcal{D}_k\mathcal{U}_k. \end{aligned} \tag{2.9}$$

We use the notations

$$\mathcal{N}_k = \text{blockdiag}\left(-ki\omega I,\ \ldots,\ -i\omega I,\ 0,\ i\omega I,\ \ldots,\ ki\omega I\right) \tag{2.10}$$

with $0, I \in \mathbb{R}^{\dim x \times \dim x}$ and the complex harmonic coefficients

$$\begin{aligned} \mathcal{X}_k &= \left[x_{-k}^T, \ldots, x_0^T, \ldots, x_k^T\right]^T, \\ \mathcal{Y}_k &= \left[y_{-k}^T, \ldots, y_0^T, \ldots, y_k^T\right]^T, \\ \mathcal{U}_k &= \left[u_{-k}^T, \ldots, u_0^T, \ldots, u_k^T\right]^T. \end{aligned}$$

Eq. 2.9 has complex values which is cumbersome for describing systems having real inputs signals $\mathcal{U}_{real,k}$. For the sake of simplification, the desired real representation of Eq. 2.9 can be derived by introducing a transformation matrix $\mathcal{T}_{\mathcal{U},k} \in \mathbb{C}^{(2k+1)\cdot\dim u \times (2k+1)\cdot\dim u}$ [100] such that

$$\mathcal{U}_{real,k} = \mathcal{T}_{\mathcal{U},k}\mathcal{U}_k$$

where the transformation matrix has the form

$$\mathcal{T}_{\mathcal{U},k} = \begin{bmatrix} \frac{1}{2}I & & & 0 & & & \frac{1}{2}I \\ & \ddots & & & & \iddots & \\ & & \frac{1}{2}I & & \frac{1}{2}I & & \\ 0 & & & I & & & 0 \\ & & -\frac{1}{2}iI & & \frac{1}{2}iI & & \\ & \iddots & & & & \ddots & \\ -\frac{1}{2}iI & & & 0 & & & \frac{1}{2}iI \end{bmatrix} \tag{2.11}$$

with $I \in \mathbb{R}^{\dim u \times \dim u}$. The real input vector $\mathcal{U}_{real}$ is described by

$$\mathcal{U}_{real,k} = \left[u_{c,k}^T, \ldots, u_{c,1}^T, u_0^T, u_{s,1}^T, \ldots, u_{s,k}^T\right]^T$$

where $u_{c,m}$, $u_{s,m}$ $(m = 1, \ldots, k)$ correspond to the real and imaginary parts of the complex Fourier coefficients u_m. The real input signal u can be reconstructed by

$$u(t) = u_0 + \sum_{m=1}^{\infty} 2u_{c,m} \cos m\omega t - \sum_{m=1}^{\infty} 2u_{s,m} \sin m\omega t. \tag{2.12}$$

Analogously transforming complex state and output harmonic vectors in Eq. 2.9 by transformation matrices $\mathcal{T}_{\mathcal{X},k}$, $\mathcal{T}_{\mathcal{Y},k}$:

$$\begin{aligned} \mathcal{X}_{real,k} &= \mathcal{T}_{\mathcal{X},k}\mathcal{X}_k \\ \mathcal{Y}_{real,k} &= \mathcal{T}_{\mathcal{Y},k}\mathcal{Y}_k \end{aligned}$$

with appropriate dimensions, the real harmonic state space representation of LTP systems approximated by k harmonics can be finally achieved as

$$\begin{aligned} s\mathcal{X}_{real,k} &= \mathcal{A}_{real,k}\mathcal{X}_{real,k} + \mathcal{B}_{real,k}\mathcal{U}_{real,k} \\ \mathcal{Y}_{real,k} &= \mathcal{C}_{real,k}\mathcal{X}_{real,k} + \mathcal{D}_{real,k}\mathcal{U}_{real,k} \end{aligned} \tag{2.13}$$

with

$$\begin{aligned} \mathcal{A}_{real,k} &= \mathcal{T}_{\mathcal{X},k}(\mathcal{A}_k - \mathcal{N}_k)\mathcal{T}_{\mathcal{X},k}^{-1} \\ \mathcal{B}_{real,k} &= \mathcal{T}_{\mathcal{X},k}\mathcal{B}_k\mathcal{T}_{\mathcal{U},k}^{-1} \\ \mathcal{C}_{real,k} &= \mathcal{T}_{\mathcal{Y},k}\mathcal{C}_k\mathcal{T}_{\mathcal{X},k}^{-1} \\ \mathcal{D}_{real,k} &= \mathcal{T}_{\mathcal{Y},k}\mathcal{D}_k\mathcal{T}_{\mathcal{U},k}^{-1} \end{aligned} \tag{2.14}$$

Eq. 2.13 provides a unified formalization for the generalized averaging modeling of a wide class of power electronic systems, which are approximated by k harmonics. By using a symbolic toolbox, e.g. Maple[4] or MATLAB, the generalized averaging modeling can be easily computed for arbitrary harmonic approximations, once the periodic state-space description in Eq. 2.3 is known. The approaches to derive harmonic

[4]Maple is a registered trademarks of Waterloo Maple Inc.

state-space representation are discussed in [98, 78**?**]. They can be significantly simplified. The knowledge on the steady-state waveforms acquired by simulating averaged models with different accuracy is important to establish an adequate setup of the optimization based steady-state analysis regarding the convergence performance.

Example

As example, a simple buck converter is selected to apply the lift technique for power electronic systems. The buck converter is depicted in Fig. 2.1. The First Harmonic Averaged Model (FHAM) of the buck converter shall be derived. Assuming, that the electrical switch works with a constant time period T_s, and dT_s is the time interval in which the switch is on, where $0 \leq d \leq 1$ is called the duty cycle. If the switch is being on, the buck converter has the topology as depicted in the upper diagram of Fig. 2.2. The topology becomes the configuration in the lower diagram of Fig. 2.2, once the switch is being off. The state space description for this buck converter is defined by

$$\begin{aligned} \dot{x} &= A(t)x + B(t)u \\ y &= C(t)x + D(t)u \end{aligned}$$

where $x = [\ i_L \quad v_C\ ]^T$ for the inductance current and capacitor voltage. Defining the inductance current i_L as the system output and v_{in} as the system input, the state space matrices can be described in

$$A(t) = \begin{bmatrix} 0 & -\frac{1}{L} \\ \frac{1}{C} & -\frac{1}{RC} \end{bmatrix} \ \forall t \in [nT_s, (n+1)T_s] \tag{2.15}$$

$$B(t) = \begin{cases} \begin{bmatrix} \frac{1}{L} \\ 0 \end{bmatrix} & \forall t \in [nT_s, (n+d)T_s] \\ \begin{bmatrix} 0 \\ 0 \end{bmatrix} & \forall t \in [(n+d)T_s, (n+1)T_s] \end{cases} \tag{2.16}$$

$$C(t) = \begin{bmatrix} 1 & 0 \end{bmatrix} \ \forall t \in [nT_s, (n+1)T_s]$$

$$D(t) = 1 \, \forall t \in [nT_s, (n+1)T_s]$$

where $B(t)$ is a periodic matrix. Since $A(t)$ is not a time variable matrix, the Fourier series coefficient matrices of $A(t)$ are

$$A_k = \begin{cases} \begin{bmatrix} 0 & -\frac{1}{L} \\ \frac{1}{C} & -\frac{1}{RC} \end{bmatrix} & \forall k = 0 \\ \begin{bmatrix} 0 & 0 \\ 0 & 0 \end{bmatrix} & \forall k \neq 0 \end{cases}$$

the Toeplitz form matrix $\mathcal{A}_k$

$$\mathcal{A}_k = \begin{bmatrix} A_0 & A_{-1} & A_{-2} \\ A_1 & A_0 & A_{-1} \\ A_2 & A_1 & A_0 \end{bmatrix}$$

where the second order Fourier series coefficient is required to compute the first harmonic averaged model. Applying Eq. 2.8 for the $B(t)$ matrix, such as

$$B_k = \frac{1}{T_s}\left(\int_0^{dT_s} \begin{bmatrix} \frac{1}{L} \\ 0 \end{bmatrix} e^{-ik\omega\tau} d\tau + \int_{dT_s}^{T_s} \begin{bmatrix} 0 \\ 0 \end{bmatrix} e^{-ik\omega\tau} d\tau\right)$$

the Fourier series coefficient matrices of $B(t)$ become

$$B_1 = \begin{bmatrix} \frac{sin(2\pi d)+i(cos(2\pi d)-1)}{2\pi L} \\ 0 \end{bmatrix} and\, B_{-1} = \begin{bmatrix} \frac{sin(2\pi d)-i(cos(2\pi d)-1)}{2\pi L} \\ 0 \end{bmatrix}$$

$$B_2 = \begin{bmatrix} \frac{sin(4\pi d)+i(cos(4\pi d)-1)}{4\pi L} \\ 0 \end{bmatrix} and\, B_{-2} = \begin{bmatrix} \frac{sin(4\pi d)-i(cos(4\pi d)-1)}{4\pi L} \\ 0 \end{bmatrix}$$

and

$$\mathcal{B}_k = \begin{bmatrix} B_0 & B_{-1} & B_{-2} \\ B_1 & B_0 & B_{-1} \\ B_2 & B_1 & B_0 \end{bmatrix}$$

According to Eq. 2.10, the $\mathcal{N}_2$ matrix can be defined by

$$\mathcal{N}_2 = \begin{bmatrix} \omega i & 0 & 0 & 0 & 0 & 0 \\ 0 & \omega i & 0 & 0 & 0 & 0 \\ 0 & 0 & 0 & 0 & 0 & 0 \\ 0 & 0 & 0 & 0 & 0 & 0 \\ 0 & 0 & 0 & 0 & -\omega i & 0 \\ 0 & 0 & 0 & 0 & 0 & -\omega i \end{bmatrix} \tag{2.17}$$

where $\omega = 2\pi/T_s$. The transformation matrices $\mathcal{T}_{\mathcal{U},2}$ and $\mathcal{T}_{\mathcal{X},2}$ with appropriate dimensions can be defined by Eq. 2.11 as

$$\mathcal{T}_{\mathcal{X},2} = \begin{bmatrix} 0.5 & 0 & 0 & 0 & 0.5 & 0 \\ 0 & 0.5 & 0 & 0 & 0 & 0.5 \\ 0 & 0 & 1 & 0 & 0 & 0 \\ 0 & 0 & 0 & 1 & 0 & 0 \\ -0.5i & 0 & 0 & 0 & 0.5i & 0 \\ 0 & -0.5i & 0 & 0 & 0 & 0.5i \end{bmatrix} \tag{2.18}$$

$$\mathcal{T}_{\mathcal{U},2} = \begin{bmatrix} 0.5 & 0 & 0.5 \\ 0 & 1 & 0 \\ -0.5i & 0 & 0.5i \end{bmatrix} \tag{2.19}$$

Applying the transformation in Eq. 2.14, the real state space description of the FHAM of the buck converter can be written as

$$\begin{bmatrix} \dot{i}_{L1r} \\ \dot{v}_{C1r} \\ \dot{i}_{L0} \\ \dot{v}_{C0} \\ \dot{i}_{L1i} \\ \dot{v}_{C1i} \end{bmatrix} = \begin{bmatrix} 0 & -\frac{1}{L} & 0 & 0 & \omega & 0 \\ \frac{1}{C} & -\frac{1}{CR} & 0 & 0 & 0 & \omega \\ 0 & 0 & 0 & -\frac{1}{L} & 0 & 0 \\ 0 & 0 & \frac{1}{C} & -\frac{1}{CR} & 0 & 0 \\ -\omega & 0 & 0 & 0 & 0 & -\frac{1}{L} \\ 0 & -\omega & 0 & 0 & \frac{1}{C} & -\frac{1}{CR} \end{bmatrix} \begin{bmatrix} i_{L1r} \\ v_{C1r} \\ i_{L0} \\ v_{C0} \\ i_{L1i} \\ v_{C1i} \end{bmatrix} + \begin{bmatrix} 0 & \frac{sin(2\pi d)}{2\pi L} & 0 \\ 0 & 0 & 0 \\ 0 & \frac{d}{L} & 0 \\ 0 & 0 & 0 \\ 0 & \frac{sin(\pi d)^2}{\pi L} & 0 \\ 0 & 0 & 0 \end{bmatrix} \begin{bmatrix} 0 \\ v_{in} \\ 0 \end{bmatrix} \tag{2.20}$$

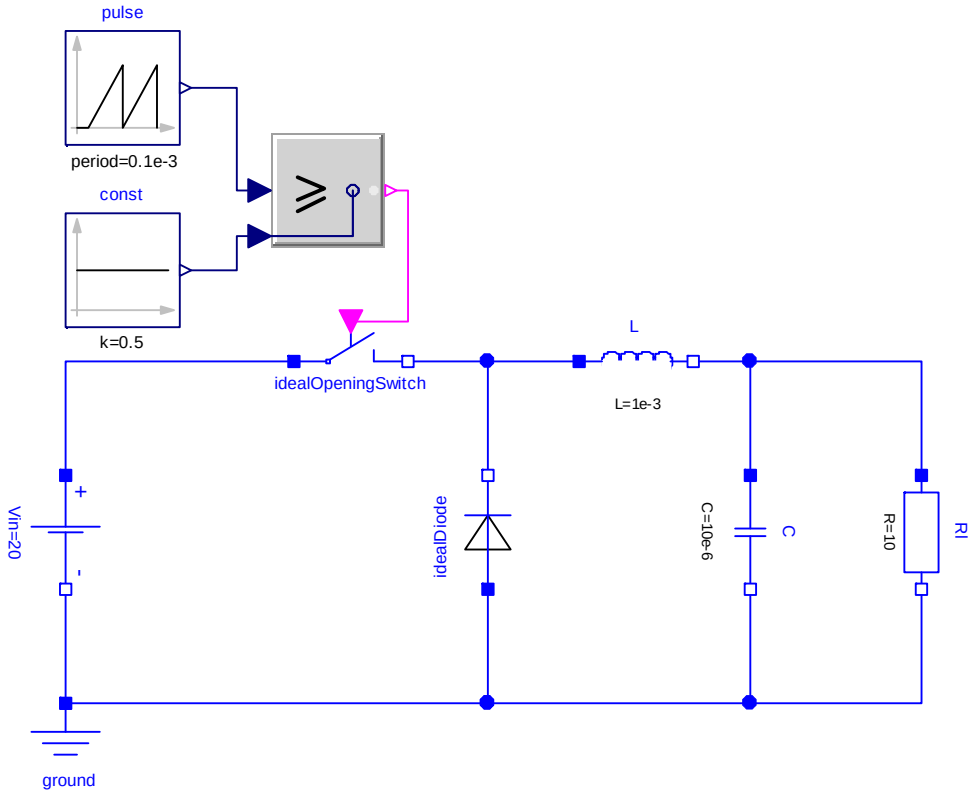

Figure 2.1.: A multi-level modeling example with a simple buck converter

where i_{Lkr} and v_{Ckr} are kth real parts of the complex Fourier series coefficients for the inductance current and capacitor voltage. i_{Lki} and v_{Cki} are the imaginary parts of the complex Fourier series coefficients. Simulation results of the inductance current in the behavioral model in Fig. 2.1, a classical DC Averaged Model (DCAM) and the FHAM in Eq. 2.20 are presented in Fig. 2.3. It is easy to see, that the oscillation performance in transient and steady-state phase of the original behavioral model can be much better reflected by using the FHAM, instead of the classical DCAM.

Finally, it could be possible to automate the derivation of generalized averaged models in a simulation platform. In every interval, where the switch is either closed or open, the behavioral model is linearized. The generalized averaged models with required harmonic number is then constructed in a similar way as described in the example.

2.2. Modeling tools for power systems

Among several available modeling techniques and tools in the current market, Modelica and Dymola[5] have been selected to implement the modeling activities of the

[5]Dymola is a commercial modeling and simulation environment from Dassault Systemes based on the open Modelica modeling language. www.3ds.com

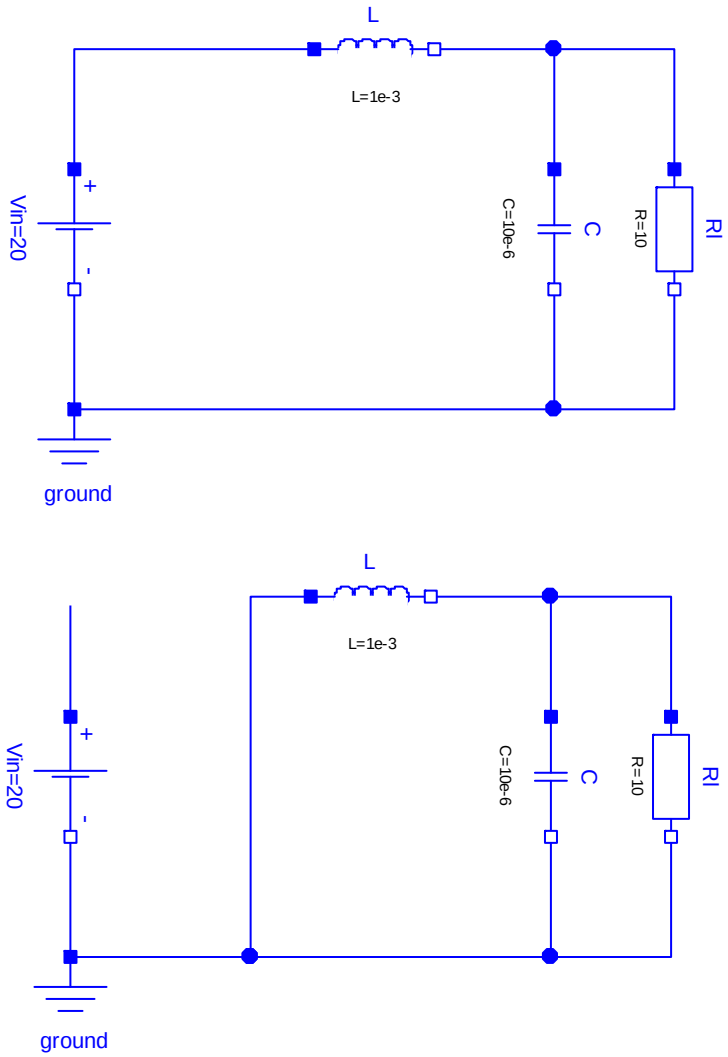

Figure 2.2.: Topologies of the buck converter with different switching modes

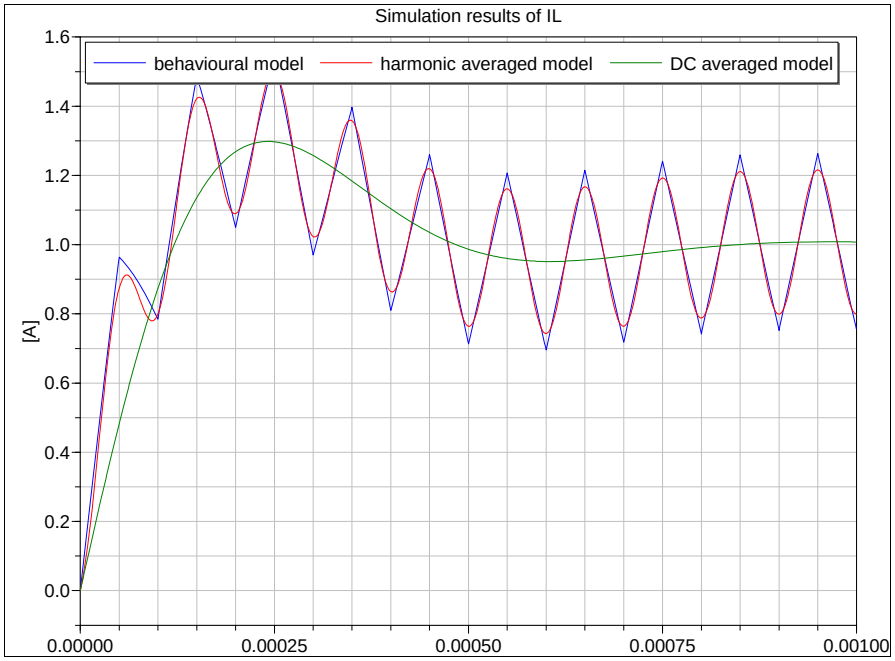

Figure 2.3.: Simulation results of the inductance currents in the multi-level models of a simple buck converter (time unit is [s])

MEA. Modelica is a non-proprietary modeling language and the name is a trademark of the Modelica Association [3]. The basic idea behind Modelica was to create a modeling language that could express the behavior of models from a wide range of engineering domains without limiting those models to a particular commercial tool. Modelica can be used to solve a variety of problems that can be expressed in terms of differential-algebraic equations describing the behavior of continuous variables. Modelica has the inherent ability to conveniently model complex physical systems containing e.g. mechanical, electrical, hydraulic, thermal, control, electric power or process-oriented sub-components.

There are many formalisms used for modeling continuous systems. Two common approaches are block diagram modeling and acausal modeling. While the block diagram approach exhibits excellent performance when modeling control algorithm, the acausal modeling approach can significantly ease the modeling of power systems. With acausal formulations, there is no explicit specification of system inputs and outputs. Instead defining the inputs and outputs, the system behavior is determined by mathematical equations. In order to formulate acausal models, it is useful to identify the flow variables and potential variables for the component being modeled. For instance, the voltage is the across variable and the current is the through variable for an electrical system. The maturity of Modelica for the modeling and simulation tools of large scale power systems in the MEA has been proven by benchmark use cases [55, 56], which have been established within the Clean Sky project [1]. In general, a Modelica based modeling tool, e.g. Dymola has following advantages to model and simulate a MEA power system:

- Multi-domain simulation program
- Equation-based modeling
- DAE solver
- Enhanced symbolic processing and manipulation in solver
- Many additional libraries available
- Co-simulation possible by specific interfaces, e.g. the Functional Mock-up Interface FMI technology [2]
- Ability to analyze simulation results

2.3. Modeling of the electric network in the MEA

In a conventional aircraft system architecture, fuel is converted into power by the engines. Most of this power is expended as thrust to propel the aircraft. The remainder is transmitted via, and converted into, four main forms of non-propulsive power: pneumatic, mechanical, hydraulic and electrical power.

- Pneumatic power generated by high-pressure compressor to power the Environmental Control System (ECS) and supply hot air for Wing Ice Protection System (WIPS).
- Mechanical power from engines to central hydraulic pumps and other mechanically driven subsystems, and to the main electrical generator.
- Hydraulic power by hydraulic pumps to drive the actuation systems for flight control, landing gear and numerous ancillary systems.
- Electrical power by the generator to supply electric energy to the avionics, to cabin and aircraft lighting, to the galleys, and to other commercial loads

Regarding the High Voltage Direct Current (HVDC) architecture for the MEA, major sub-systems, such as electric generator, auto-transformer rectifier, DC-DC converter, Permanent Magnetic Synchronous Machine (PMSM) are frequently considered. In order to perform the virtual testing activities, an integrated electrical power network model is needed including every necessary sub-system and component. Normally, the behavioral and functional models are both required when building the integrated electrical power network for diverse design tasks.

Although the aircraft industry clearly tends to design future aircraft with more electric power energy, discussions about the optimal energy power network is still ongoing. Comparing with an AC power distribution system, a HVDC distribution system is gaining more attention [97] thanks to the benefits like mass/volume saving in the feeders, possible use of regeneration energy from electric actuators etc. For instance, a possible DC power distribution network configuration is depicted

in Fig. 2.4. This architecture contains a 18-pulses ATRU, which transfers 230V AC voltage to 540V DC voltage supplying DC loads such as electric environmental system (ECS) and electric actuators. By replacing the VFG in the proposed architecture by a switched reluctance generator, which directly generates 540V DC voltage, the ATRU can even be saved [38, 53]. High quality models of components and the integrated power network is a precondition for the model based design, e.g. the virtual testing process in the aircraft system verification design phase. An electric power network in the MEA typically covers several physical domains such as electrical systems, magnetic systems, mechanical systems and control. Therefore, a modeling language to be selected for the virtual testing process has to be capable for modeling multi-domain systems. Furthermore, powerful solvers which can well deal with complex dynamic systems including switching actions are needed. An electric power network often is a very complex large scale system, for instance, a proposed aircraft power network containing a VFG, a high power 18-pulses ATRU, a 3 phase auto-transformer, a DC/DC converter unit (DCCU), a PMSM and a 115V AC constant power load (CPL) typically has more than 100 dynamic state variables.

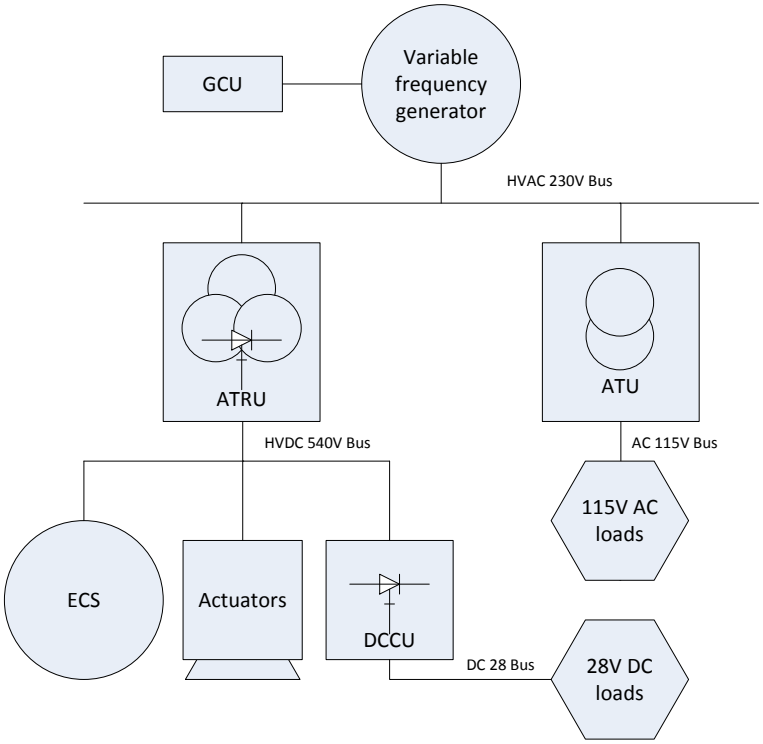

Figure 2.4.: An electric network architecture for the MEA

2.3.1. Requirement of modeling activities

A key-factor for the success of developing the MEA is to incorporate high quality system models in the complete aircraft design process [12], which briefly can be

Design phase	Typical task	Required model
Concept	Architecture optimization	Level 1
System specification	Stability studies	Level 2/3
System development	Control design	Level 2/3
System verification	Virtual testing	Level 2/3

Table 2.1.: Model requirements in different aircraft design phases

divided into 4 major phases: concept phase, system specification phase, system development/validation phase and system verification phase [36]. Today, aircraft industry utilizes a multi-level approach for the design of the aircraft system [67]. Tab. 2.1 presents an overview of model requirements in all aircraft design phases. In this thesis, only functional and behavioral models are considered.

2.3.2. Modeling of electric generators

Currently, aircraft loads are supplied from a combination of individually optimized hydraulic, electrical, pneumatic, and mechanical power sources. With the MEA concept, use of electrical power alone will enable global optimization and significant system level performance improvements. Although preferred architectures for the MEA power systems have yet to be established, they will feature multiple distributed power electronic converters for flight control surface actuation, environmental control, and numerous DC and AC loads [24]. Furthermore, the HVDC power network in the MEA would include a variable speed embedded power generation, which is likely to favor switched reluctance (SR) machine technology because of its high power density, its ability to operate in harsh environments and the fact that it offers a degree of fault-tolerance [23].

Synchronous generator model

VFGs provide simplified power generation solutions for aircraft designs that incorporate variable frequency electrical systems. The VFG essentially eliminates the need for a constant speed drive, as the generator is allowed to rotate at a variable speed. Through the use of power electronics and conversion equipment, this type of electrical power can be used to power a variety of aircraft electrical loads. Two essential parts of a VFG are the synchronous generator and the Generator Control Unit (GCU). After d-q transformation, an external excited three phase Synchronous Generator (SG) can be described as

$$\begin{aligned} \dot{\Phi}_{fd} &= V_{fd} - R_{fd} I_{fd} \\ \dot{\Phi}_{kD} &= -R_{kD} I_{kD} \\ \dot{\Phi}_{kQ} &= -R_{kQ} I_{kQ} \\ \dot{\Phi}_{d} &= V_{d} + R_{s} I_{d}^{gen} + \omega_s \Phi_q \\ \dot{\Phi}_{q} &= V_{q} + R_{s} I_{q}^{gen} - \omega_s \Phi_d \end{aligned} \tag{2.21}$$

where V_{fd} and I_{fd} are the exciter field voltage and current, R_{fd} is the field winding resistance, R_{kD} and R_{kQ} are equivalent d- and q axis damper winding resistance, respectively. I_{kD} and I_{kQ} are the d- and q axis rotor damper winding currents and Φ_{fd}, Φ_{kD} and Φ_{kQ} are the magnetic flux-linkages of the field winding and the d- and q axis damper windings. V_d and V_q are the d- and q axis stator output voltages, R_s is the phase resistance of the stator winding, Φ_d and Φ_q are the d- and q axis flux linkages of the stator winding and ω_s is the synchronous angular velocity of the generator. By ignoring the magnetic saturation effect, the fluxes equations in the dq system for the stator and rotor are given by

$$\begin{bmatrix} \Phi_d \\ \Phi_q \\ \Phi_{fd} \\ \Phi_{kD} \\ \Phi_{kQ} \end{bmatrix} = LL \begin{bmatrix} I_d^{gen} \\ I_q^{gen} \\ I_{fd} \\ I_{kD} \\ I_{kQ} \end{bmatrix} \tag{2.22}$$

$$LL = \begin{bmatrix} -(L_s + L_{md}) & 0 & L_{md} & L_{md} & 0 \\ 0 & -(L_s + L_{md}) & 0 & 0 & 0 \\ -L_{md} & 0 & L_{fd} + L_{md} & L_{md} & 0 \\ -L_{md} & 0 & L_{md} & L_{kD} + L_{md} & 0 \\ 0 & -L_{mq} & 0 & 0 & L_{kQ} + L_{mq} \end{bmatrix} \tag{2.23}$$

where L_s is the stator winding leakage inductance and L_{md}, L_{mq} are the d- and q axis magnetizing inductances. L_{kD} and L_{kQ} are the d- and q axis leakage inductances of the rotor damper windings.

GCU model

Another important part is the GCU. It regulates the field excitation voltage demand and a thyristor rectifier provides the dc excitation current to the field winding in the synchronous machine. The comparison result between the reference three phase voltage V_m^* and the terminal voltage V_m is eliminated by a proportional-integral control. The exciter is therefore represented by a first-order delay element with a time constant T_{gcu}. The mathematical description of the GCU is given by

$$\begin{aligned} \dot{V}_{fd} &= -\tfrac{V_{fd}}{T_{GCU}} + \tfrac{\alpha_{PI}}{T_{GCU}} - \tfrac{K_{ps}}{T_{GCU}}\sqrt{V_d^2 + V_q^2} + \tfrac{K_{ps}}{T_{GCU}} V_m^* \\ \alpha_{PI} &= -K_{is}\sqrt{V_d^2 + V_q^2} + K_{is} V_m^* \end{aligned} \tag{2.24}$$

where α_{PI} is the output of the integrator of the controller, K_{ps} and K_{is} are the gains of the controller.

Implementation with Modelica

The VFG consists of a synchronous machine, an exciter and a GCU. The VFG model has been completely modeled with Modelica. Both behavioral models with 3 phase AC power connector and functional model using 3 phase RMS power connector are

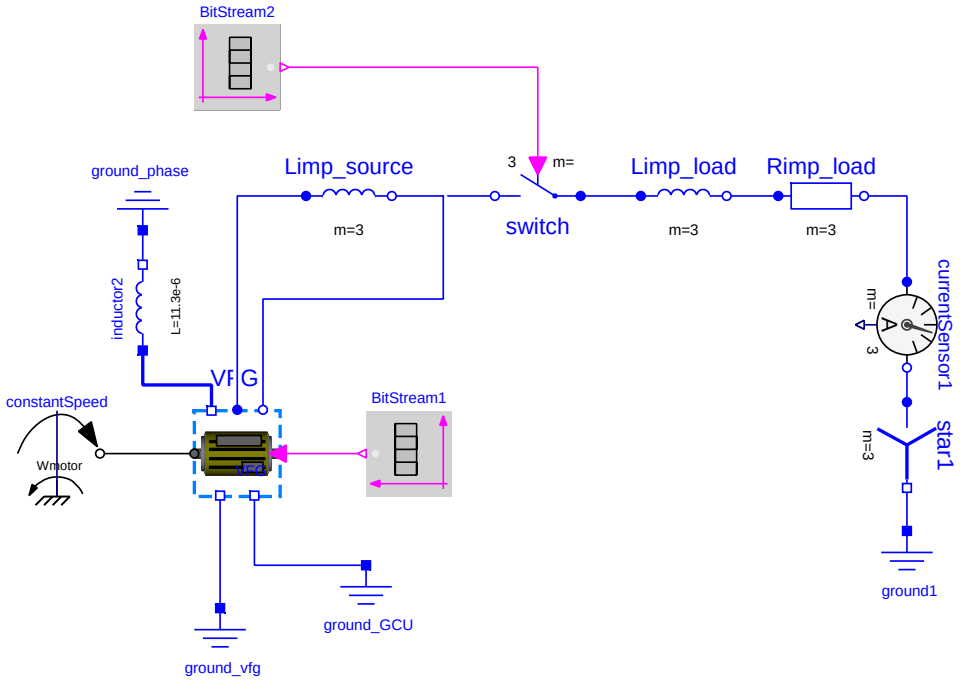

Figure 2.5.: The Modelica model of the VFG

implemented. The Modelica model of the VFG is depicted in Fig. 2.5. The VFG is fed by a constant speed and provides three phase voltages for a three phase load. To check the VFG model, the power load connection tests have been established, where the VFG is powered at 0.1 second. The simulation results for both behavioral and functional level are depicted in Fig. 2.7 and Fig. 2.8. The BitStream2.y curve in Fig. 2.7 and the BitStream.y curve in Fig. 2.8 present the signals to power up the behavioral and functional VFG models, respectively. In the simulation result in Fig. 2.8, the RMS values of three output currents and voltages are toltoally identical. It can be seen, that a voltage sag at the point of regulation of the VFG occurs at the 0.1 second.

Switched reluctance generator modeling

Most primary electrical AC power generators are based on the compound generator concept, which has some issues concerning reliability and maintenance limitation. When replacing the VFG by a Switched Reluctance Generator (SRG), the rectifier unit for the AC/DC transformation can be saved. The SRG is usually connected to the DC bus via asymmetric H-bridges. The torque of the switched reluctance machine is produced by the natural tendency of the stator poles to attract the nearest rotor poles. If the phase is excited as the rotor poles rotate through the aligned position when the phase inductance decrease with the rotor position, the rotor experiences torque opposing to its direction of rotation and therefore the machine operates as a generator. Details about how to implement switch reluctance drives with Modelica are described in appendix A.

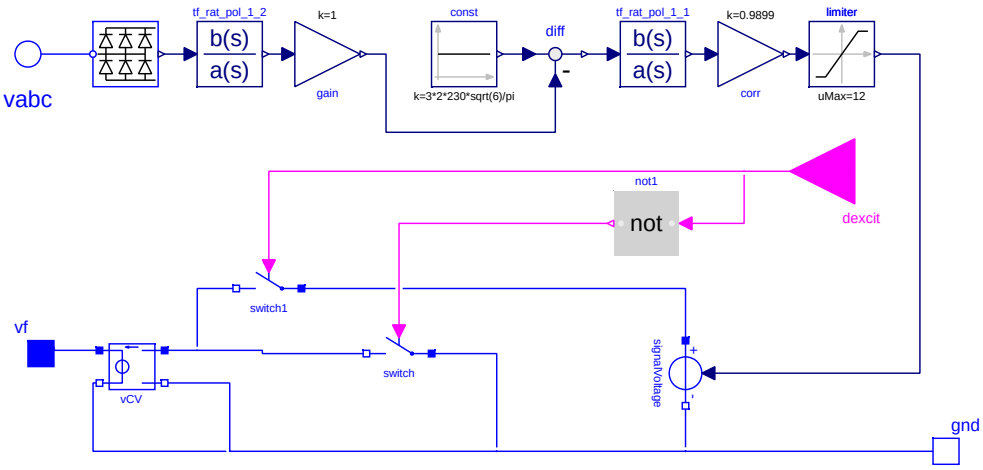

Figure 2.6.: The Modelica GCU model

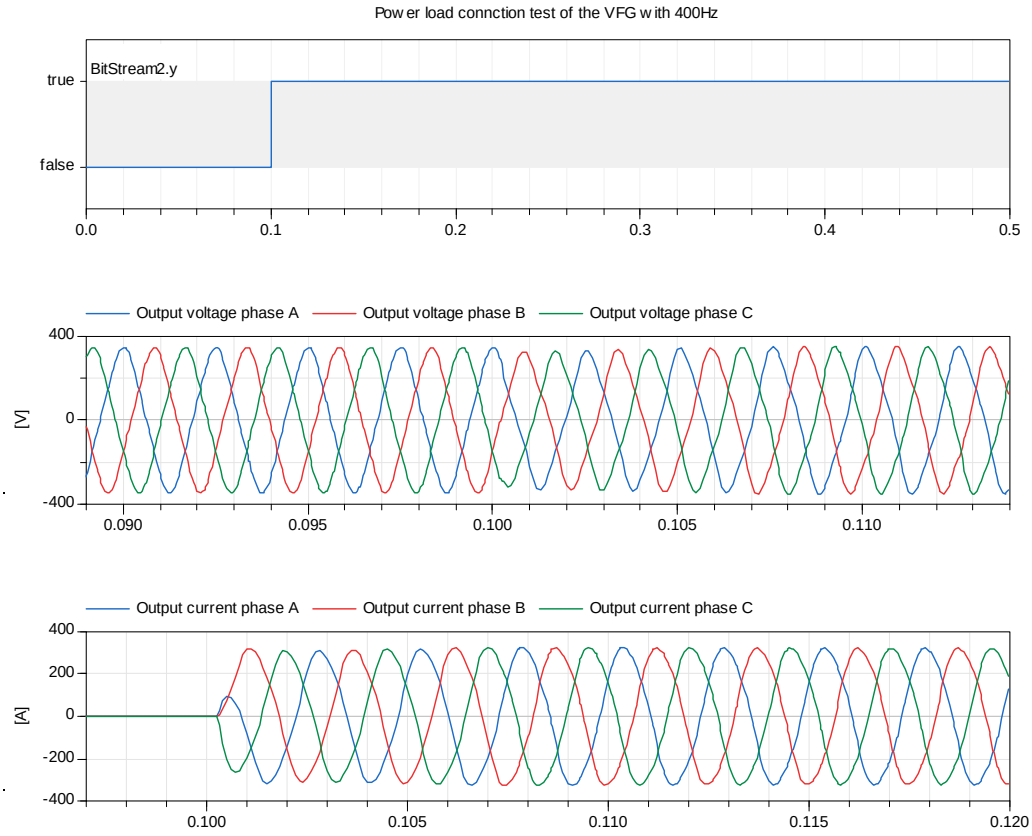

Figure 2.7.: Simulation results of output voltages and currents in power load connection test of the VFG behavioral model with 400Hz (time unit is [s])

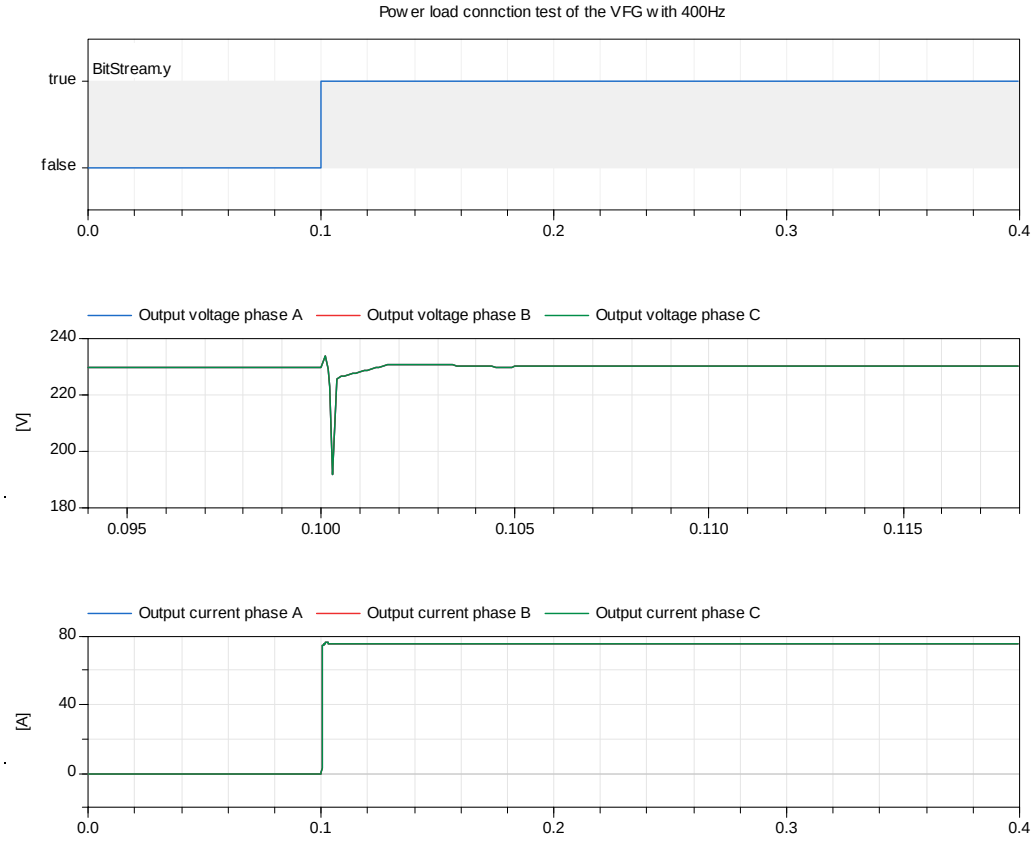

Figure 2.8.: Simulation results of output voltages and currents in power load connection test of the VFG functional model with 400Hz (time unit is [s])

2.3.3. Modeling of electromagnetic actuators

The key applications of electromagnetic actuators in the MEA are flight actuators, fuel pumps and landing gear nose wheel steering systems. Regarding several machine options for the EMA applications, such as induction motors, reluctance motors and permanent magnetic motors, the permanent magnetic motors usually provide higher torque density than other motor types [19].

Mathematical description of the PMSM

The PMSM can be mathematically described in the synchronous reference dq frame, the stator voltage equations of a PMSM are given by

$$\begin{aligned} v_{sd} &= R_S i_{sd} + \frac{d\psi_{sd}}{dt} - \omega_{pmsm}\psi_{sq} \\ v_{sq} &= R_s i_{sq} + \frac{d\psi_{sd}}{dt} + \omega_{pmsm}\psi_{sd} \end{aligned} \tag{2.25}$$

The result flux is a sum of the mutual flux generated by the stator windings and the permanent magnet rotor flux. When ignoring the leakage inductance and magnetic cross coupling, the stator flux linkage can be simply described in the rotor reference frame such as

$$\begin{aligned} \psi_{sd} &= L_d i_{sd} + \psi_{PM} \\ \psi_{sq} &= L_q i_{sq} \end{aligned} \tag{2.26}$$

The torque experienced by the PMSM can be divided into two parts, i.e. electromagnetic torque and the reluctance torque, which can be described by

$$T_{pmsm} = \tfrac{3}{2} p \psi_{PM} i_{sq} + \tfrac{3}{2} p (L_d - Lq) i_{sd} i_{sq} \tag{2.27}$$

The mechanical equation of the PMSM is given by

$$\frac{d\omega_{pmsm}}{dt} = \frac{1}{J_{pmsm}} (T - T_l) \tag{2.28}$$

where J is the moment of inertia of the PMSM and T_l is the load torque. The PMSMs in the MEA normally are driven by a three-phase voltage source inverter applying sinusoidal Pulse Width Modulation (PWM) technique [7].

Implementation with Modelica

The Modelica EMA model addresses all important components in an electric actuator unit such as the PMSM, an input filter, power inverters with dead-time, protections for over/under voltage, a precharge and a motor control unit. Friction in the bearings also considered. The behavioral EMA model deals with three phases currents/voltages in the PMSM as well as in the power inverter. The functional PMSM model has been derived by replacing power inverters by continuous transfer functions and transforming 3-phase values into RMS values. The Modelica model of the EMA unit is depicted in Fig. 2.9. In the behavioral modeling level, the control unit in Fig. 2.10 for speed and current control has to address the park transformation

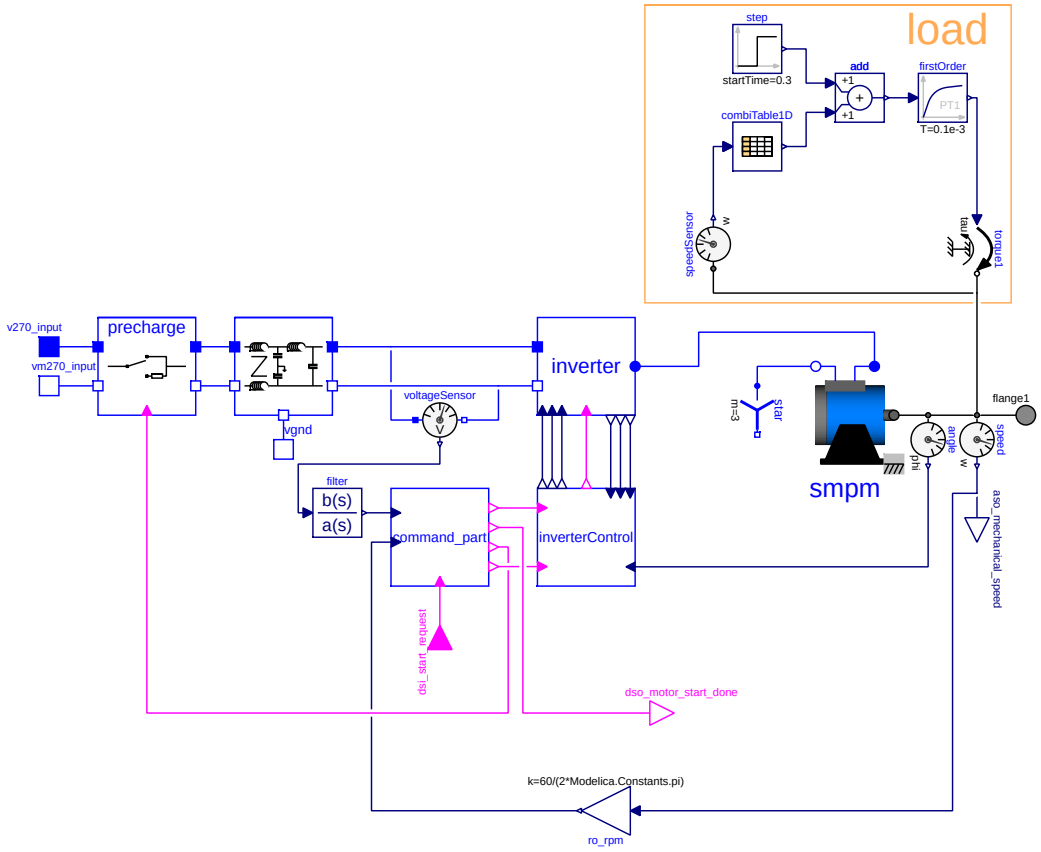

Figure 2.9.: The Modelica model of an EMA

to transform three phases currents/voltages into dq reference. Fig. 2.11 shows the power inverter for DC-AC transformation by applying sinusoidal PWM techniques. The simulation results for inrush current tests when powering up the EMA are depicted in Fig. 2.12 and Fig. 2.13 at both behavioral level and functional level. In the test, both behavioral and functional EMA models are powered at 0.01 second. In order to limit input inrush currents due to charging the DC capacitor in input filter (see simulation results), the inverters in PMSMs have been activated after 0.1 second precharging time. In the precharging time, large value resistors are connected to the DC power network. The input currents in the inrush current test of the behavioral and the functional PMSM mdoels with 230V input voltage are depicted in Fig. 2.12 and the DC input voltages before the power inverter of the behavioral and functional PMSM models are depicted in Fig. 2.13. The voltage sag effects of the input voltages are also seen in the simulation results, when the inverter are activated.

2.3.4. Modeling of 3 phase Auto-Transformer Units

The use of HVDC power transmission e.g. 540V DC network gives some advances, such as reduction in the size of current carrying conductors therefore minimizing

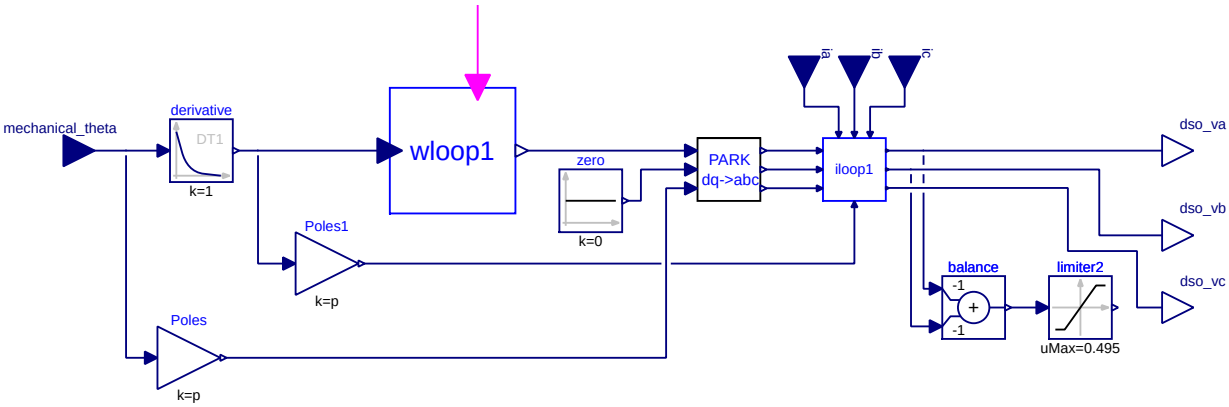

Figure 2.10.: The control unit of the PMSM in Fig. 2.9

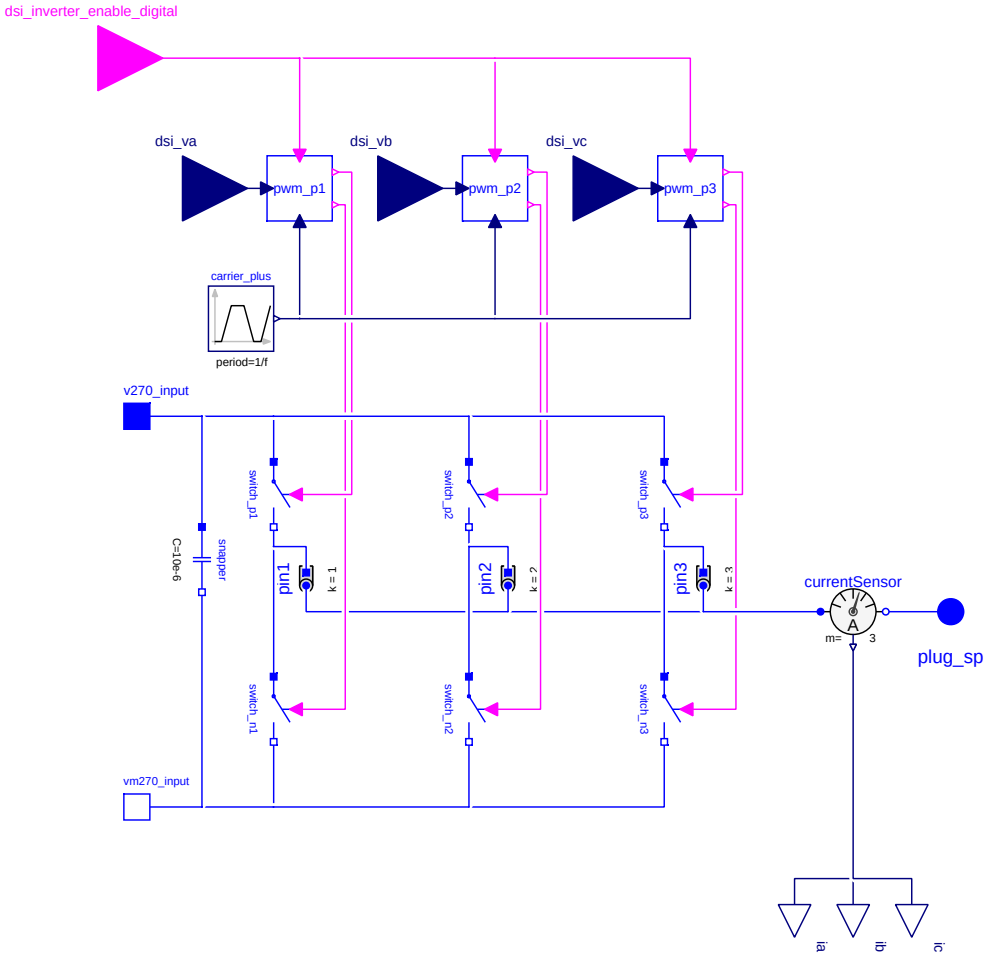

Figure 2.11.: The power inverter of the PMSM in Fig. 2.9

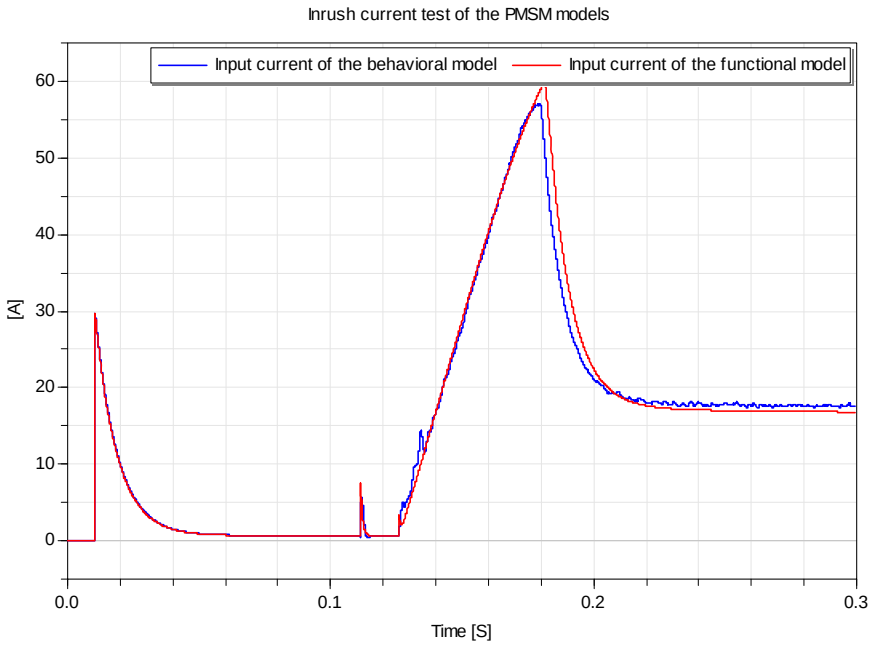

Figure 2.12.: Simulation results of input currents in the inrush current test of the behavioral and functional PMSM models with 230V input voltage

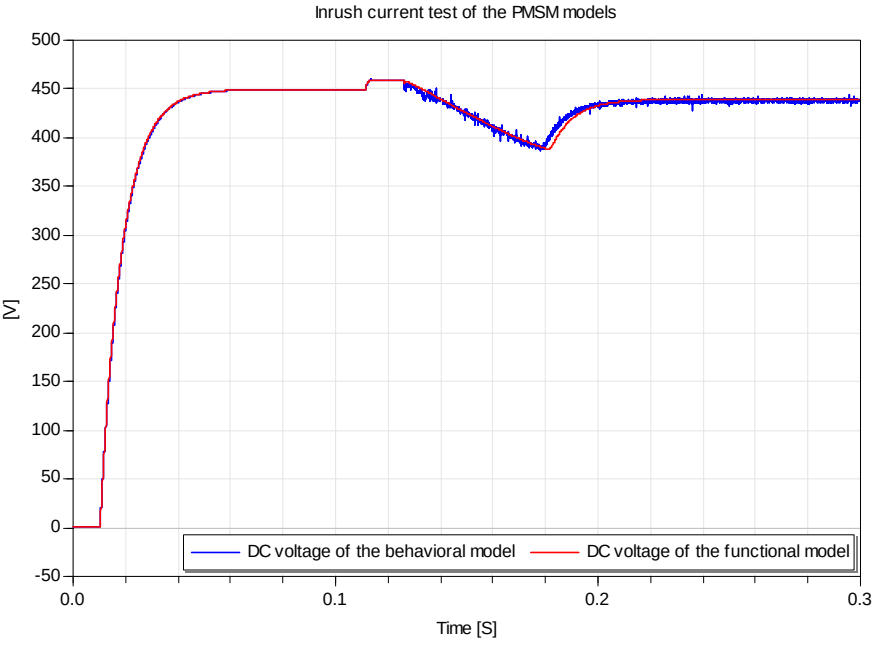

Figure 2.13.: Simulation results of DC input voltages in the inrush current test of the behavioral and functional PMSM models with 230V input voltage

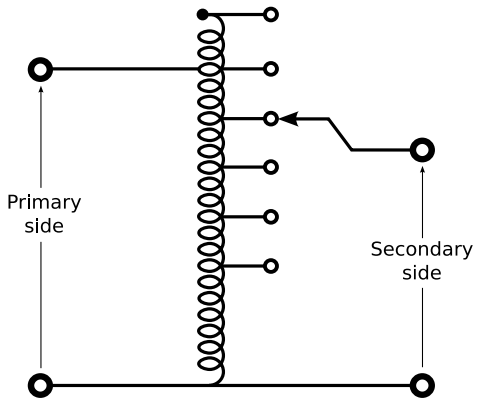

Figure 2.14.: The schematic diagram of a auto-transformer

weight and power dissipation. However , a number of aircraft services still require 115V AC supplies. A three phase Auto-Transformer Unit (ATU) transforms the output voltage of the VFG into 115V AC which supplying AC loads e.g. some constant power loads.

Mathematical description of the ATU

While an ordinary transformer typically has separate primary and secondary windings with turns $N1$ and $N2$, which are not connected, an auto-transformer is an electrical transformer with only one winding for one phase. Comparing with the ordinary transformer, the auto-transformer has the advantages of often being smaller, lighter and cheaper but the disadvantage of losing the electrical isolation between the primary and secondary power units. The ideal auto-transformer can be described by Eq. 2.29, where V_{in}, V_{out}, a are the primary, secondary voltage and turn ratio.

$$\frac{V_{in}}{V_{out}} = \frac{N_1}{N_2} = a \tag{2.29}$$

When the magnetic hysteresis effect is being considered, the inrush current often arises when powering up the ATU. A steel core's remanence means that it retains a static magnetic field when power is removed. When power is then reapplied, the residual field will cause a high inrush current until the effect of the remaining magnetism is reduced, usually after a few cycles of the applied AC waveform. Overcurrent protection devices such as fuses must be selected to allow this harmless inrush to pass. In the power network of the MEA, Inrush current related issues such as over-current in AC transformers and sympathetic effects among several AC transformers have to be thoroughly modeled and analyzed.

Implementation with Modelica

The three phase ATU with input 230V AC voltage and output 115V AC voltage is modeled with the Modelica Magnetic library [119]. The geometry parameters of

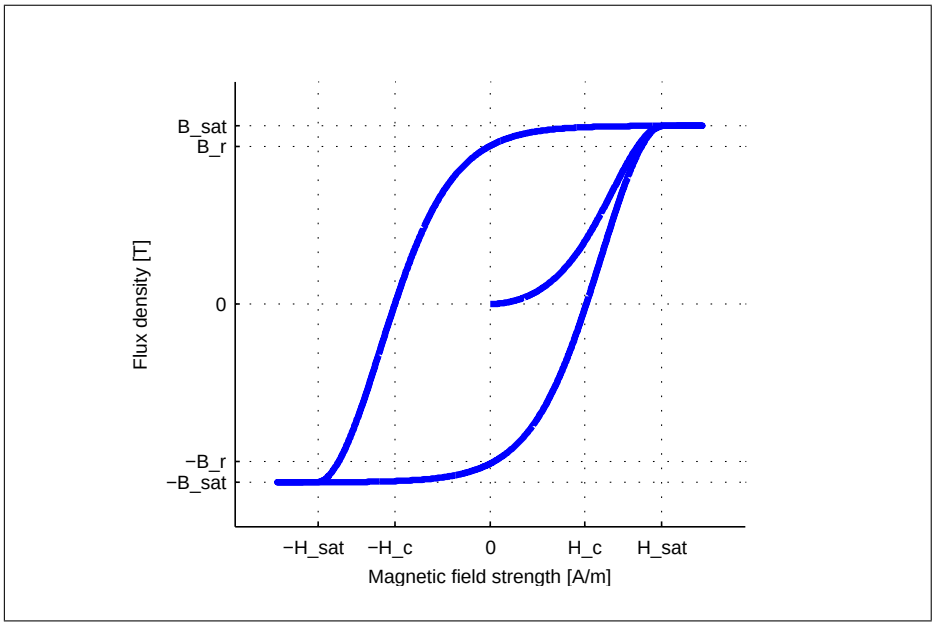

Figure 2.15.: Simulated hysteresis for flux density B vs. magnetic field strength H

magnetic circuit, such as area and length of magnetic core as well as the characteristics of magnetic hysteresis loop e.g. coercive field and permanent magnetic field, can be conveniently set by users. For efficient modeling of magnetic circuits, the free Modelica.Magnetics.FluxTubes library [16] is used. Material properties can be taken into account by linear and nonlinear permeability. For the study of inrush currents, the so called "Tellinen hysteresis model" showed to model the flux density B versus the magnetic field strength H in relationship of a measured ferromagnetic material well via moderate complex equations and by efficient simulation. Details and comparisons about the first release of the magnetic hysteresis models for Modelica were published in [119]. The so called static hysteresis links the flux density B in relation to the magnetic field strengths H for a ferromagnetic material where

$$B = \mu_r \cdot H \tag{2.30}$$

The saturation curve with its typical shape is depicted in Fig. 2.15. The most basic shape parameters are B_r and H_c. B_r is the remanence which means the magnetization left from a saturation at no external magnetic field strength. H_c is the coercitivity which means the intensity of the applied magnetic field strength required to compensate a B_r which was generated by saturation to zero flux density. The shape of minor loops in the BH area which do not drive the material into saturation, differs for the hysteresis models and maybe adjusted for the more advanced ones. A generalization in this area often is acceptable, since there is little measurement data of material available. The hysteresis models differ in the number and type of input variables, internal states or history data used to calculate the nonlinear permeability μ_r. This is not only of supreme importance for the simulation but also for the initialization, where a consistent initial condition must be found for an equation

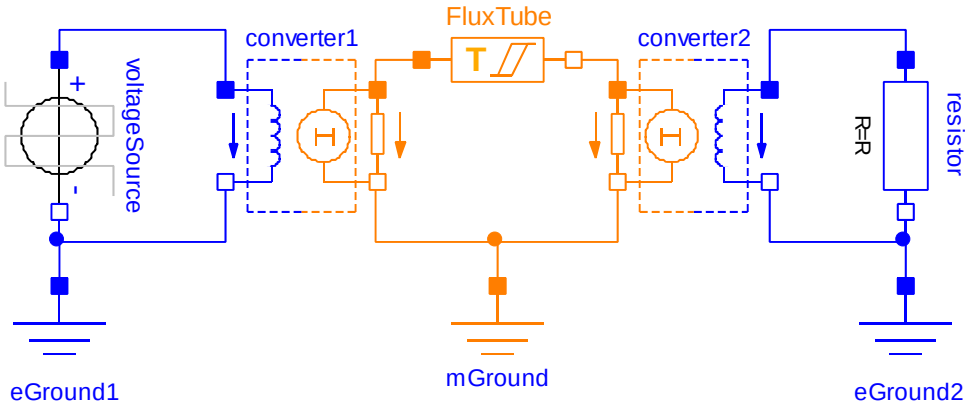

Figure 2.16.: Test model of an electromagnetic circuit

system which may contain several of these hysteresis elements. The Tellinen model is very efficient in this sense. All information to determine the actual value of μ_r is based on the recent value of H and the sign of the derivative of H where

$$\mu_r = \begin{cases} \mu_r^-(H) & \text{for } \dot{H} < 0 \\ \mu_r^+(H) & \text{for } \dot{H} > 0 \end{cases} \tag{2.31}$$

without the use of history data. In case the equations must be inverted to calculate H from B, it is advantageous to guarantee a monotonically increasing of $B(H)$. Since for saturation μ_r often is set to zero by a hysteresis equation, it is advantageous to add an additional linear term

$$B = \mu_r(H, sign(\dot{H})) \cdot H + \mu_0 \cdot H \tag{2.32}$$

A small demonstration system depicted in Fig. 2.16 is used to present the hysteresis modeling. It is a graphical view of a Modelica model of a transformer, consisting of an circuit with electric and magnetic parts. It was constructed by the use of the modeling and simulation environment Dymola. Blue parts are part of the electrical model (voltage source, resistor) while the magnetic circuit is colored orange (flux tube) They are linked by electromagnetic converters. The magnetic model's equations are similar to a resistive electrical network where magnetic potential difference V_m is equivalent to electrical voltage and magnetic flux Φ is equivalent to electrical current. In the model there is an ideal circular coupling of the fluxes without leakage paths. At the converters, the electric and magnetic part is linked by Ampere's law

$$V_{mx} = i_x \cdot N_x \tag{2.33}$$

and Faraday's law

$$N_x \cdot \dot{\Phi}_x = -v_x \tag{2.34}$$

where x denotes the variables of converter 1 or 2. The FluxTube object embeds the equations for the material including the hysteresis. Internally B and H are deduced

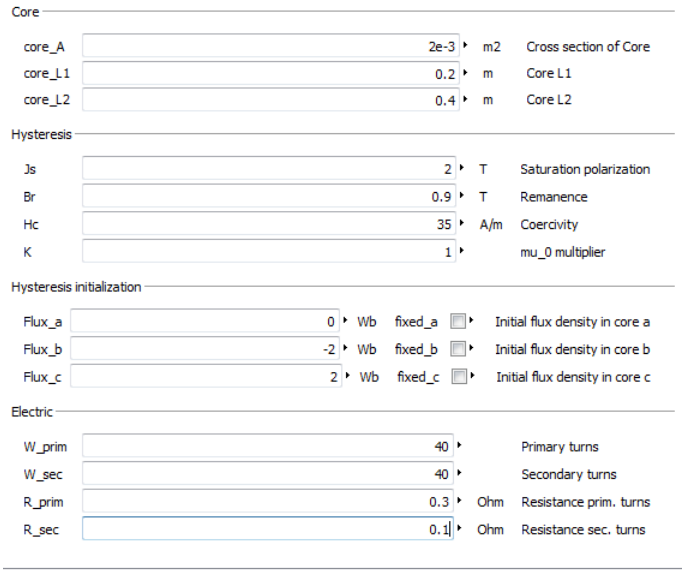

Figure 2.17.: The parameter menu of ATU model

from Φ respectively V_m by geometric properties area and lengths of the magnetic "tube". So for the material equation 2.32 we write

$$\Phi = \mu_r(V_m, sign(\dot{V}_m) \cdot V_m + \mu_0 \cdot V_m \tag{2.35}$$

Finally, the set of equations for the magnetic part consists of the (double) equations 2.33 and 2.34, 2.35 and Kirchhoff's equations

$$\Phi_1 = -\Phi_2 = -\Phi_{FT} \tag{2.36}$$

and

$$V_{m1} = V_{FT} + V_{m2} \tag{2.37}$$

Using the magnetic hysteresis model, the Modelica model of the 3-phase ATU with input 230V AC voltage and output 115V AC voltage (in Fig. 2.18) is built in Dymola. The geometry of magnetic circuit such as area and length of magnetic core as well as the magnetic hysteresis loop, e.g. coercive field and remanent magnetic field are defined in the FluxTube block as parameters, which can be conveniently set. The leakage magnetic paths in the magnetic core and air behave linearly with fixed permeability. This can be modeled with linear magnetic flux tube elements. In terms of setup for an ATU model, Fig. 2.17 shows all possible parameters and the hysteresis initialization. The ability to initialize magnetic flux in the ATU for simulation is crucial for inrush current studies. The Modelica model of the ATU has been tested by an inrush test simulation for the behavioral level, which is depicted in Fig. 2.19. In this inrush test, the behavioral ATU model without no load have been connected to the AC power at 0.01 second, where the flux density in core a, b and c are initialized by 0Wb, $1e-3$Wb and 0Wb. The simulation results of the inrush current test are shown in Fig. 2.20, where a remarkable input current for phase B arises. Since the

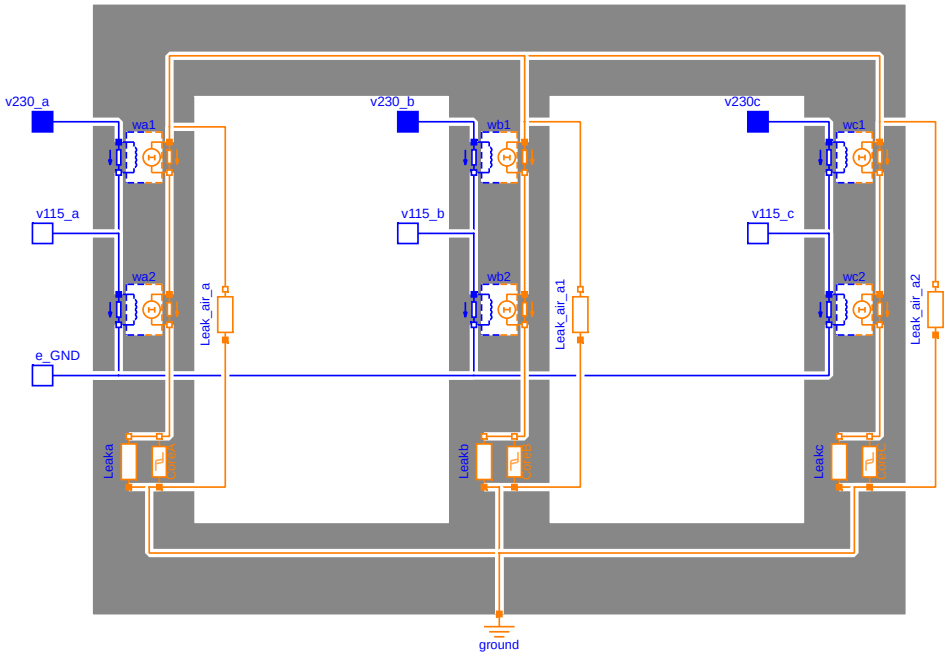

Figure 2.18.: The behavioral model of ATU

input currents for phase A and phase C are identical, the blue curve of input current phase A is hidden by the green curve in Fig. 2.20. The functional ATU model calculated with RMS values has been tested by the power dis-connection test, in which the functional ATU model is connected with a 100kw load at 0.01 second and dis-connected again at 0.05 second. Simulation results of secondary output currents and voltages are depicted in Fig. 2.21, where the BitStream1.y curve presents the signal to control the connection of the ATU to voltage source. In this simulation, the RMS values of three output currents and voltages are toltoally identical.

2.3.5. Modeling of 18-pulses ATRU

When using the VFG for the power generation in MEA, the AC-DC conversion is used to generate the DC bus, which supplies power to both DC-DC and DC-AC secondary converters. Under various types of AC-DC conversion candidates such as the PWM active front ends converter and multi-pulse diode based converters, the 18-pulse autotransformer rectifier unit seems to be a suitable choice for the MEA, in order to comply with the stringent requirements on the power quality to both AC and DC loads for military and civil aircrafts [87].

Description of the ATRU

The circuit of the ATRU depicted in Fig. 2.22 can be built with the US patent [89]. When the autotransformer is supplied by a set of three phase AC voltages, a set of nine phase voltages is produced on the output side with a 40 degree phase

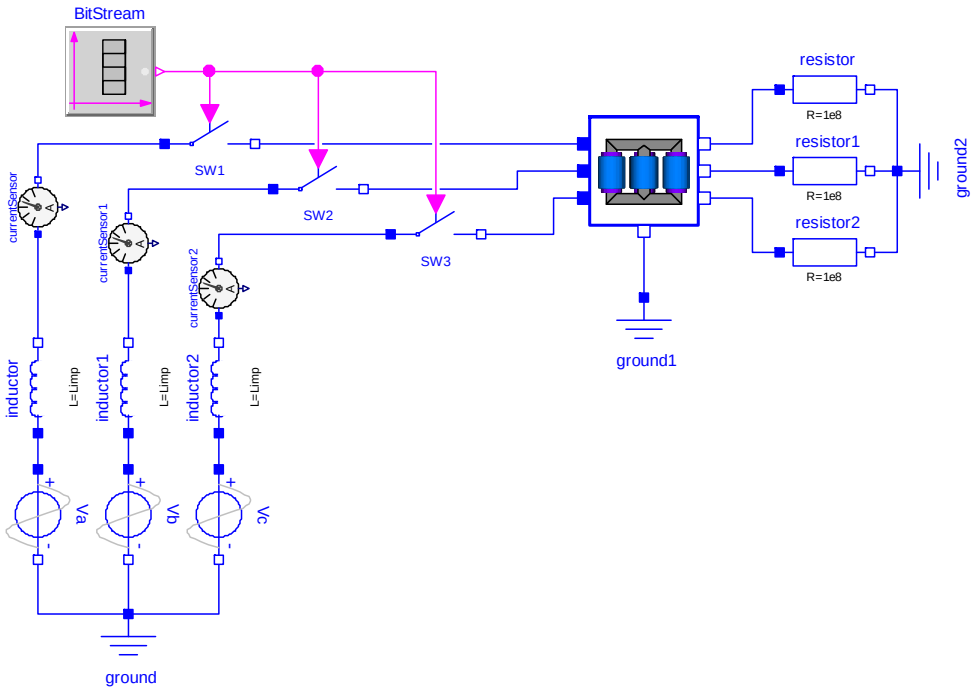

Figure 2.19.: The inrush test setup of the behavioral ATU model

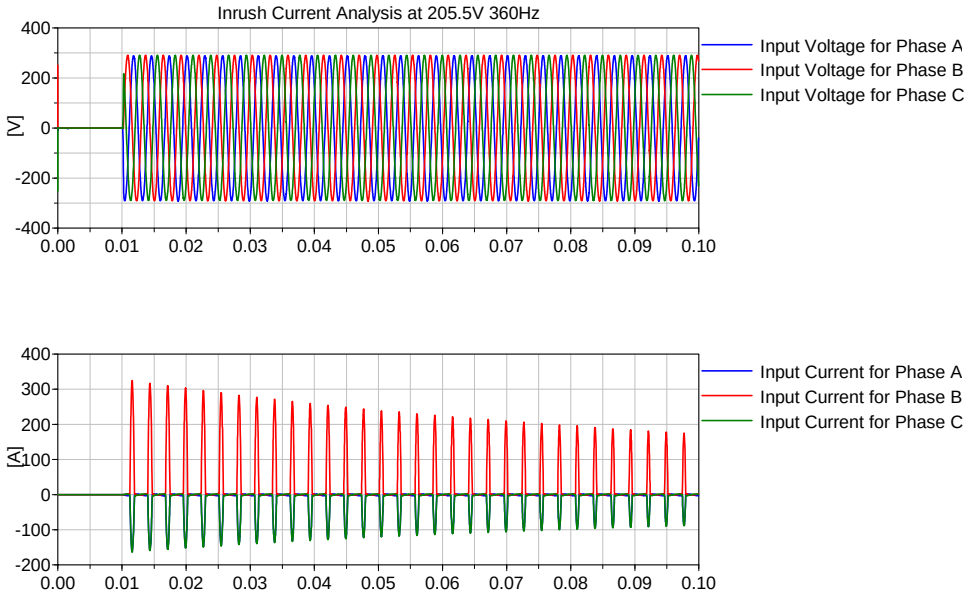

Figure 2.20.: Simulation results of input currents and voltages in inrush current test of the behavioral ATU model (time unit is [s])

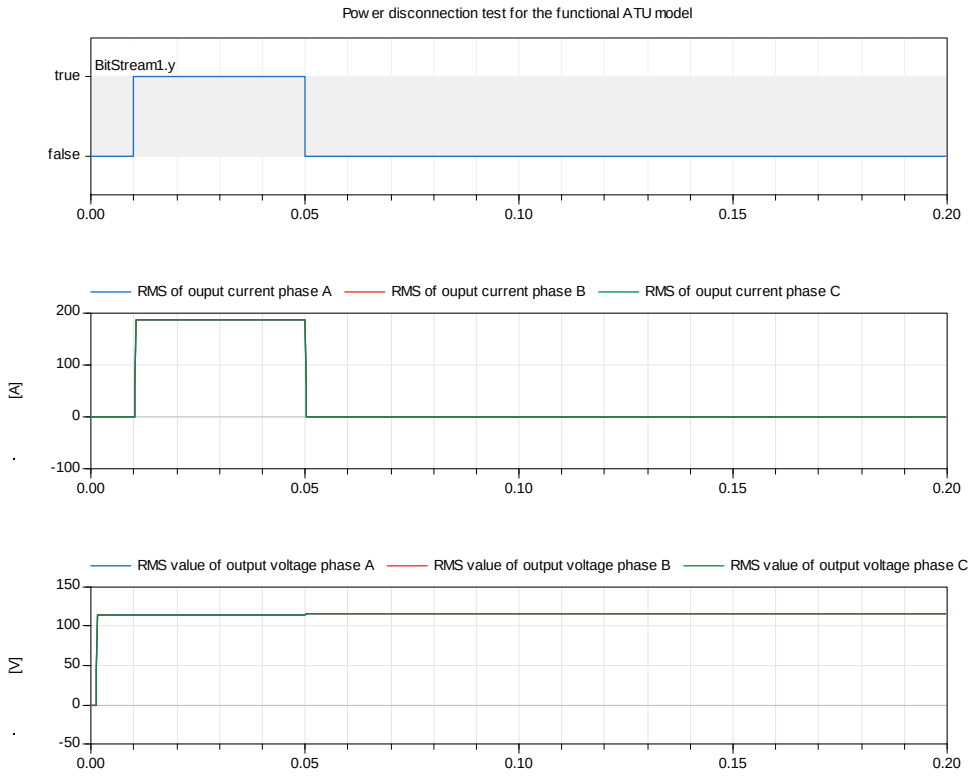

Figure 2.21.: Simulation results of output currents and voltages in power disconnection test of the functional ATU model (time unit is [s])

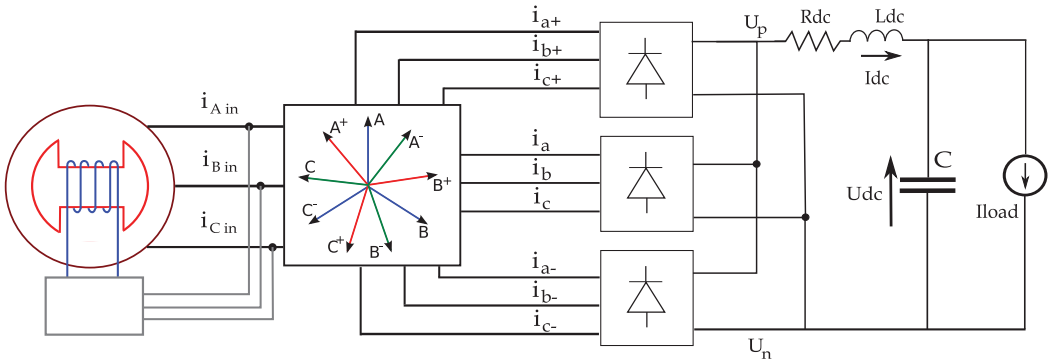

Figure 2.22.: The schematic diagram of an 18 pulses ATRU

angle. The nine phase output voltages can be considered as three sets of three phase output voltages. The 9 phase set of voltages feed three six-pulse rectifier bridges that are connected in parallel at the output side and the resultant DC voltage is finally used to power the load. To do this, the transformer turn ratios between primary turns and the long and short secondary turns have to be set properly. Additionally, when modeling the high power 18-pulse ATRU model at the behavioral level, the inrush current effect at switching-on has to be included by considering the magnetic hysteresis effect. By applying the state-space averaging approach in [37], the functional model of the ATRU can be derived.

Implementation with Modelica

Using the diode model in the Modelica standard library, the topological model of 6/18-pulse bridge rectifier (RU) can be made very easily. Detailed parameters in diodes such as forward state-on resistance and forward threshold voltage can be freely tuned to best match the real performance of physical components. The geometrical and physical parameters about the magnetic core can be defined by the users in the same manner as the ATU model. The Modelica model of the ATRU at the behavioral level is depicted in Fig. 2.23 and the 18-pulses autotransformer including magnetic hysteresis effect is modeled in Fig. 2.24. The nine phase output voltages of the autotransformer can be seen in the simulation results for a power-up test of the ATRU in Fig. 2.25, where the three phase input currents and DC output voltage are also demonstrated. In this test, the behavioral ATRU model is turned on at 0.01 second and after a 0.1 second precharging process, the DC load is connected to the ATRU. The simulation results of the functional model for the same test are presented in Fig. 2.26, where the RMS values of the 3 phase input currents/voltages and DC output currents are plotted.

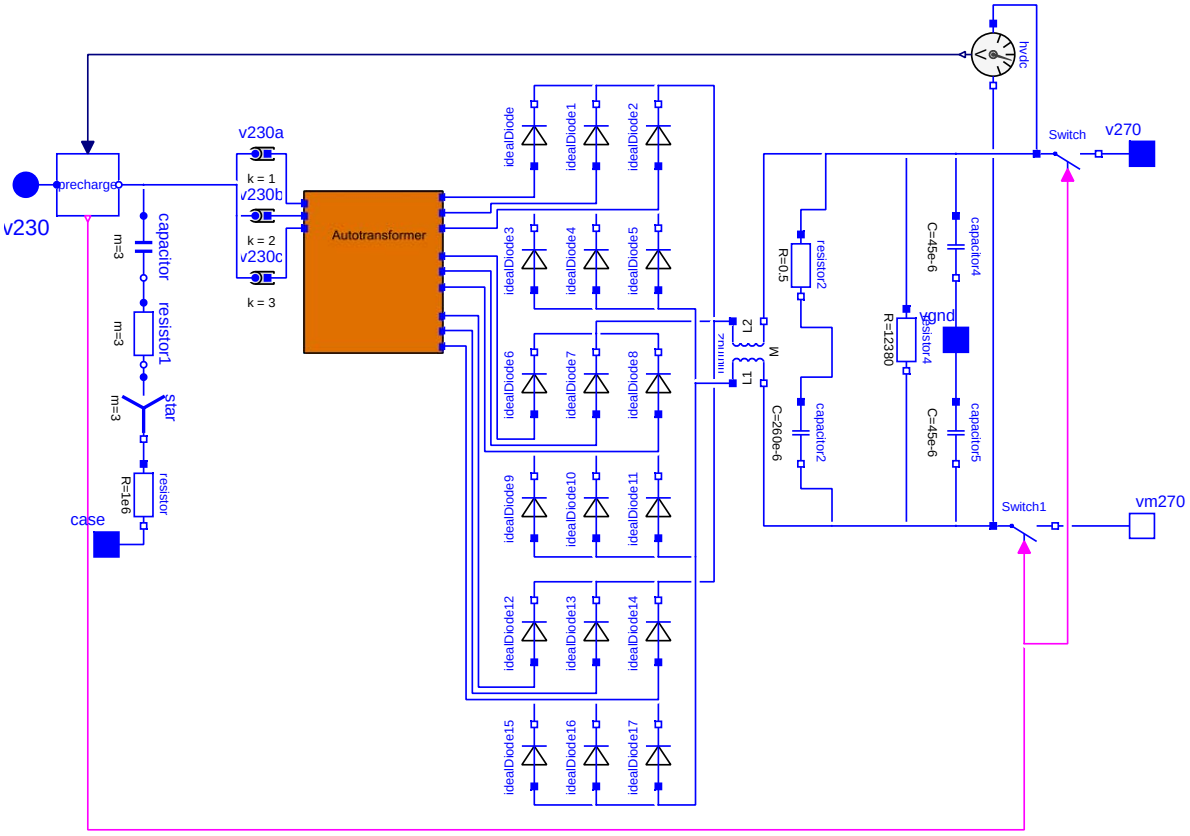

Figure 2.23.: A Modelica behavioral model of an ATRU

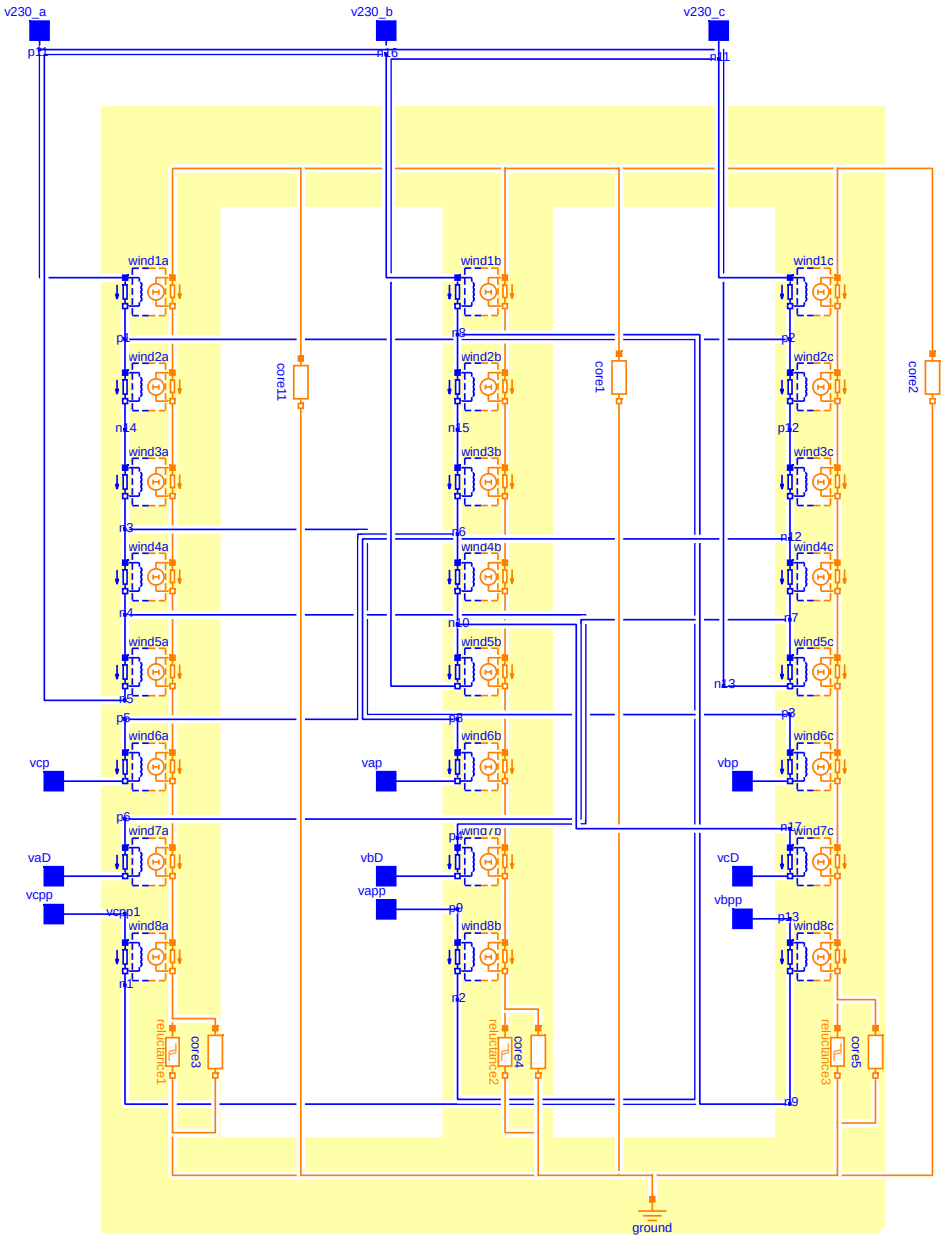

Figure 2.24.: The Modelica behavioral model of an 18 pulses auto-transformer

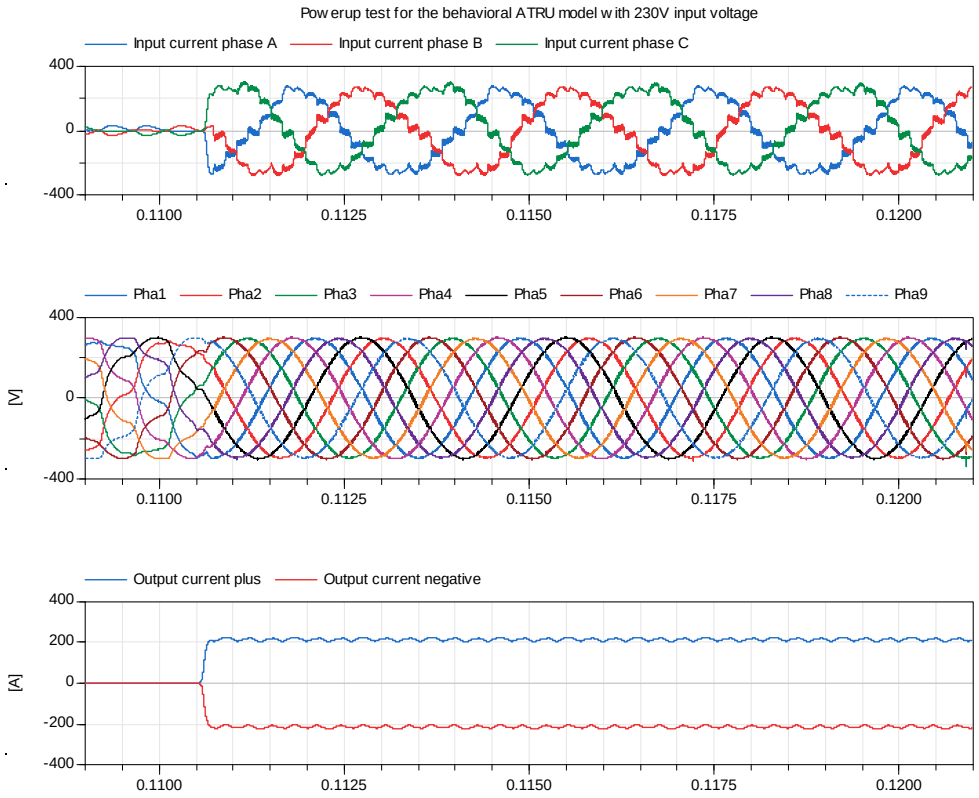

Figure 2.25.: Simulation results of input currents, voltages and output currents in power-up current test of the behavioral ATRU model with 230V input voltage (time unit is [s])

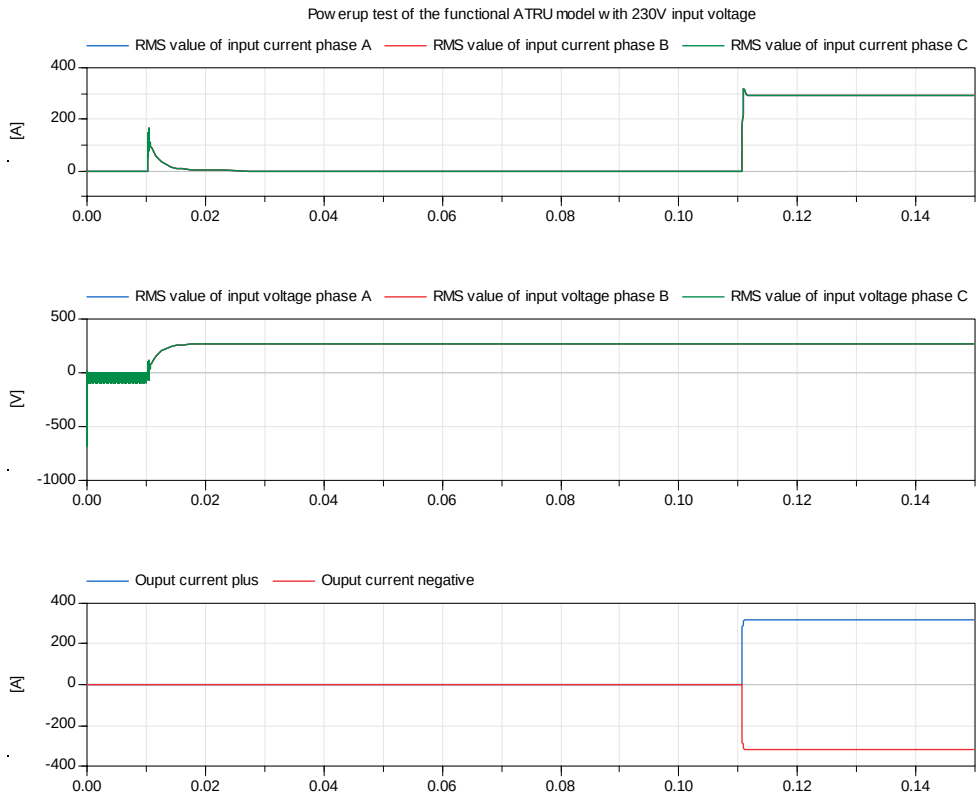

Figure 2.26.: Simulation results of input currents, voltages and output currents in power-up test of the functional ATRU model with 230V input voltage (time unit is [s])

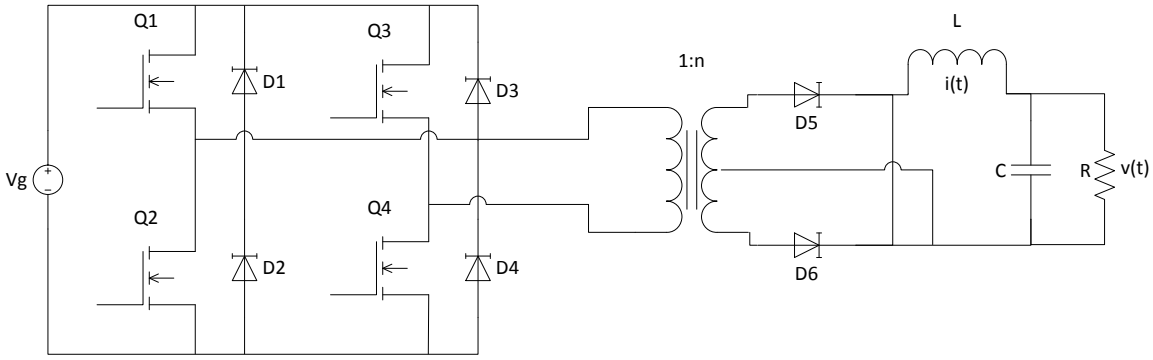

Figure 2.27.: The schematic diagram of a full-bridge transformer isolated DCCU

2.3.6. Modeling of DC/DC buck converters

The main advantages of the proposed HVDC power bus in the MEA are reduced feeder numbers and the possibility to minimize the size of the input stage in the electro-mechanical conversion process. The DC/DC buck converter is needed to convert the 540V DC bus voltage into various low voltages such as 28V for supplying some electrical loads like lighting systems.

Description of the DC/DC buck converter

The circuit diagram of a full-bridge transformer isolated buck converter is sketched in Fig. 2.27. Defining the D_{buck} as the duty cycle of the time period T_{sbuck} for the buck converter, the transformer primary voltage $v_T = V_g$, the output current $i(t) = I_{Q5}$ (diode Q_5 is on), if the transistors Q_1 and Q_4 are switched on and the transistors Q_2 and Q_3 are off within the time $D_{buck}T_{sbuck}$. Let the transistors Q_2 and Q_3 be conducting and the transistors Q_1 and Q_4 be off within the time $D_{buck}T_{sbuck}$, the output current of the buck converter $i(t) = I_{Q6}$ (diode Q_6 is on) and $v_T = V_g$. During the sub-interval $(1 - D_{buck})T_{sbuck}$, all transistors $Q_1 - Q_4$ are switched off, and $i_{D5} = i_{D6} = 0.5i(t)$. The output voltage of the buck converter $v = nD_{buck}V_g$, where n is the transformer turn ratio in the buck converter. The output voltage of the buck converter can be adjusted by the duty cycle typically with a PI control loop.

Implementation with Modelica

The full bridge isolated DCCU contains a full bridge inverter, magnetic transformer, input filter and phase-shifted control. The DCCU typically supplies 28V DC low voltage loads in the electric power network. The scheme of the modeled DC/DC buck converter is depicted in Fig. 2.27. Modeling and simulation of DC/DC converter units is a challenging job, since this component inherently works with very high frequency PWM modulation. This high frequency switching operation could lead to a great amount of event actions which will significantly slow down or break

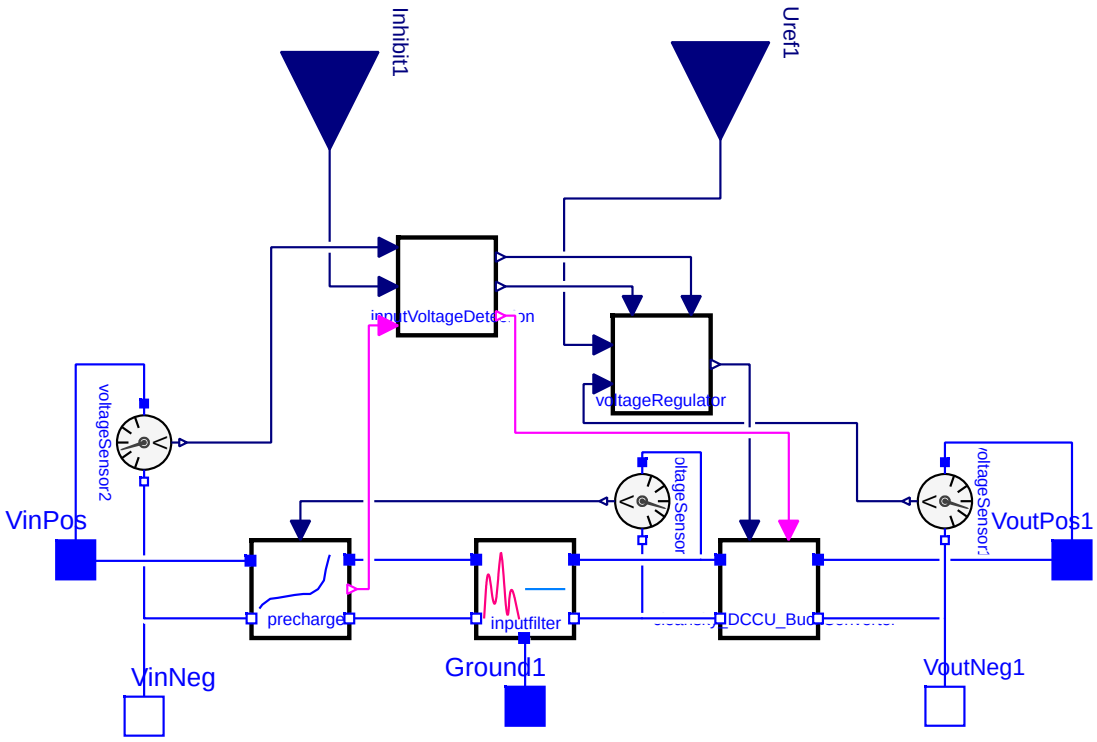

Figure 2.28.: The behavioral model of the DCCU

the simulation process. The synchronous feature [88] provided by Modelica can efficiently solve this issue by transferring the state events into time events. The behavioral model of the buck converter including voltage control unit, precharge unit and DC/DC converter is depicted in Fig. 2.28. Inside of the behavioral model, the transformer and power switches with defined dead time to prevent shoot-through current are modeled and shown in Fig. 2.29. The classical averaging technique has been utilized to implement the functional DC/DC buck converter. The simulation results of the power-up test for the behavioral model are depicted in Fig. 2.30, where the output voltage and input currents in the buck converter are plotted. In this test, the behavioral DCCU model is connected to a 540V DC voltage source at 0.01 second. A 40kw DC load is connected to the DCCU after a precharging process with 0.1 second. The same test for the functional buck converter model has no switching effect any more, and the averaged output voltage and input currents can be seen in Fig. 2.31.

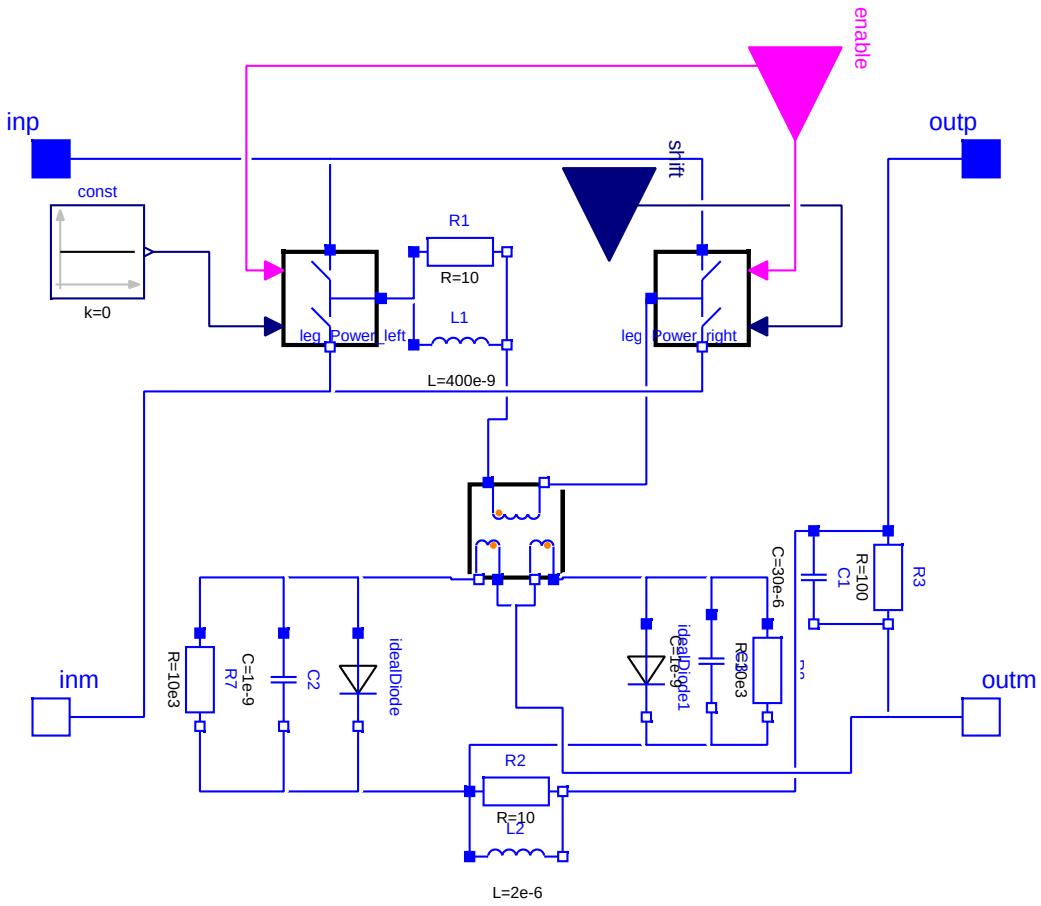

Figure 2.29.: The Modelica buck converter model within the behavioral DCCU model in Fig. 2.28

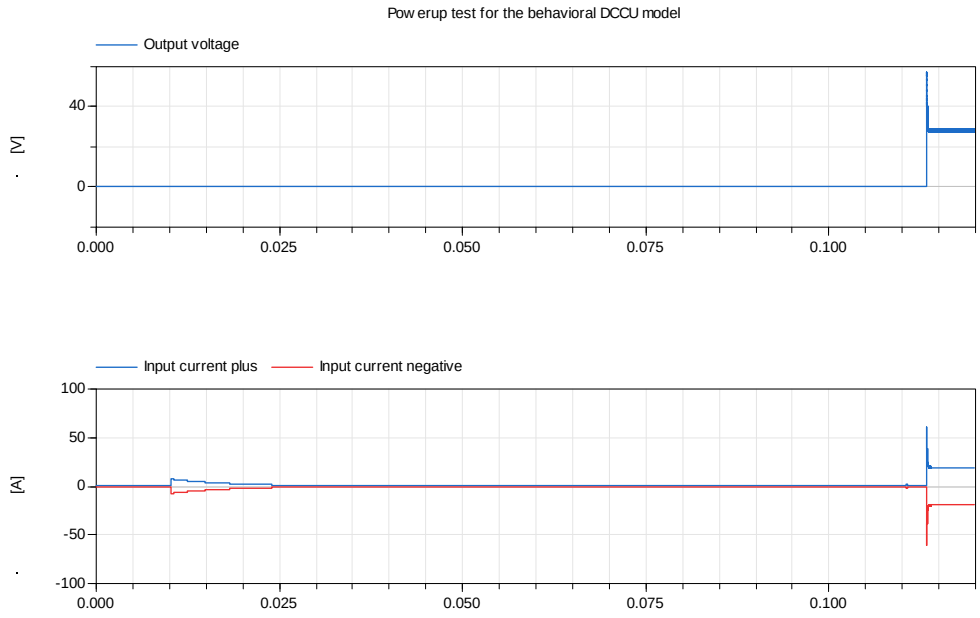

Figure 2.30.: Simulation results of output currents and voltage in power-up test of the behavioral buck converter model (time unit is [s]

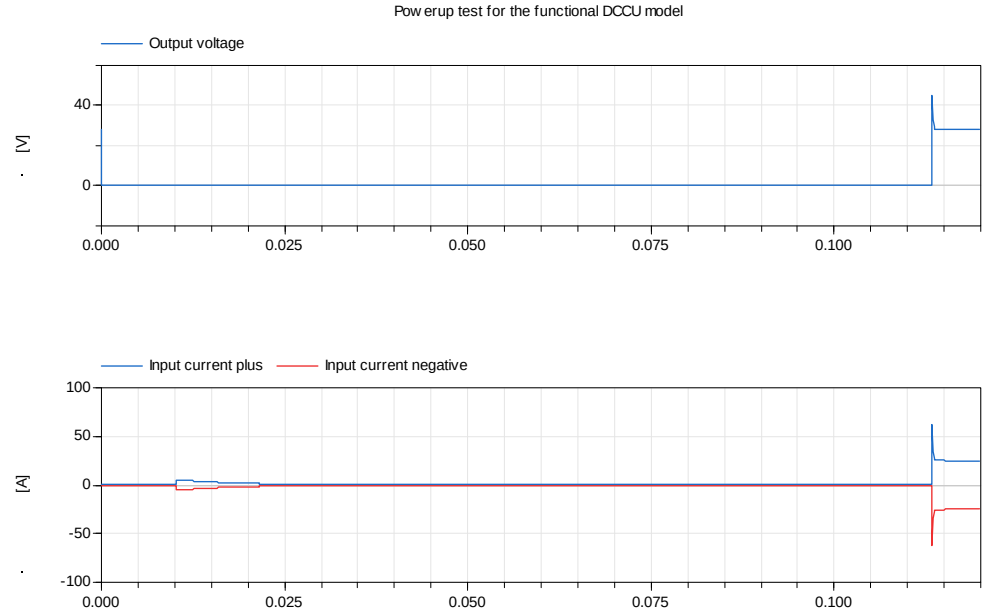

Figure 2.31.: Simulation results of output currents and voltage in power-up test of the functional buck converter model (time unit is [s])

3. Stability studies for electrical networks

As previously mentioned, the electric network in the MEA tends to be unstable, because the system load can change swiftly and without warning due to a large range of duty cycles and unpredictable spikes. Therefore, the stability issue has to be thoroughly examined. Power system stability may be broadly defined as property of a power system that enables it to remain in a state of operating equilibrium under normal operating conditions and regain an acceptable state of equilibrium after being subjected to a disturbance [68]. Instability in the electrical network of the MEA may be manifested in several different ways depending on the system configuration and operation mode. Traditionally, the stability has been one of maintaining synchronous operation. Since many power systems rely on synchronous machines for generations of electrical power, a necessary condition for satisfactory system operation is that all synchronous machines remain in synchronicity. This aspect of stability is influenced by the dynamics of generator rotor angles and power angle relationships. Voltage stability is the stability of a power system to maintain steady acceptable voltages at all buses in the system under normal operating conditions and after being subjected to disturbances. A system enters a state of voltage instability when a disturbance, increase in load demand, or change in system condition caused a progressive and uncontrollable drop in voltage. The main factor causing instability is the inability of the power system to meet the demand for reactive power. The heart of the problem is usually the voltage drop that occurs when active power and reactive power flow through inductive reactance, which is associated with the transmission network.

While the MEA architecture will demonstrate significant weight gains, reduced maintenance requirements, increased reliability and passenger comfort, the electric network tends to instability because the system load can change swiftly and without warning due to a large range of duty cycles and unpredictable spikes [76], especially for modern power optimized architectures using large HVDC networks. Therefore, it is necessary to investigate the stability of the whole electric network both at the small signal level for steady state conditions and at the large signal level for transients, impacts and network reconfiguration. The applied methods must be capable of handling systems becoming more and more complex for future airplanes. One key problem is to investigate when and how the electric on-board system could become unstable.

3.1. Introduction to buck converters

It is already recognized that the regulated DC/DC converter, e.g. the buck converter, is one of the most critical components in on-board electric networks [14]. Switching-mode regulators have a negative input resistance at low frequencies and may become unstable by adding an input filter [83]. An electric-mechanical actuator in the MEA has similar stability issues once it behaves as a constant power load [74]. The topological block diagram for the buck converter to be studied is depicted in Fig. 3.1. By applying the average modeling technique in [77], a time continuous model can be derived. All nominal parameters except the controller of the buck converter model are taken from [14]. The parameters including the PI controller parameter are given in Tab. 3.1. The differential equations of the buck converter become

$$\begin{aligned}
\frac{d}{dt}i_{Lf} &= \frac{1}{L_F}(E - R_f \cdot i_{Lf} - V_c) \\
\frac{d}{dt}V_{Cf} &= \frac{1}{C_f}(i_{Lf} - \alpha \cdot i_L) \\
\frac{d}{dt}i_L &= \frac{1}{L_h}(\alpha \cdot V_{Cf} - V_c) \\
\frac{d}{dt}V_C &= \frac{1}{C}(i_L - \frac{V_c}{R}) \\
\frac{d}{dt}\alpha &= -\frac{K_p}{C}(i_L - \frac{V_c}{R}) + K_i(V_{ref} - V_c)
\end{aligned} \tag{3.1}$$

$X = (x_1,\ x_2,\ x_3,\ x_4,\ x_5) = (i_{Lf},\ V_{Cf},\ i_L,\ V_C,\ \alpha)$ represent the five states of the buck converter system where α is the duty cycle. u includes all system inputs. The linear state space system

$$\begin{aligned}
\Delta\dot{X} &= A\Delta X + B\Delta u \\
\Delta Y &= C\Delta X + D\Delta u
\end{aligned} \tag{3.2}$$

of the buck converter is obtained by symbolic linearization for all equilibrium points

$$\begin{bmatrix} x_{1,eq} \\ x_{2,eq} \\ x_{3,eq} \\ x_{4,eq} \\ x_{5,eq} \end{bmatrix} = \begin{bmatrix} \frac{350-\sqrt{350^2-\frac{4\cdot 28^2}{R}\cdot R_f}}{2R_f} A \\ \frac{28^2}{R}\cdot\frac{1}{x_{1,eq}} V \\ \frac{28}{R} A \\ 28V \\ \frac{28}{x_{2,eq}} \end{bmatrix} \tag{3.3}$$

The resulting state space matrices in Eq. 3.2 are

$$A = \begin{bmatrix} -\frac{R_f}{L_f} & -\frac{1}{L_f} & 0 & 0 & 0 \\ \frac{1}{C_f} & 0 & -\frac{x_{5,eq}}{C_f} & 0 & -\frac{x_{3.eq}}{C_f} \\ 0 & \frac{x_{5,eq}}{L} & 0 & \frac{1}{-L} & \frac{x_{2,eq}}{L} \\ 0 & 0 & \frac{1}{C} & -\frac{1}{RC} & 0 \\ 0 & 0 & -\frac{K_p}{C} & \frac{K_p}{RC} - K_i & 0 \end{bmatrix} \tag{3.4}$$

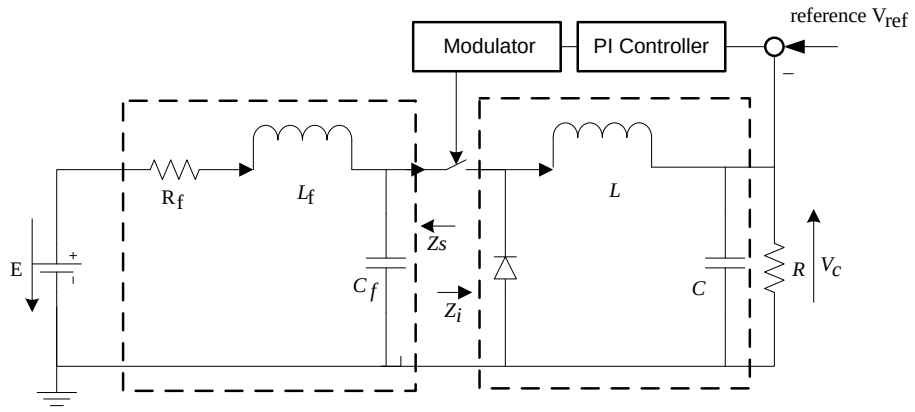

Figure 3.1.: The schematic block diagram of a buck converter with PWM controller

Parameter	Value	Unit
voltage source E	350	Volt
reference output voltage V_{ref}	28	Volt
output power P	5000	Watt
output resistance R	0.1568	Ohm
inductance L	290e-6	Henry
capacitance C	399e-6	Farad
resistance of input filter R_f	250e-3	Ohm
inductance of input filter L_f	100e-6	Henry
capacitance of input filter C_f	100e-6	Farad
gain of I controller K_i	5	-
gain of P controller K_p	0.05	-

Table 3.1.: The nominal parameters of the examined buck converter

$B = [\frac{1}{L_f}\ 0; 0\ 0; 0\ 0; 0\ 0; 0\ K_i]$, $C = [0\,0\,0\,1\,0]$, $D = [0\,0]$.

3.2. Small signal based methods

Due to the inherent character of the DC distribution system, various methods for the investigation of its stability exist. For a given operating point, most power systems can be simplified into a LTI presentation. Then, classical methods for stability analysis of linear systems can be applied. Some existing small signal based methods are Middlebrook criterion and Nyquist criterion, Modal analysis method as well as the recently applied robust μ analysis.

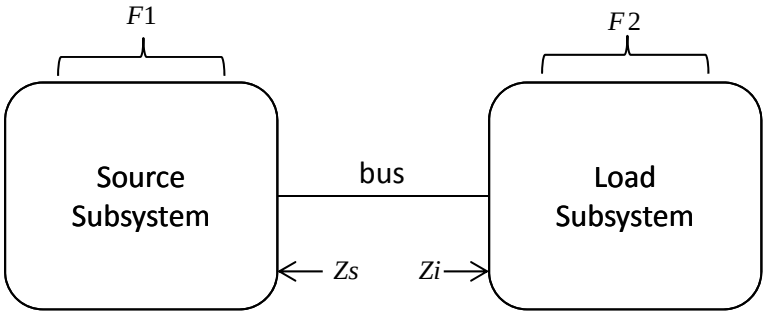

Figure 3.2.: The series connection of two stable subsystem

3.2.1. Impedance based approaches

The Middlebrook criterion is intended originally for investigating the stability of a power converter system including two subsystems. Let Z_s be the output impedance of the source subsystem and Z_i be the input impedance of the load subsystem, respectively (see Fig. 3.2). The system is stable if the amplitude of the output impedance Z_s is smaller than the amplitude of the input impedance Z_i within the studied frequency range. The Middlebrook criterion is a conventional method and has been applied for power system stability analysis for a very long time. Unfortunately, the analysis results by the Middlebrook approach often reveal a much larger stability margin as necessary [26]. For the buck converter in Fig. 3.1 the output impedance of the input filter is

$$Z_s = \frac{R_f + sL_f}{s^2 L_f C_f + sR_f C_f + 1}$$

The peak Z_{smax} (in Fig. 3.3) of the magnitude of the output impedance of the input filter is $L_f/C_f R_f$. The frequency ω_s at which the maximum output impedance Z_{smax} appears equals $1/\sqrt{L_f C_f}$. Varying an input filter for a given regulated buck converter, the system could become unstable in two ways:

- the peak Z_{smax} crosses over the input impedance of the buck converter Z_i due to the variations of R_f
- the frequency ω_s moves to the left, so that the peak Z_{smax} crosses over the input impedance Z_i (mainly L_f and C_f are responsible)

3.2.2. Modal analysis method

Another interesting small signal based stability analysis method is the so-called modal analysis, which was used in [14] and [38] for design and stability studies of MEA architectures. For the linearized form of Eq. 3.2, ϕ_i and ψ_i are the right and left eigenvectors and λ_i is the corresponding eigenvalue. The sensitivity of the eigenvalue to the element a_{kj} of the state matrix A in Eq. 3.4 can be calculated by

$$\frac{\partial \lambda_i}{\partial a_{kj}} = \Psi_{ik} \Phi_{ji} \tag{3.5}$$

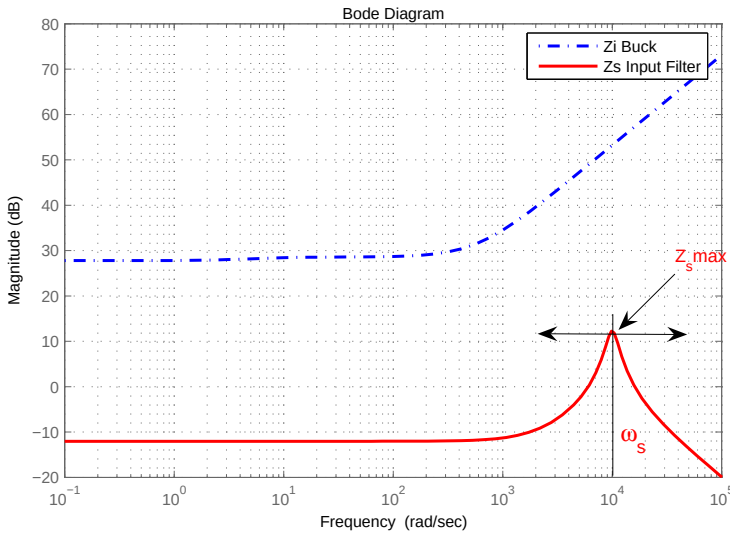

Figure 3.3.: Bode diagram of output impedance of source Zs and input impedance of load Zi

where $\Psi = [\ \psi_1^T \quad \psi_2^T \quad \cdots \quad \psi_n^T\ ]^T$ and $\Phi = [\ \phi_1 \quad \phi_2 \quad \cdots \quad \phi_n\ ]$. A matrix P is called the participation matrix, which uses right and left eigenvectors to get a measure of the association between the state variables and the modes. The element $p_{ki} = \phi_{ki}\psi_{ik}$ is defined as participation factor [113]. The participation factor can also be presented by the sensitivity of the eigenvalue λ_i to the diagonal element a_{kk} of the state matrix A

$$p_{ki} = \frac{\partial \lambda_i}{\partial a_{kk}} \tag{3.6}$$

The correlation between state variables and eigenvalues of a numerically linearized system can be found by calculating the participation factors, i.e. whether a state variable has influence on an eigenvalue. Applying the modal analysis to the buck converter at equilibrium points

$$[\ i_{Lf,eq} \quad V_{Cf,eq} \quad i_{L,eq} \quad V_{C,eq} \quad \alpha_{eq}\ ]^T = [\ 14.27A \quad 346V \quad 178.57A \quad 28V \quad 0.08\ ]^T$$

results in the following state matrix A:

$$A = \begin{bmatrix} -2.5e3 & -1e4 & 0 & 0 & 0 \\ 1e^4 & 0 & -8e3 & 0 & 1.78e6 \\ 0 & 275.86 & 0 & -3.4e3 & 1.2e6 \\ 0 & 0 & 2.5e3 & -1.6e4 & 0 \\ 0 & 0 & -150.4 & 954.13 & 0 \end{bmatrix} \tag{3.7}$$

	λ_1	λ_2	λ_3	λ_4	λ_5
i_{Lf}	0	0.5099	0.5099	0.0131	0.0131
V_{Cf}	0	0.4892	0.4892	0.0209	0.0209
i_L	0	0.0266	0.0266	0.6058	0.6058
V_C	0.9662	0.0248	0.0248	0.6814	0.6814
α	0.0406	0.0269	0.0269	0.5789	0.5789

Table 3.2.: The participation factor of the buck converter

The eigenvalues and eigenvectors of the state matrix A in Eq. 3.7 can be calculated as

$$\begin{bmatrix}\lambda_1\\ \lambda_2\\ \lambda_3\\ \lambda_4\\ \lambda_5\end{bmatrix} = \begin{bmatrix}-78.37\\ -1168.4+9703.7i\\ -1168.4-9703.7i\\ -8034.3+1137.5i\\ -8024.3-1137.5i\end{bmatrix} \tag{3.8}$$

and

$$\Phi = \begin{bmatrix}0.15 & -0.71 & -0.71 & 0.24+0.49i & 0.24-0.49i\\ -0.04 & 0.09+0.69i & 0.09-0.69i & 0.69 & 0.69\\ 0.98 & 0.01+0.02i & 0.01-0.02i & -0.36-0.27i & -0.36+0.27i\\ 0.15 & 0 & 0 & -0.07+0.02i & -0.07-0.02i\\ 0 & 0 & 0 & 0 & 0\end{bmatrix} \tag{3.9}$$

$$\Psi = \begin{bmatrix}0 & 0 & -0.01 & 6.28 & 1e20\\ -0.7+0.12i & 0.02+0.69i & -1.02+0.59i & 7-3.39i & 7.05e-1.27e2i\\ -0.7-0.12i & 0.02-0.69i & -1.02-0.59i & 7+3.39i & 7.05e+1.27e2i\\ -0.02+0.01i & 0.02+0.02i & -0.45-1.26i & 2.58+7.9i & 1.14e2+3.06ei\\ -0.02-0.01i & 0.02-0.02i & -0.45+1.26i & 2.58-7.9i & 1.14e2-3.06ei\end{bmatrix} \tag{3.10}$$

Utilizing the definition of the participation factor, the correlation between state variables and eigenvalues can be shown by the participation matrix in Tab. 3.2. It is easy to see from the participation matrix that the state variables $i_{L,}V_{C,}\alpha$ mainly depend on the system modes $\lambda_{4,5}$. The system modes $\lambda_{2,3}$ have the most influence on the state variables i_{Lf} and V_{Cf}, while the system mode λ_1 is only responsible for the state variable V_C. An overview of all eigenvalues in the buck converter and their most corresponding state variables is depicted in Fig. 3.4. From the result of computing eigenvalue sensitivity in [14] is known that

- λ_1 is mainly sensitive to K_p, K_i and R
- $\lambda_{2,3}$ are mainly sensitive to L_f and C_f
- $\lambda_{4,5}$ are mainly sensitive to L, C and K_p

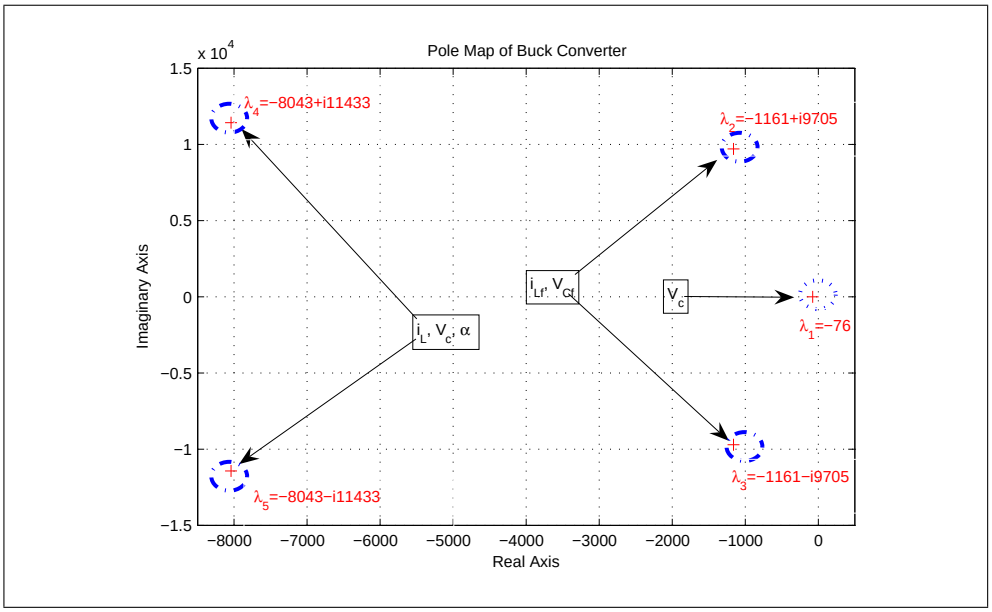

Figure 3.4.: Poles and their corresponding state variables of the buck converter

The combined information from the participation factors and the eigenvalue sensitivity can be used by a system designer to determine suitable parameters for pole displacement e.g. for a higher stability margin or a better dynamic performance. For example, the state variables i_{Lf} and V_{Cf} can be significantly influenced by changing the parameter L_f and C_f because of the large participation factor of the state variables i_{Lf} and V_{Cf} to the eigenvalues $\lambda_{2,3}$ and the great sensitivity from L_f and C_f to the eigenvalues $\lambda_{2,3}$. Although the modal analysis is very suitable for the design, it is not reliable to look for the most critical parameters with respect to system stability. It is easy to see in Fig. 3.4, that the most critical eigenvalue for stability in the nominal system now is the first eigenvalue λ_1, which is the nearest to the imaginary axis. However, an equal perturbation of all parameters will first let the eigenvalues $\lambda_{4,5}$ cross over the imaginary axis, although the eigenvalues $\lambda_{4,5}$ are the most uncritical ones in the nominal system. The modal analysis cannot explain the phenomenon at all. Once again, the standard way for doing global stability analysis is exhaustive iterative parameter variation, linearization at equilibrium and calculation of the eigenvalues, e.g. by Monte Carlo simulation. There is no guarantee to find all critical parameter variations.

3.2.3. Robust stability analysis

The Linear Fractional Representation (LFR) of uncertain systems is often used as the basis for stability analysis and controller synthesis in Robust Control. The structured singular value μ, the skewed-structured singular value ν and μ sensitivity are some of the most important definitions for robust stability analysis and robust controller design.

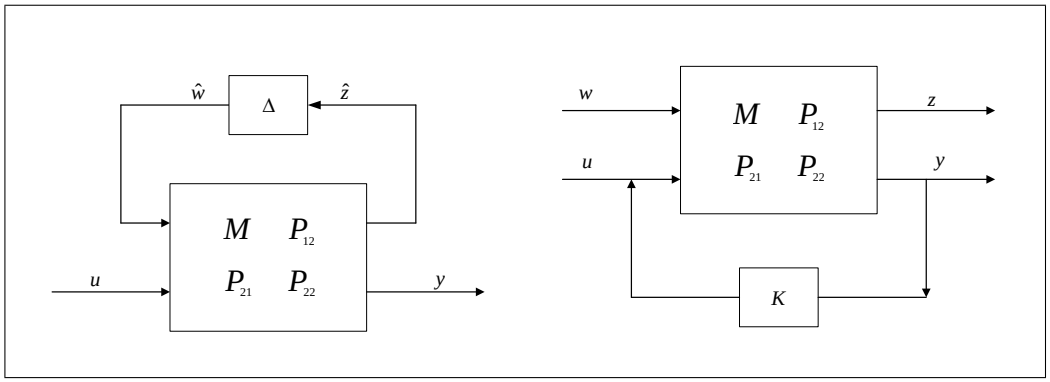

Figure 3.5.: Linear Fractional Transformation framework

Linear Fractional Transformation (LFT)

Suppose P is the transfer matrix of a nominal system with $P = [M\ P_{12};\ P_{21}\ P_{22}]$. K and Δ represent the controller and system uncertainties of the parameters, respectively. The lower Linear Fractional Transformation $\mathcal{F}_l(P, K)$ of P and K is defined as

$$\mathcal{F}_l(P, K) = M + P_{12}K(I - P_{22}K)^{-1}P_{21} \tag{3.11}$$

The lower LFT represents the transfer function from signal w to z when closing the lower loop. In general, w can account for all uncontrollable signals, e.g. disturbance and noise and z denotes the signal that allows to characterize whether a controller has certain desired properties. z is called controlled variable e.g. z equals the control error [103] (see the left figure in Fig. 3.5). u and y include the controller inputs and the system outputs. Similarly, the upper LFT $\mathcal{F}_u(\Delta, P)$ is defined as

$$\mathcal{F}_u(\Delta, P) = P_{22} + P_{21}\Delta(I - M\Delta)^{-1}P_{12} \tag{3.12}$$

(see the right one in Fig. 3.5). The upper LFT is the transfer function from $\widehat{w}$ to $\widehat{z}$, which defines all uncertainty outputs and inputs in the system when closing the upper loop. All system uncertainties are normalized to ± 1 and pulled out into the Δ matrix. The row dimension of Δ is called the order of the LFR. The above defined two Linear Fractional Transformations play a very important role in Robust Control. The LFR-toolbox [42] for MATLAB can build the LFR models '$\Delta - P$' (Fig. 3.5) automatically. Low order LFT-based uncertainty models can be obtained with the new version of the LFR-toolbox for MATLAB using symbolic preprocessing and numeric reduction techniques [40]. This allows the utilization of the LFT based stability analysis for industrial relevant complex systems [39].

Structured and skewed-structured singular value

Let the Δ matrix in terms of a '$\Delta - P$' model in Fig. 3.5 be diagonal or block-diagonal. It includes all system uncertainties and its norm remains less than 1. Then the structured singular value $\mu_\Delta(M)$ of P with respect to the structured uncertainty matrix Δ is defined as:

$$\mu_{\Delta}(M) = \frac{1}{\min_{\Delta}\{\overline{\delta}(\Delta) : det(I - M\Delta) = 0\}} \tag{3.13}$$

where $\overline{\sigma}(\Delta)$ is the largest singular value of matrix Δ, i.e. $||\Delta||_{\infty}$ and $\mu_{\Delta}(M) = 0$, if there is no Δ that satisfies the determinant condition. The structured singular value defines the reciprocal of the minimal $\mathcal{H}_{\infty}$ norm of the uncertainty matrix which makes the term $I - M\Delta$ singular. The nominal system M has to be stable. Then the linear formulation of an uncertain system given by Eq. 3.12 can only be unstable if the term $I - M\Delta$ is singular. Therefore,

- $\mu_{\Delta}(M) \leq 1$ implies that $I - M\Delta$ is non-singular for all uncertainties, which satisfy $||\Delta||_{\infty} \leq 1$
- $\mu_{\Delta}(M) \geq 1$ implies that there exists a system uncertainty which makes $I - M\Delta$ singular

Robust Stability

The system described by the left structure in Fig. 3.5 is robustly stable against all uncertainties in the specified uncertainty range if [117]

$$\mu_{\Delta}(M) < 1 \text{ for } ||\Delta||_{\infty} \leq 1 \tag{3.14}$$

A system tends to be unstable as the structured singular value increases [117]. The structured singular value is usually determined by calculating its upper and lower bounds because the exact computation of $\mu_{\Delta}(M)$ is in general NP-hard [115]. The upper bound is used to calculate the μ sensitivity, which will be introduced in the following section. The lower bound of μ is suitable for the determination of the worstcase combination of the uncertain parameters. It is calculated by algorithms using local optimization. Numerous methods for computing bounds of μ are introduced in [10] and [27].

If a subset Δ_f of Δ (in Fig. 3.5) may not vary freely and $||\Delta_f|| < 1$ when computing the μ, while the norm of another subset Δ_v in matrix Δ may increase without restriction then it is called the skewed structured singular value $\nu_{\Delta s}(M)$ of matrix M with respect to the uncertainty matrix $\Delta_s = diag(\Delta_v, \Delta_f)$. It is defined as:

$$\nu_{\Delta s}(M) = \frac{1}{\min_{\Delta}\{\overline{\sigma}(\Delta_v) : det(I - M\Delta_s) = 0\}} \tag{3.15}$$

where $||\Delta_f|| \leq 1$. $\nu_{\Delta s}(M)$ is zero if no Δ_s exists that makes $det(I - M\Delta_s) = 0$ [28]. The skewed Structured Singular Value gives a solution for determining the maximum allowable range for a subset of uncertain parameters, while other parameters are fixed in a specified range. $\mu_{\Delta}(M)$ is a special case of $\nu_{\Delta s}(M)$.

μ sensitivity

In the last paragraph the relationship between the stability of a system against uncertainties and μ was defined. Also important is the identification of the most

critical parameters of a system. This is equivalent to the uncertain parameters which are most sensitive with respect to μ. The most sensitive parameters are those parameters which lead to the greatest increase of μ by a variation of their normalized range. Consider there is a Δ with two parametric uncertainties $\Delta = [\Delta_1\ 0;\ 0\ \Delta_2]$ of the nominal system M, $\delta\beta$ represents the perturbation of the first uncertain parameter with $\beta = 1 + \delta\beta$. The uncertainty matrix Δ_β perturbed with $\delta\beta$ becomes

$$\Delta_\beta = \begin{bmatrix} \Delta_1 & 0 \\ 0 & \Delta_2 \end{bmatrix} \begin{bmatrix} \beta I & 0 \\ 0 & I \end{bmatrix} \tag{3.16}$$

The perturbation in the uncertainty matrix Δ can be absorbed into M_β, so that the original uncertain matrix Δ remains. The new system matrix with absorbed perturbation $\beta\Delta_1$ becomes

$$M_\beta = \begin{bmatrix} \beta I & 0 \\ 0 & I \end{bmatrix} \begin{bmatrix} \beta M_{11} & \beta M_{12} \\ M_{21} & M_{22} \end{bmatrix} \tag{3.17}$$

The μ sensitivity with respect to the j^{th} uncertainty parameter in Δ_1 can be defined as:

$$Sen^{\mu}_{p_j} = \lim_{\delta\beta_j \to 0} \frac{\mu_\Delta(M(\beta_j) - \mu(M(\beta_j - \delta\beta_j))}{\delta\beta_j} \tag{3.18}$$

with $j \in 1 \ldots n$. It is proven, that the skewed μ is equivalent to μ sensitivity [81]. Thus, the μ sensitivity can be calculated easily in two ways. In the first way, the parametric perturbation is absorbed into the system matrix. μ sensitivity is computed using definition in Eq. 3.18 by the computation of the Structured Singular Value μ. The μ sensitivity can also be calculated with the help of skewed μ. Both can be done with the skew μ toolbox [27]. All elements in the state space matrix must be constant or of polynomial type in order to use the LFR Toolbox to generate a LFR. The application of the robust analysis method to the buck converter is addressed in [65].

3.2.4. Discussion

Some small signal based methodologies for stability analysis were demonstrated with a DC/DC buck converter model, which is a small but critical system component in the electric on-board network of the MEA. Two standard methods for stability investigations, the Middlebrook criterion and the modal analysis, were briefly shown and compared with the new approach. The analysis was shown to be superior in the characterization of the robustness level and identification of the critical parameters. While the computation is more complex than e.g. the modal analysis, it is more reliable for a broader range of operating points due to the symbolic linearization. The Middlebrook criterion basically shows a result for the critical parameters similar to the μ analysis. Determination of the critical parameter combination or the allowed range is quite unhandy with the Middlebrook criterion. It is necessary to be well aware of the interpretation of the Bode plot. The standard way to determine

the stability bound is a time consuming parameter variation. The method is just applicable to input filter considerations of the DC/DC converter while μ analysis is applicable to all LTI systems. The Middlebrook criterion cannot give a quantitative analysis for the critical level of uncertain parameters.

3.3. Large signal based methods

An industrial applicable definition of stability is the ability of a system to keep a certain system variable of interest within desired limits. Those limits may be defined for steady state operation and transient state operation. They can be given in time domain or frequency domain and are often combined criteria for network stability, power quality and performance. The requirements of the standards must be fulfilled for any combination of parametric uncertainties and over the whole operation range. Using just analytic methods from classical control theory for industrial defined criteria might therefore not be straightforward, conservative or just impossible. For large power networks it might be impracticable to prove stability in general and industrial demands in particular other than by simulation due to the usually high nonlinear and wide ranging dynamics coming from very fast switching. For example, a state could be oscillating at low damping. The eigenvalues could be in the stable area while the industrial defined limits of overshoot, steady state limits and permitted frequencies are violated. Therefore, for aircraft electrical systems, the current industrial verification process relies basically on checking the limits repeatedly for the parameter range and operation envelope, often by use of a mass of simulations. The limits are given by general aviation standards and airframers' directives. Parameter combinations are chosen by gridding or Monte-Carlo simulation for a few parameters. In the case of too many tuner parameters and grids, the Monte-Carlo simulation quickly becomes infeasible. This demands extensive computation and no guarantee for hitting the worst case combination can be given. Anti-optimization or worst-case search has been proposed to improve the verification process. The basic idea is to reformulate a stability criterion as a minimum distance problem which is minimized to determine worst-case parameter combinations and operation conditions leading to worst performance. This is the reason why it is also called anti-optimization. Since the search is directed, it is likely to be much faster and more accurate than gridding or Monte-Carlo analysis[1].

3.3.1. Technical preliminary

With the theory of [29], let p be the parameter vector and OC the operating condition. The clearance problem for a given performance criterion $c(p, OC)$ can be formulated as a distance minimization problem to find the worst-case parameter combination/operating condition leading to the worst performance. With c0 being the limiting acceptable value of $c(p, OC)$ as defined in a requirements specification,

[1] This section is an extended and improved version of [65]

the difference

$$d(p, OC) = c(p, OC) - c_0 \tag{3.19}$$

is to be minimized by variation of p within the parameter space of all possible operating conditions OC. The minimum distance

$$d(p, OC) = c(p, OC) - c_0 \tag{3.20}$$

can be interpreted as the robustness measure how far the system is away from the limiting acceptable performance c_0. For flight control the optimization-based approach was used with parametric nonlinear aircraft models which were linearized for eigenvalue based analysis [112]. But the approach is general, being able to address all kinds of mathematically formulated criteria for linear, non-linear and switching models. This is necessary for industrially defined stability criteria [87] since they are mixed criteria for network stability, power quality and performance for complex models which can not necessarily be treated with linear systems control theory. It is applicable for

- simulation based stability studies with behavioral systems for large signal stability by applying the industrial stability criteria
- stability studies, by testing non-switching functional systems with linearized equations for small signal stability
- robust stability for parameter variations in a predefined range
- design by determination of maximum parameter variations which are tolerable for a nominal system to be still stable (for multiple parameters, the ratio must be weighted by a cost function)
- design by iterative optimization of design parameters (e.g. controller), optimized for worst operating conditions identified by anti-optimization [11]. The evaluation of criteria based on linearised models involves trimming, linearization and frequency response or eigenvalue computation. The evaluation of criteria based on nonlinear models usually involves simulations, preceded by trimming.

The anti-optimization based approach for stability analysis of nonlinear electrical network has been proposed in this thesis. The aim is to find the maximum range for a design parameter not violating a stability, performance or quality criterion. The optimization problem is proposed to be as follows

$$\begin{aligned} &\min_{\bar{P}} f(\bar{P}) \\ &\min_{k,\bar{p}} d_k(\bar{p}, \bar{P}, OC) \overset{!}{\leq} 0 \\ &c_i(\bar{p}, \bar{P}) \geq 0 \\ &l_j \leq p_j \leq u_j \end{aligned} \tag{3.21}$$

Assuming there is a range in the design parameters $\bar{P}$ where the defined stability criteria can not be violated within the system variation $\bar{p}$ or operation conditions range OC. The optimization problem is to size $\bar{P}$ to find the minimum solution of $f(\bar{P})$ which will make the distance to instability $d_k(\bar{p}, \bar{P}, OC)$ to zero for the criterion which is "easiest" to violate. The vector of uncertain system parameters lies within the limits $l_j \leq p_j \leq u_j$. Additional constraints to exclude certain parameter combinations $c_i(\bar{p}, \bar{P}) \geq 0$ may be stated (e.g. combinations not occurring for the real system or exclusion of areas where stability is already known).

Considerations about the optimization method and problems are stated in an extra paragraph. For several design parameters the problem is non trivial since $f(\bar{P})$ has to be formulated to destabilize the system just in case of growing. Non-convex problems will prevent good solutions. Therefore, as much analytic information as possible should be inserted in the problem formulation.

3.3.2. Formulation of stability criteria

While it is advantageous for a single evaluation or in hardware certification tests to have binary indicators like "criterion fulfilled/ not fulfilled", just stochastic algorithms suitable for discrete problems could be used to optimize a criteria built upon them. For using faster converging algorithms such as genetic algorithms or Particle Swarm Optimization (PSO), the problems have to be redrafted to be continuous. This requires a thorough formulation of the objectives by means of smooth optimization criteria. It is crucial to formulate criteria aiming for internal stability, especially eigenvalue based approaches, and methods for output stability, such as limits from the standards checked by simulation.

Eigenvalue criteria

The eigenvalues give information about small-signal stability and settlement of a linear time-invariant representation. In case the largest eigenvalue of a system passes the imaginary axis of the complex plain, the system is unstable. With the l eigenvalues λ calculated from the linearized functional model, the distance criterion can be defined as

$$d_{ev} = \min_{l}(-\epsilon - \mathrm{Re}(\lambda_l)) \tag{3.22}$$

where ϵ is an additional stability margin which can be used to limit the maximum settling time. From the practical point of view, one might mainly be interested in the behavior of a monitored state. This may not be dependent upon all λ s. The correlation between the k states of a linear system and its l eigenvalues can be determined by the participation factor:

$$p_{kl} = \frac{\delta \lambda_l}{\delta a_{kk}} \tag{3.23}$$

In any case one can say the states $\bar{x}$ of a linear asymptotically stable system will return to the OC the equilibrium point $\bar{x}^*$ exponentially with at least the "speed" of the largest eigenvalue:

$$||\bar{x} - \bar{x}^*|| \leq ke^{\chi t},\ k > 0,\ \max_l(\lambda_l) < \chi < 0 \tag{3.24}$$

This information could be used to transfer the demands of the industrial standards for settlement to the eigenvalue criterion.

Eigenvalue damping criterion

The damping of the eigenvalues is important for attenuation of oscillations. The distance criterion can be defined as the minimum of the distance of the damping of the eigenvalue to the accepted one:

$$d_D = \min_l(\frac{-\mathrm{Re}(\lambda_l)}{|\lambda_l|} - D),\ \zeta = \arccos D \tag{3.25}$$

3.3.3. Investigation of stability according to industrial standards

The stability requirements firstly have to be converted into the optimization problem formulation. For the demonstration of the methodology, limits in the style of the often applied Military Standard 704F are used, see [87], for the specification of a 28V DC network. Here there is just a concentration on the limits for the system, not on tests on equipment level. The following cases of stability regarding the industrial standards can be defined:

Case1: For steady state, maximum and minimum voltages are given. Upper and lower boundaries are not necessarily equidistant from nominal value.

Case2: For transients, the voltage of the DC network must remain within time variable limits after a displacement. After the settling time steady state limits apply. As for the steady state case, upper and lower boundaries envelopes may differ in extent but also in the shape of Fig. 3.8 shows a typical operation envelope, the permitted range is in color.

Case3: This distortion has to be bounded to a maximum voltage amplitude (time domain).

Case4: For the frequencies spectrum of the network voltage, limits in the amplitudes are given.

Case5: The total distortion may not exceed a certain ratio of the DC signal. For special conditions as over voltage or power-up, other limits may apply. They are not treated here since they are variations of the mentioned cases.

To perform the anti-optimization based approach, the pre-defined cases of stability have to be described by the corresponding mathematical formulations.The cases may be used for optimization criteria formulation as follows:

For case 1: Since this is a performance criterion for steady state condition of the base voltage, both functional and behavioral models apply. For the functional model,

trimming the model at steady state already gives the network voltage. For the used simulation environment Dymola, steady state initialization at zero and fixed value initialization (e.g. $\varphi = 400$Hz) can be mixed easily. Since the initialization problem may be nonlinear it is advantageous to set guess values for the iteration variables which are close to the actual ones. As guess values, the result of a former simulation run with similar parameters can be used. Using just the steady state solution for the functional model is similar as using architectural models as used for system architecture optimization in [101]. For behavioral models, while the mean voltage does not change at stationary operation it is superposed by alternating voltages mentioned in case 3. The former can be separated as the DC part of the Fourier-transformed result of a simulation run. As stability distance criterion the distance between the actual net voltage V, the upper and lower boundaries V_u/V_l shall be defined, normalized by the distance between the nominal value V_0 and the bounds. If the criterion is below 0 the standard is violated.

$$d_{DC} = \begin{cases} \left(\frac{V-V_u}{V_0-V_u}\right), V \geq V_0 \\ \left(\frac{V-V_l}{V_0-V_l}\right), V < V_0 \end{cases} \tag{3.26}$$

A gradient based optimizer is not applicable for this criterion since the sign of the function changes at V_0.

For case 2: This limit can be formulated most effectively when simulating an operation scenario with some sort of induced transition, e.g. step response on a load change. Some typical scenarios are given by the standards such as power-up or -down, network reconfiguration, load variation and short circuits. In practice often the scenario most critical to stability is not known a priori but fixed scenarios without guarantee in targeting the worst case violations are applied. The scenarios must be processed consecutively. Another method could include parameters defining the operation condition in the unknown parameter vector and anti-optimize for the most critical condition. In [82] the flexibility of global optimization methods was exploited to show how continuous regions of the flight envelope could be cleared in a single analysis. Furthermore, for time-dependent inputs a scheme for worst-case inputs computation was proposed. The idea was to represent discretized times and amplitudes for switching as "genes", which are varied by a genetic algorithm.

The distance criterion for the limit itself can be formulated similar to the formula in Eq. 3.26. With the simulation results discretized at time steps i, the criterion is the maximum value of the formula 3.26 evaluated at all i's. If it is below 0 the requirement is violated.

$$d_{trans1} = \min_{i \in 0 \ldots n} \left\{ \begin{cases} \left(\frac{V_i-V_{ui}}{V_{0i}-V_{ui}}\right), V_i \geq V_{01} \\ \left(\frac{V_i-V_{li}}{V_{0i}-Vli}\right), V_l < V_{0i} \end{cases} \right\} \tag{3.27}$$

Filtering can be achieved by calculation of the mean value by using integration:

$$d_{trans2} = \min_{j \in 0 \ldots m} \left\{ \frac{1}{T_{j+1}-T_j} \int_{T_j}^{T_{j+1}} \begin{cases} \frac{V(t)-V_u(t)}{V_0(t)-V_u(t)} dt & \forall V(t) \geq V_0(t) \\ \frac{V(t)-V_l(t)}{V_0(t)-V_l(t)} dt & \forall V(t) < V_0(t) \end{cases} \right. \tag{3.28}$$

Care must be taken to choose the intervals j long enough to limit the frequencies' content but not to hide local overshoots. It is convenient to use the integration algorithm of the simulation programme for the evaluation of this criterion.

For case 3: The voltage ripple can be seen as the reciprocal problem of the former limits cases. For behavioral model constant operation and both modeling levels transients simulation, the ripple is superposing the slowly varying part. It can be separated by high-pass filtering or subtraction of the low-pass filtered or averaged signal from the simulation result.

For case 4: This limit resembles case 2 but for the frequency domain. The criterion for optimization can be formulated as the minimum of the distances of the amplitudes $A(f_k)$ at frequencies f_k to their applicable limits $\lim(f_k)$:

$$d_{fs} = \min_k \{\lim(f_k) - A(f_k)\}\,,\ k = 1 \ldots l \tag{3.29}$$

For the discrete Fourier transformation (DFT) the sampling time has to be chosen low enough to cover the highest frequencies appearing in the simulation or specified in the requirements. The number of sampling points determines the spectral resolution and therefore must be chosen high enough not to mask peaks of close-by frequencies. For heavy switching systems the results with the DFT might be wrong since the algorithm demands a fixed sampling rate. To cover the events generated by switching, it might be noteworthy to use the Lomb periodogram [75, 106] which allows frequency analysis for possibly non-uniformly sampled data.

For case 5: The criterion for the total distortion factor (TD) [69] is quite straightforward. With the TD calculated as the RMS value of the alternating voltage component divided by the DC voltage and the limit TD_{lim}:

$$d_{TD} = TD_{lim} - TD \tag{3.30}$$

3.3.4. Simulation based Anti-optimization approach

To assess the stability criteria defined in industrial standards[87], the simulation based approach seems to be a proven method. Concerning the time domain criteria such as transient envelop, the functional models usually can provide sufficient results with the benefits of fast simulation time. For some tasks such as assessment in frequency domain, the behavioral or generalized averaging models can be utilized.

For stability analysis, it is sufficient to find one solution in the parameter range which will result in a boundary violation. For design it is essential to find the global solution of the optimization problem since otherwise the design limit is overestimated. It is quite easy to see that the optimization problem in Eq. 3.21 is very affine for local minima since just the worst criterion has to be minimized. Local optimization algorithms such as gradient based optimization will minimize just one criterion with the minimum located next, neglecting other solutions in the parameter space for this criterion at all other criteria in general. It is essential to normalize the criteria at the start conditions to prevent strong favoring already in the beginning. As a basis one could perform a first evaluation run for the nominal model and scale

the criteria by the nominal values. For the global optimization there exist stochastic and deterministic solvers such as the well known stochastic genetic algorithm and the PSO or the deterministic differential evolution algorithm [95]. The possibility to parallelize the computation is seen as being essential for the efficient computation. Therefore the PSO is used, and in this thesis no comparison with other algorithms is given. The implementation in the DLR optimizer Multi-Objective Parameter Synthesis (MOPS) [59] of the PSO is extended for constraint optimization problems and has additional hybrid (combined local/global) optimization features to overcome slow convergence of stochastic search methods to some extent.

The PSO tries to simulate the social behavior of a population (swarm), for example a swarm of birds. This is a successful application of the philosophy of bounded rationality and decentralized decision-making to solve the global optimization problems [104, 13, 30]. A swarm of birds or insects searches for food, protection, etc. in a very typical manner. If one of the members in the swarm finds a desirable path, e.g. nearest to the goal, the rest of the swarm will follow quickly. Each member of the swarm searches for the best in its locality and learns from its own experience, simultaneously it learns from the others, typically from the best performer among them. PSO has been extended to many variants after the introduction in [60] e.g. the repulsive particle swarm for finding the global optimum more effectively [108] and other variants using dynamic scheme [72, 43]. The basic algorithm is easy to implement. A given problem (tuner) space is firstly explored randomly. In iteration k, for each particle (tuner vector) $x^i(k)$ in the population a new candidate $c^i(k+1)$ is computed as

$$\begin{aligned} c^i(k+1) &= x^i(k) + v^i(k+1) \\ v^i(k+1) &= I(K)v^i(k) + \alpha\omega_1(k)(\bar{x}^i(k) - x^i(k)) \\ &\quad + \beta\omega_2(k)(\bar{\bar{x}}(k) - x^i(k)) \end{aligned} \tag{3.31}$$

Where

- $I(k)$ is a weighting factor (called inertial parameter) linearly interpolated between initial and final value after maximum iterations.
- $\bar{x}^i(k)$ is the best solution on position of the population so far.
- $\bar{\bar{x}}(k)$ is the overall best solution at iteration k.
- α, β are weighting factors (called cognition and social parameters respectively).
- $\omega_j(k)$ is a random number uniformly drawn from (0,1).

In the terminology of PSO, v is also called velocity. A candidate is then taken as a new particle in population $k+1$ if it outperforms the corresponding particle of the iteration before.

3.3.5. Tool chain

As tools, the object-oriented simulation environment Dymola and MOPS is used. To this end, MOPS offers a basic control system criteria library, a generic multi-model structure for multi-disciplinary problems and a generic multi-case structure for robust control law design, as well as visualization tools for monitoring the design progress. The user is provided with a clear application program interface and a graphical user interface both implemented in MATLAB. To solve the underlying optimization problem different optimization procedures are available [59]. The parameters to be optimized are called "tuners" in MOPS to distinguish them from all other parameters appearing in a setup, such as the ones describing model uncertainties. While the tuners remain always the same for an optimization run, different models need to be used, e.g. network wiring or level of detail. This can be done via different "Models". Models just differing from different parameters not being tuned are treated as "cases".

For the MOPS environment, different scenarios can be treated in a single optimization setup. For a common understanding, our definition of "tuner", "model" and "case" in MOPS shall be given first:

- "Tuners" is an optimization parameters subset of the model parameters.
- "Model" is a run script for interface, computation and visualization.
- "Case" is a model instantiation for a specific parameter set.

3.3.6. Application for a buck converter

The methodology is demonstrated with a parametric variable model consisting mainly of a DC/DC buck converter in an aviation use case. A Thévenin type voltage source is feeding the 270 HVDC power network. This Thévenin's source is seen as a simple model of a transformer rectifier unit. The parameters are functions of the replaced AC source and the load. While the load is known for this use case it would not be so straightforward for several loads and the AC source. Therefore the parameters are treated as independent uncertain ones. Via a feeder line the DC/DC converter supplying the 28 Volts network is connected (original source: [65]). The low voltage network load is variable, too. For the models, different levels of complexity are used as reported in [66]: Behavioral models are complex models including switching and HF injection behavior. They are representative even for network power quality studies but simulation speed is low. Functional models are averaged models valid for steady-state power consumption and mean-value transient behavior. Equations related to the net frequency have to be transformed to a net-frequency fixed system which gives a time independent steady state solution for stationary operations. Linearization can be applied on the functional models for network stability investigations and network logic is studied via them. The behavioral model and the functional model can be seen in Fig. 3.6 and Fig. 3.7 respectively. The source voltage, feeder resistance and inductance and the load resistance ($R_{feq} = l \cdot R_{per\,meter}$, $L_{feq} = l \cdot L_{per\,meter}$)

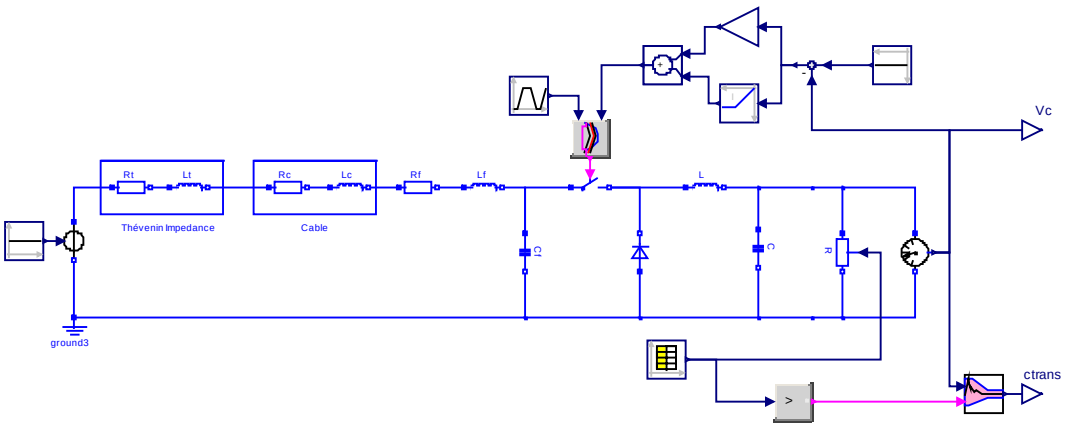

Figure 3.6.: The behavioral model of a DCDC buck converter

are system variables which are variable in a predefined range. The design parameter is the Thévenin inductance. For the behavioral model, instead of a variable load parameter, a load step is used and the limits are checked according to industrial criterion 2.

To demonstrate the proposed approach, three distance criteria are used. These are the formulas for the eigenvalue criterion in Eq. 3.22, the eigenvalue damping in Eq. 3.25 and the transient limits criterion in Eq. 3.28. The former two are evaluated with the functional model while the latter one is checked with the behavioral model. The criterion used for optimization which makes use of the former three was implemented as proposed in Eq. 3.21. The optimization converges after 48 steps and a population size of 20. From the MOPS result window in Fig. 3.10 one can see that the damping criterion was the most critical one (> 1 means "violated"). The other criteria are not violated. This minimum distance is also the value of the stability criterion used for optimization (stab in cfinal). The critical size of the source inductance is 148 mH. Fig. 3.11 and Fig. 3.9 show the results of the single distance criteria at the most critical parameter combination.

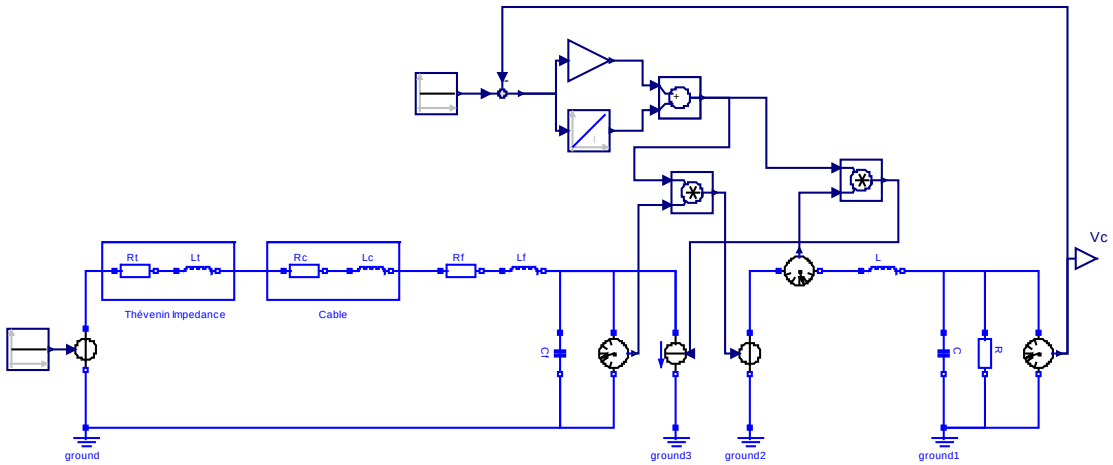

Figure 3.7.: The functional model derived from behavioral model of the DC/DC buck converter of Fig. 3.6

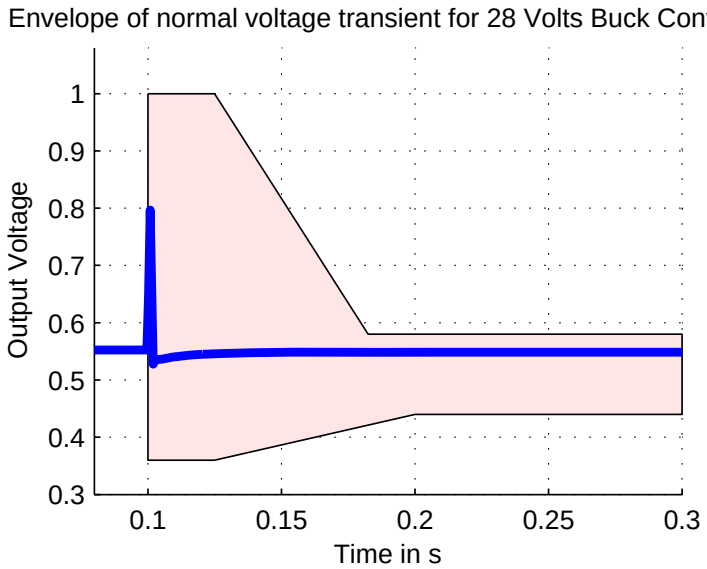

Figure 3.8.: The transient criterion

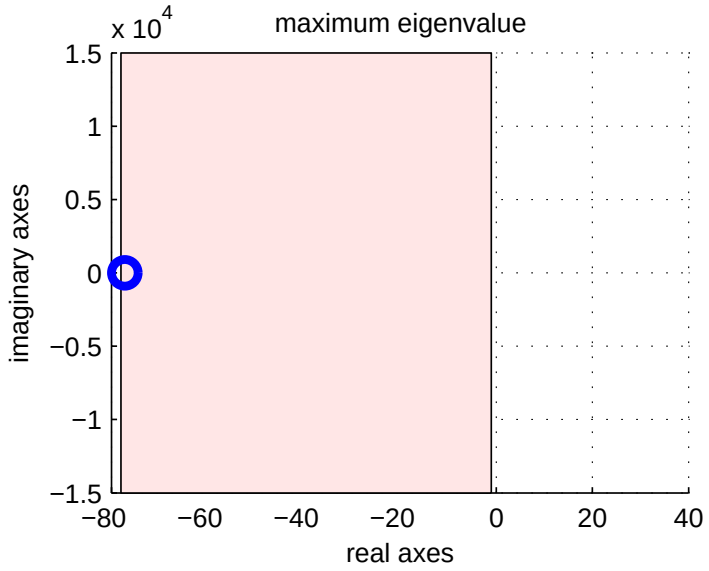

Figure 3.9.: The eigenvalue criterion

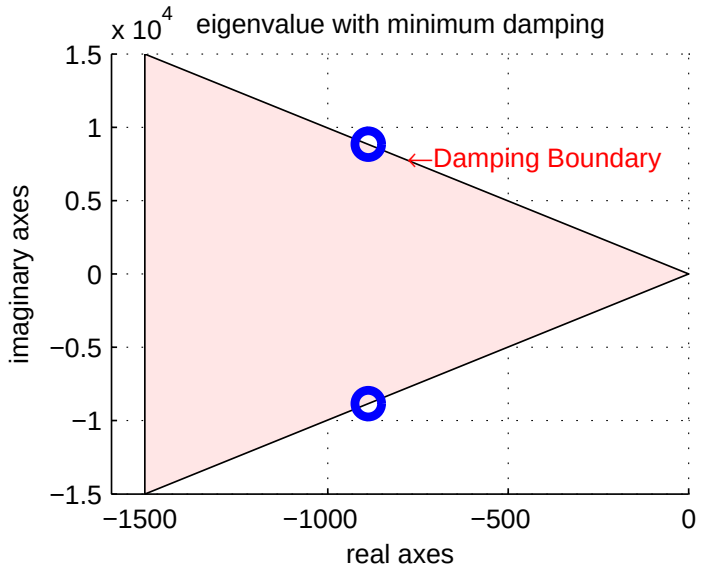

Figure 3.10.: The damping criterion

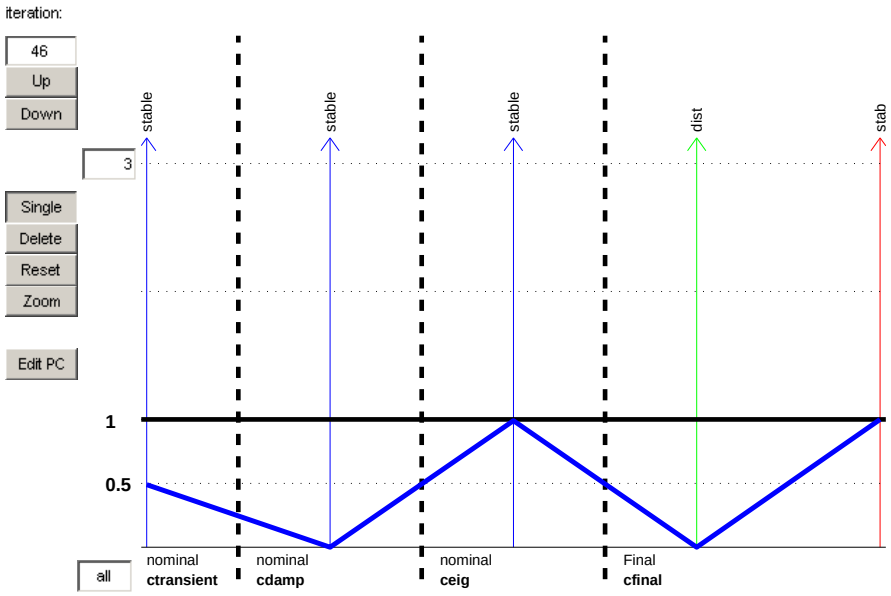

Figure 3.11.: The results as displayed by MOPS

4. Advanced power quality analysis

The power quality assessment of the electric power distribution network is generally of great interest to the MEA. The provisions of voltages and system design have to ensure that power loads successfully utilize electric energy without interference or interruption. Moreover, power quality is also usually necessary when checking network stability described in industrial standards, since the system has to keep the system variables of interest within desired limits. Those limits in time or frequency domain may be defined for steady state and transient state operation.

Power quality is a set of electrical boundaries that allow a piece of equipment to function in its intended manner without significant loss of performance of life expectancy [99]. Any power-related problem that compromises either performance or life expectancy is a power quality concern. Some power quality issues in the traditional power systems include but not limited to power frequency disturbance, power system transients, power system harmonics, electro-magnetic interference, power factor. Dealing with power quality issues for the power system of the MEA, a special consideration has to be paid. According to the specific aircraft type, requirements for power generation systems and supplied equipments are defined. The requirements define the acceptable limit for different values e.g. AC voltage performance, DC voltage performance. One of the mostly considered criteria for the assessment of power quality is the frequency spectrum at steady state. Concerning the complete development process of the future MEA, large scale testing of energy systems using virtual rigs gain increased attention. The virtual tests will allow a quick check of the overall performance, anticipating any problem on the hardware and extrapolating results with real hardware test. Some major tasks within the virtual testing such as electrical system performance and network quality analysis usually need precise steady-state voltage and current waveforms of the relevant components.

4.1. Current issues with power quality analysis

The conventional brute force simulation to yield the steady-state waveforms of a large scale system containing high frequency switching components is very expensive and suffering from numerical instabilities. Existing methods to efficiently solve the steady-state analysis problem can be principally divided into two groups. The methods in the first group such as the harmonic balance based approach [8] integrated in SimulationX or the Quasi-Newton based approach [79] provided by PLECS [5] try to compute the steady-state waveforms with possibly minimum simulation iterations. In another group, the original topological models including high frequency switching components are transformed into the accurate approximated ones without

switching effect by generalized averaging technique or discrete wavelet decomposition, to improve the speed of executing simulation. However, every method has disadvantages. The harmonic balance based approach is well suitable for analyzing an oscillation problem in mechanical systems but seldom applicable to power electronic systems due to numerical problems. With the Quasi-Newton based method, good convergence performance is strongly subject to appropriate start values. By the approximation based approaches such as generalized averaging technique or wavelet decomposition, a trade-off between simplicity and speed of execution is inevitable. The approximated models normally cannot reveal the exact waveforms in the original topological systems.

4.2. Steady state analysis of power electronic systems[1]

The analysis of a steady-state solution for switched power electronic systems consists of the determination of a long-term periodic solution. The focus of the work is to compute solutions in the time domain with a known period $T > 0$. The electrical system is modeled by an initial value problem

$$\dot{x}(t) = f(x,t), \quad x(0) = x_0 \tag{4.1}$$

with initial values $x_0 \in \mathbb{R}^n$ of the states x. The right hand side f is a non-smooth (probably discontinuous) function that describes the dynamics of the system including switching effects. Assuming that there exists a periodic solution $x(t) = x(t+T)$ for $t \geq 0$. Consequently, the task is to find initial values x_0 such that

$$\dot{x}(t) = f(x(t),t), \quad t \in [0,T], \quad x(0) = x(T) = x_0.$$

In order to find the periodic solution at the system steady state, a system of n nonlinear equations

$$z(x) = F_T(x) - x = 0 \tag{4.2}$$

has to be solved, from a mathematical point of view. $F_T(x)$ is the mapping by integrating Eq. 4.1 over the period T.

4.2.1. Fixed-point iteration

The simplest method to find the steady state of periodic power switching systems is the so-called fixed-point iteration. This method is essentially equivalent to the brute force method to run out transients by long simulations. In a switching power converter, transients can converge very slowly, and the fixed-point iteration normally needs a large number of simulation runs. In practice, this method should only be used to find a reference to compare with other methods.

[1] This section is an extended and improved version of [58].

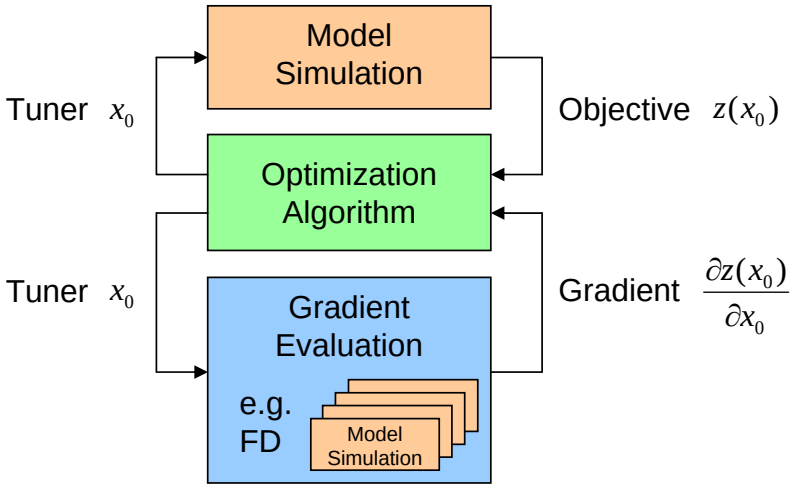

Figure 4.1.: Optimization process for steady-state analysis. FD = Finite Differences

4.2.2. Quasi-Newton methods

To solve the steady state problem formulated in Eq. 4.2, a wide variety of Newton-based methods can be used. The basic idea in all of the methods is to approximate $z(x)$ in the k^{th} iteration with

$$z(x) \approx z^*(x) = J^k \cdot (x - x^k) + z(x^k) \tag{4.3}$$

and to calculate the next iterate x^{k+1} by solving $z^*(x^{k+1}) = 0$,

$$x^{k+1} = x^k - (J^k)^{-1}(x^k - F_T(x^k)) \tag{4.4}$$

The main difference among various Newton-based methods is how the Jacobian matrix J^k is derived.

4.2.3. Optimization based approach

The periodic solution is actually identical to the solution of the following optimization problem:

$$\min_{x_0} z(x_0), \quad z(x_0) := \|x(T) - x_0\|_2^2. \tag{4.5}$$

In the field of numerical optimization a couple of algorithms are available, that have different properties and application areas [85]. This variety can be used to handle the finding of a periodic solution as optimization problem.

In Fig. 4.1 the numerical optimization process applied to the problem in Eq. 4.5 is shown. Model simulations and gradient evaluations are driven by an optimization algorithm that iteratively generates new initial values x_0 of the periodic system. The gradient computations are optional and only necessary for corresponding algorithms like sequential quadratic programming (SQP) methods [85]. A classical separation of optimization methods leads to globally and locally converging algorithms. Stochastic approaches like genetic algorithms tend to find a global optimum

whereas gradient based methods quickly converge close to the solution point. An adequate speed of convergence of a gradient based algorithm requires the reliable numerical evaluation of the objective function's gradient. Especially for dynamical systems with discontinuous right hand sides numerical finite differences (FD) of $\partial z(x_0)/\partial x_0$ may have a poor accuracy. Alternative approaches for the evaluation of gradients that integrate the sensitivity equation allow to generate more accurate results [92]. The optimization based approach to compute periodic steady state initial conditions based on Eq. 4.5 was implemented by Andreas Pfeiffer and included in the commercial Dymola Optimization library [93]. In the following subsections, this library is the basis for the periodic steady state computation.

4.2.4. Determination of start values

Both the solution of the nonlinear equation system in Eq. 4.2 with a Quasi-Newton method, as well as the solution of the optimization problem in Eq. 4.5 require start values for x_0 that are already close to the solution. Otherwise, the numerical methods to do not converge. With the following new technique, such start values can be determined:

1. Perform a simulation with a DCAM model and determine roughly the time instant t_{DCAM} where steady-state occurs. This simulation is very fast.

2. Perform a simulation with one of the averaged models of section 2.1.2 , for example the first harmonic approximation of the original topological model, up to t_{DCAM}. Around t_{DCAM} determine the time instant t_{AV} where a new period starts and extract the state x_{AV} at this time instant.

3. Solve the nonlinear equation system in Eq. 4.2 or the optimization problem in Eq. 4.5 with the original topological model using $T = t_{AV}$ and $x_0 = x_{AV}$as start values.

4.2.5. Case study for the buck converter

Generally, there are three major steps to conduct the optimization based steady-state analysis. First, the DCAM shall be simulated to point out the settling time when the steady-state arrives. Afterwards, more accurate averaged models introduced in the section 2.1.2 e.g. first harmonic approximation of the original topological model shall be simulated only until the settling time. Finally, the optimization setup regarding start values, tuner ranges, criteria demands can be established by means of the simulation results of the generalized averaged models. In this section a buck converter including an input filter is used to demonstrate the proposed optimization based steady-state analysis approach. With respect to the stability analysis result in [65], the stability reserve can be improved by increasing the capacitance value of the input filter C_f, which leads a longer time duration until the steady-state arrives. For the sake of simplicity, only the open loop model of the buck converter in continues

conduction mode is considered in this thesis. The modeling of a closed loop DC/DC converter taking into account the PWM is addressed in [18].

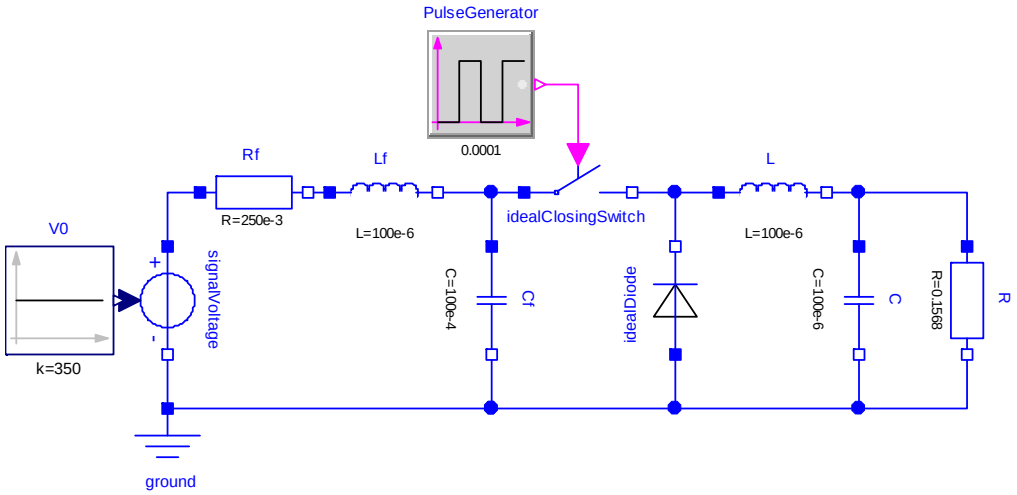

Figure 4.2.: Topological model of a buck converter in Modelica

Modeling of the buck converter

To present the proposed steady state analysis method, the topological Modelica model of a buck converter without the control loop is depicted in Fig. 4.2. By introducing the duty ratio d and switching period T_s of the pulse generator, the performance of the switcher can be defined as on for $0 < t < dT_s$ and off for $dT_s < t < T_s$, where T_s is the time period of the PWM. The state space representation is defined as

$$\dot{x} = A(t)x + B(t)u \tag{4.6}$$

where $x = [i_{L_f},\ v_{C_f},\ i_L,\ v_c]^T$, $B(t) = [1/L_f,\ 0,\ 0,\ 0]^T$, $u = V_0$ and the periodic matrix

$$A(t) = \begin{cases} \begin{bmatrix} -\frac{R_f}{L_f} & -\frac{1}{L_f} & 0 & 0 \\ \frac{1}{C_f} & 0 & -\frac{1}{C_f} & 0 \\ 0 & \frac{1}{L} & 0 & -\frac{1}{L} \\ 0 & 0 & \frac{1}{C} & -\frac{1}{RC} \end{bmatrix} & \text{for } t \in [0, dT_s) \\ \begin{bmatrix} -\frac{R_f}{L_f} & -\frac{1}{L_f} & 0 & 0 \\ \frac{1}{C_f} & 0 & 0 & 0 \\ 0 & 0 & 0 & -\frac{1}{L} \\ 0 & 0 & \frac{1}{C} & -\frac{1}{RC} \end{bmatrix} & \text{for } t \in [dT_s, T_s) \end{cases} \tag{4.7}$$

Applying the unified harmonic state space representation in Eq. 2.13 with $n = 0$, the 0th order average model (DC term approximation) of the buck converter can be

easily derived as

$$\frac{d}{dt}\begin{bmatrix} i_{L_f} \\ v_{C_f} \\ i_L \\ v_C \end{bmatrix} = A_0 \begin{bmatrix} i_{L_f} \\ v_{C_f} \\ i_L \\ v_C \end{bmatrix} + \begin{bmatrix} \frac{V_0}{L_f} \\ 0 \\ 0 \\ 0 \end{bmatrix}$$

with

$$A_0 = \begin{bmatrix} -\frac{R_f}{L_f} & -\frac{1}{L_f} & 0 & 0 \\ \frac{1}{C_f} & 0 & -\frac{d}{C_f} & 0 \\ 0 & \frac{d}{L} & 0 & -\frac{1}{L} \\ 0 & 0 & \frac{1}{C} & -\frac{1}{RC} \end{bmatrix}$$

Since $B(t)$ and u in Eq. 4.6 are constant during a period, the complex Fourier coefficients have the property $B_k = 0$ and $u_k = 0$ for $k \neq 0$. The first order harmonic state space representation with twelve state variables of the buck converter is described by A_{-1} and A_{-2} are conjugate to A_1 and A_2, respectively. Applying the transformation in Eq. 2.13 with the transformation matrices $\mathcal{T}_{\mathcal{X},1} \in \mathbb{C}^{12\times12}$ and $\mathcal{T}_{\mathcal{U},1} \in \mathbb{C}^{3\times3}$, the first order real harmonic state space representation of the buck converter is

$$\dot{\mathcal{X}}_{real,1} = \mathcal{A}_{real,1}\mathcal{X}_{real,1} + \mathcal{B}_{real,1}\mathcal{U}_{real,1} \tag{4.8}$$

where $\mathcal{X}_{real,1} = [x_{c,1}^T,\ x_0^T,\ x_{s,1}^T]^T, \mathcal{U}_{real,1} = V_0, \mathcal{B}_{real,1} = [0,\ 0,\ 0,\ 0,\ 1/L_f,\ 0,\ 0,\ 0,\ 0,\ 0,\ 0,\ 0]^T$, and $\mathcal{A}_{real,1} = [\mathcal{A}^*_{real,1}, \mathcal{A}^{**}_{real,1}, \mathcal{A}^{***}_{real,1}]$ with

$$\mathcal{A}^*_{real,1} = \begin{bmatrix} -\frac{R_f}{L_f} & -\frac{1}{L_f} & 0 & 0 \\ \frac{1}{C_f} & 0 & -\frac{\sin(4\pi d)+4\pi d}{4C_f\pi} & 0 \\ 0 & \frac{\sin(4\pi d)+4\pi d}{4L\pi} & 0 & -\frac{1}{L} \\ 0 & 0 & \frac{1}{C} & -\frac{1}{CR} \\ 0 & 0 & 0 & 0 \\ 0 & 0 & -\frac{\sin(2\pi d)}{C_f\pi} & 0 \\ 0 & \frac{\sin(2\pi d)}{L\pi} & 0 & 0 \\ 0 & 0 & 0 & 0 \\ -\omega & 0 & 0 & 0 \\ 0 & -\omega & -\frac{\cos(4\pi d-1)}{4C_f\pi} & 0 \\ 0 & \frac{\cos(4\pi d-1)}{4L\pi} & -\omega & 0 \\ 0 & 0 & 0 & -\omega \end{bmatrix}$$

$$\mathcal{A}^{**}_{real,1} = \begin{bmatrix} 0 & 0 & 0 & 0 \\ 0 & 0 & -\frac{\sin(2\pi d)}{2C_f\pi} & 0 \\ 0 & \frac{\sin(2\pi d)}{2L\pi} & 0 & 0 \\ 0 & 0 & 0 & 0 \\ -\frac{R_f}{L_f} & -\frac{1}{L_f} & 0 & 0 \\ \frac{1}{C_f} & 0 & -\frac{d}{C_f} & 0 \\ 0 & \frac{d}{L} & 0 & -\frac{1}{L} \\ 0 & 0 & \frac{1}{C} & -\frac{1}{CR} \\ 0 & 0 & 0 & 0 \\ 0 & 0 & \frac{\cos(2\pi d-1)}{2C_f\pi} & 0 \\ 0 & \frac{\cos(2\pi d-1)}{2L\pi} & 0 & 0 \\ 0 & 0 & 0 & 0 \end{bmatrix}$$

$$\mathcal{A}^{***}_{real,1} = \begin{bmatrix} \omega & 0 & 0 & 0 \\ 0 & \omega & -\frac{\cos(4\pi d-1)}{4C_f\pi} & 0 \\ 0 & \frac{\cos(4\pi d-1)}{4L\pi} & \omega & 0 \\ 0 & 0 & 0 & \omega \\ 0 & 0 & 0 & 0 \\ 0 & 0 & -\frac{\cos(2\pi d-1)}{C_f\pi} & 0 \\ 0 & \frac{\cos(2\pi d-1)}{L\pi} & 0 & 0 \\ 0 & 0 & 0 & 0 \\ -\frac{R_f}{L_f} & -\frac{1}{L_f} & 0 & 0 \\ \frac{1}{C_f} & 0 & -\frac{\sin(4\pi d)-4\pi d}{4C_f\pi} & 0 \\ 0 & \frac{-\sin(4\pi d)+4\pi d}{4L\pi} & 0 & -\frac{1}{L} \\ 0 & 0 & \frac{1}{C} & -\frac{1}{CR} \end{bmatrix}$$

The transient and steady-state simulation results of the output voltage of the buck converter are depicted in Fig. 4.3 to illustrate the diverse characteristic of DCAM and the first order harmonic averaged model. The parameters of the buck converter used for the simulation are shown in Tab. 4.1. It is remarkable in the simulation result, that the DCAM which is least computation intensive does not reflect sufficient details e.g. ripples of the original topological model. However, the DCAM is still very helpful to provide the setting time when the steady-state arrives at a rough estimation of the steady-state waveforms. In contrast to DCAM, the FHAM provides a much more accurate approximation of the waveforms of the topological model. This approximation can be used to accomplish the setup of the optimization based steady-state analysis afterwards. Concerning more computation cost for simulating the harmonic averaged model, the simulation end time is set by the settling time acquired by the simulation result of the DCAM.

Table 4.1.: Parameters of the buck converter

Parameter	Description	Value	Unit
L_f	Inductance of input filter	10^{-4}	Henry
R_f	Resistance of input filter	0.25	Ohm
C_f	Capacitance of input filter	10^{-2}	Farad
L	Inductance of buck converter	10^{-4}	Henry
R	Resistance of buck converter	0.1568	Ohm
C	Capacitance of buck converter	10^{-4}	Farad
T_s	Switching period	0.0001	Second

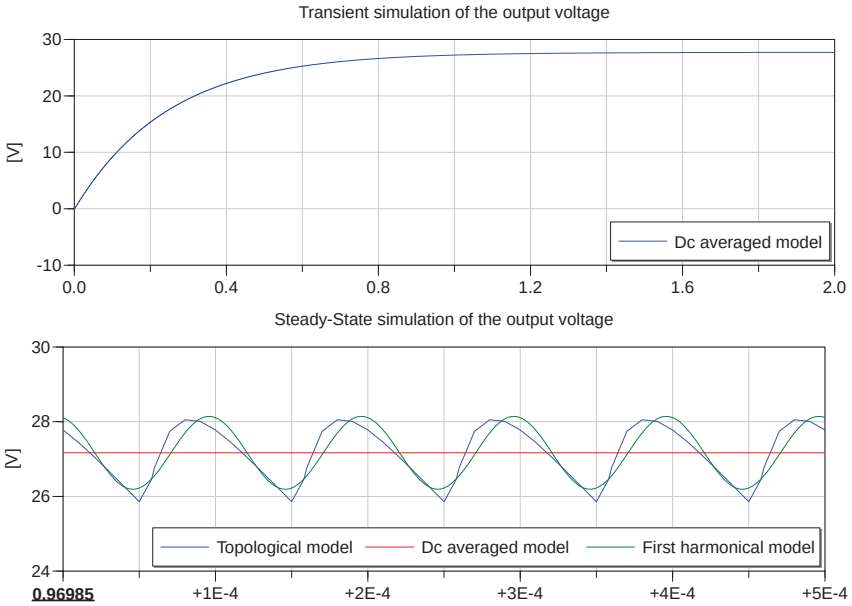

Figure 4.3.: Simulation results of the buck converter output voltage (time unit is [s])

Optimization based steady-state analysis of the buck converter

In order to apply the optimization based steady-state analysis to the buck converter described in Eq. 4.6 and Eq. 4.7, the initial values of the state variables $x = [i_{L_f},\ v_{C_f},\ i_L,\ v_c]^T$ are defined as tuners for the optimization algorithm. In this case, three experiments have been conducted by using diverse start values of the tuners for the optimization to show the effect of the optimization start values on the convergence performance. Firstly, we assume that there is no previous knowledge on the steady-state waveforms of the buck converter, the tuner start values for the optimization are set to zeros. In the second experiment, the start values of the optimization are set by taking the simulation result of the DCAM when the steady-state arrives at $t = 1.4$ seconds (see Fig. 4.3). The varying range of turners are set to ± 20 percent of the simulation values at $t = 1.4$ seconds and criteria demands are set to 1. Finally, the start values are set by the simulation result at $t = 1.4$ seconds of the

FHAM. Setup for the varying range of tuners and criteria demands are the same as in the second experiment. The convergence performance and the required number of numerical integrations for achieving the steady-state are listed in Tab. 4.2. The steady-state analysis result is depicted in Fig. 4.4, which fully covers the waveforms simulated with the topological model. It is easy to see that the convergence performance of the optimization has been significantly improved by using more accurate estimation of state variables as start values by generalized averaged models.

Table 4.2.: Comparisons with diverse start values for optimization

Method	Start value	Conv.	T-Integrations
Integration	0	Yes	12000
Optimization	0	No	N.A.
Optimization	simulation (t=1.4) of DCAM	Yes	56
Optimization	simulation (t=1.4) of FHAM	Yes	39

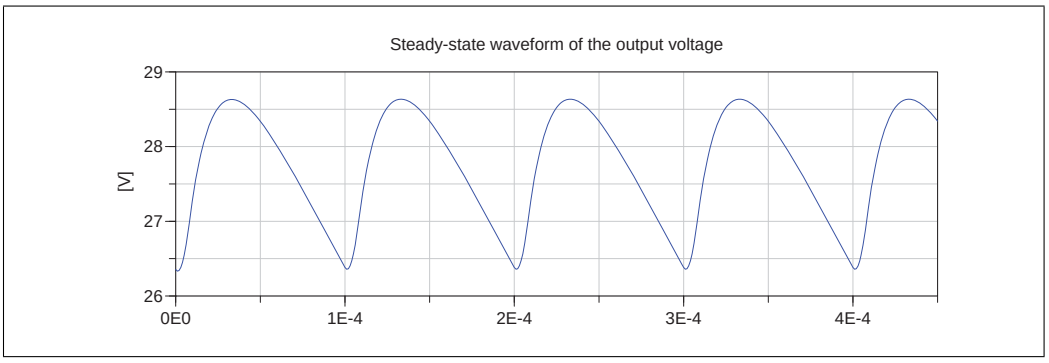

Figure 4.4.: Result of the optimization based steady-state analysis (time unit is [s])

4.3. Multilevel power quality analysis approach

Depending on the analysis tasks with different objectives, power quality assessments with diverse accuracies are needed. To get a rough knowledge on the system performance, the so-called mean value averaged model is often sufficient. At this power quality assessment level, only the fundamental frequency element is considered. For the next level, the generalized averaging technique can be used to achieve a selective multi-frequency model from the original topological system model. Power quality assessment taking more system harmonics into account can be subsequently performed by the multi-frequency harmonic averaged model. For this purpose, a unified harmonic state space representation valid for a wide class of power electronic systems is presented to allow an automated generation of the averaged models with selective approximation accuracy. Finally, to fulfill the highest requirement of power quality analysis, e.g. for EMC study and filter design, the exact finding of the power electronic waveforms is necessary.

For the multi-level power quality analysis, the result of the steady state analysis addressed in the previous section can be applied. The first sub-figure in Fig. 4.5 shows the simulation result of the output voltage of the behavioral model using the optimization based steady-state analysis approach. The functional model and FHAM are used to achieve the DC and first harmonic simulation results are depicted in the second sub-figure of Fig. 4.5. The rough and approximated power quality assessment of the output voltage (V_c) can be directly executed by reading the steady-state values of the DC (V_c_DC) and the first harmonic ($V_c\_1stHarmonic$) simulation results. The exact power quality analysis is conducted by Fast Fourier Transformation of the behavioral model simulation result. The frequency spectrum and the total harmonic distortion analysis of the output voltage are depicted in Fig. 4.6. The Modelica signal analysis tool introduced in [52] is used to perform the fast Fourier transformation and total harmonic distortion analysis. It is easy to see, that the first harmonic simulation result of the steady-state in the 2nd sub-figure of Fig. 4.5 correctly reflects the first harmonic peak in the frequency spectrum.

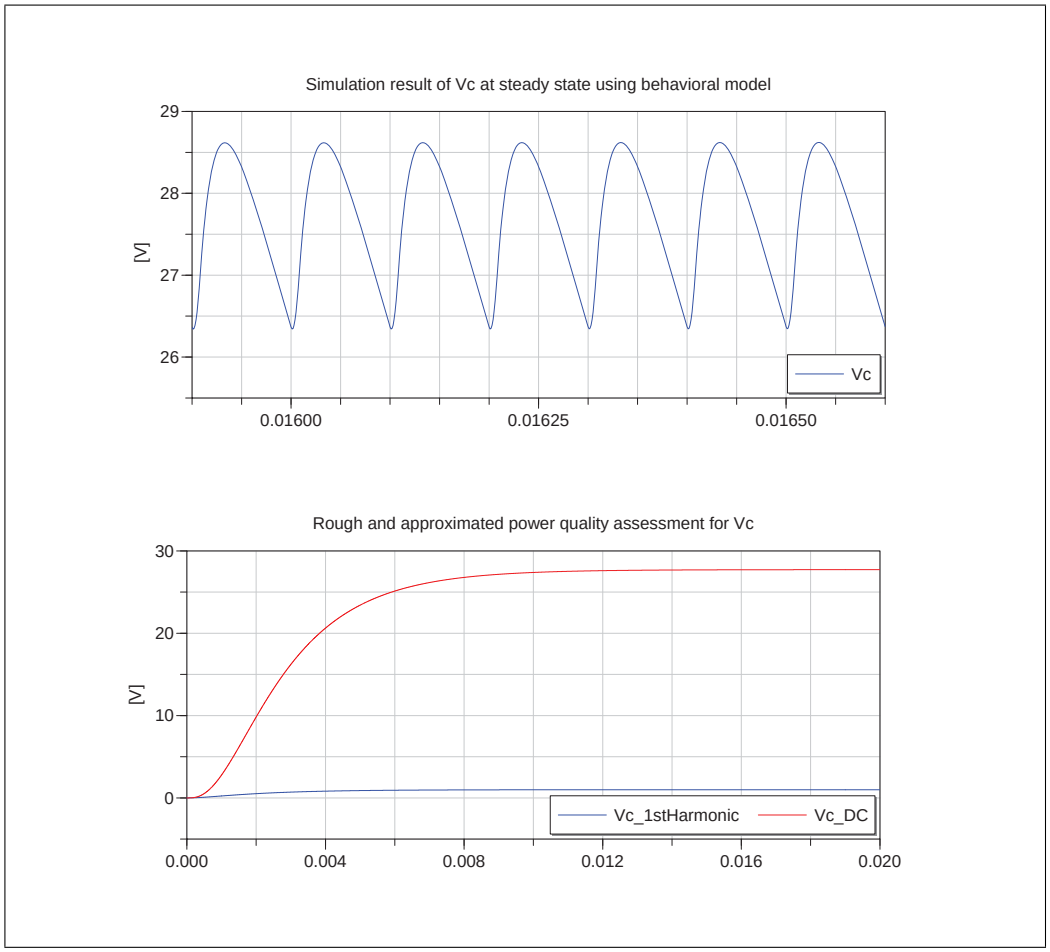

Figure 4.5.: Simulation results of the buck converter output voltage (time unit is [s])

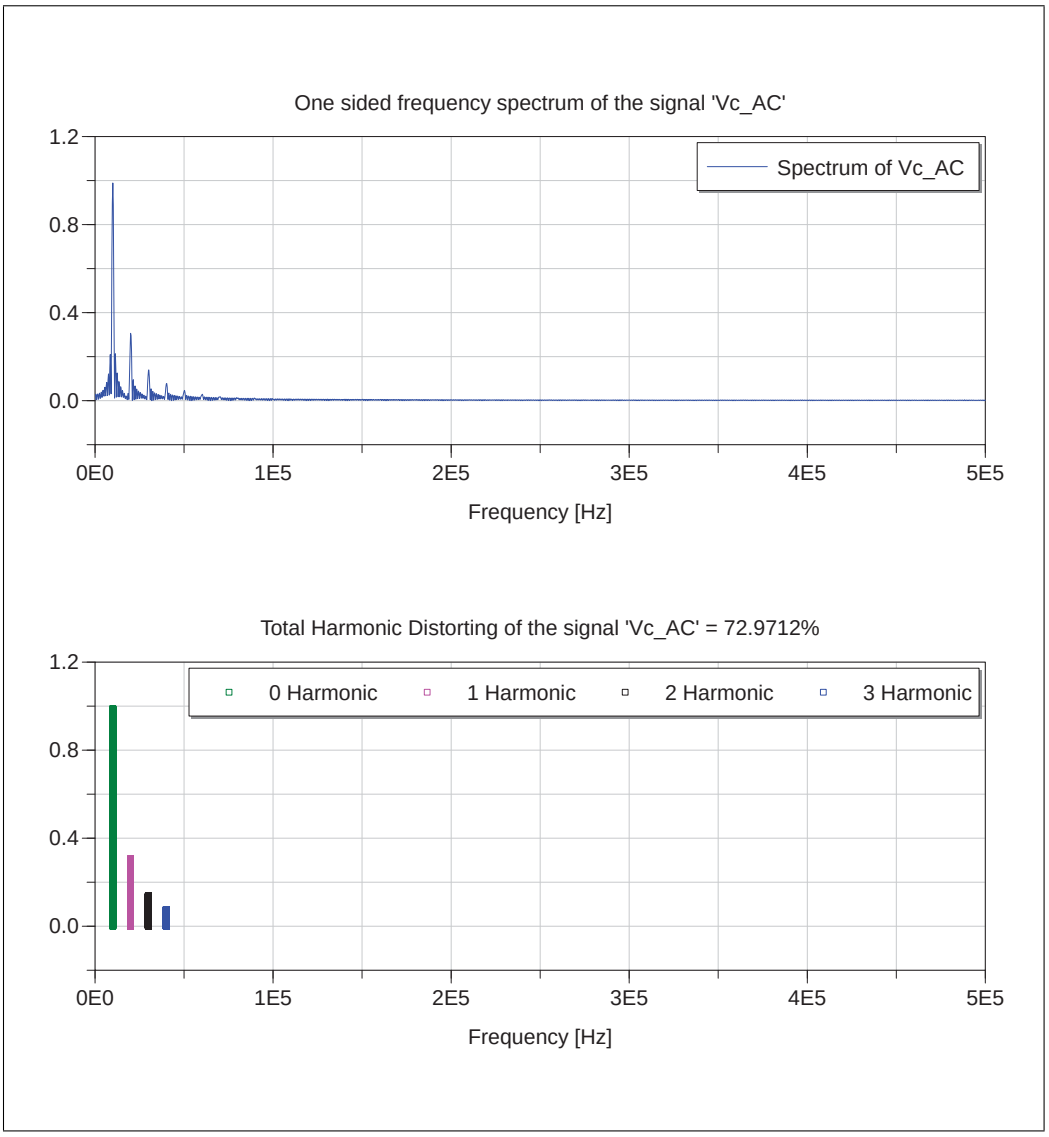

Figure 4.6.: Multi-level power quality assessment results of the buck converter output voltage

5. Fault analysis of the electrical network

A fault is an un-permitted deviation of at least one characteristic property of the system from the acceptable, usual and standard condition [47]. System reliability of the MEA can be improved by enhancing the quality, reliability and robustness of individual system components such as sensors, actuators, generators or controllers. Even so, it is very difficult to ensure a fault-free system operation. Failure analysis and design of fault diagnosis systems become indispensable during the aircraft design process. Actually, the localization of faulty units in the electrical network for power by wire systems with a dramatically increased number of electrical components and equipments is a very challenging task for the MEA design. The prognostic and health management of the power system in an aircraft is obtaining more attentions with the increasing dependency on electrical power. By means of the result of stability studies, the fault detection and health monitoring of the stability critical components e.g. the capacitor in the input filter of a DC/DC buck converter or a EMA is crucial to ensure the operation of the aircraft power system. In contrast to the present scenario of aircraft maintenance where a central maintenance computer on board will receive failure information of the corresponding component just after its fail, the health management systems in a more intelligent manner using modern fault diagnosis techniques shall be applied in the future aircraft to achieve more cost benefit, more flight reliability, decreased flight delay and more accurate information for ground maintenance after landing. Therefore, a scheme suitable for the fault detection and isolation of the power system in the MEA is becoming one key issue. Regarding how faults may develop, there can be two types of faults, namely abrupt type (stepwise) and incipient type (driftwise). Both types of faults are considered in this thesis.

5.1. Fault detection of power electronic circuit using wavelet analysis

Wavelet transform can be considered as a further development of Fourier transform, or more precisely, of short time Fourier transform (STFT) [48]. Using STFT, people try to localize the signal changing with time by selecting suitable time window. This transformation, however, is limited in time-frequency resolution capability due to the uncertainty principle. Wavelet transform overcomes this problem. This transform is defined as [80]:

$$[W_{\psi,f}](a,b) = \frac{1}{\sqrt{|a|}} \int_{-\infty}^{\infty} \overline{\psi\left(\frac{t-b}{a}\right)} f(t)dt \tag{5.1}$$

It is described as the wavelet transform of the square-integrable function f, using wavelet function ψ, a dilation (or scale) a, and a position (or translation) b. The bar above function ψ, stands for conjugation. For given a and b, the transform result is a single real number, a wavelet coefficient. Obviously wavelet transform is the integral of the multiplication of the signal f, with a wavelet function ψ. It has the same form as the STFT. However, unlike STFT, where only sine and cosine functions are used for the transformation, wavelet transform uses different wavelet functions, which can be selected according to the specific problems from a principally unlimited set. Nevertheless, the wavelet function must fulfill some conditions, namely, it must be an orthonormal function. The precise mathematical description of orthonormality is easily found in almost every book about wavelet transform, e.g. [80]. Parameter a, defines the width and height of the wavelet function. A smaller scale a makes ψ narrower; thus the wavelet represents fast changes and the transform focuses on the high frequency components of the signal. Parameter b, shifts the wavelet function along the time axis, so that the transform represents different locations of the signal. Using different values of scale a, and position b, it is able to observe the signal at different position and in different frequency ranges with only one transformation. Thanks to these special properties, wavelet transform is especially suitable for analyzing changing processes. Two forms of wavelet transform are available. They are Continuous Wavelet Transform (CWT) and Discrete Wavelet Transform (DWT). In CWT both scale and position parameters are continuous real values. CWT expresses the signal changes in continuous details. It is more suitable for visual examination.

In DWT only discrete values of the scale and location parameters are used. The values are selected in a discrete form, namely

$$\psi_{j,k} = 2^{-\frac{j}{2}} \psi(a^{-j}x - kb) \tag{5.2}$$

where $a > 1$, $b > 0$ and $j, k \in \mathbb{Z}$. The transform results, i.e. the wavelet coefficients, are therefore also discrete. In the numeric calculation of DWT, an extra scaling function, in addition to the wavelet function, is used to carry out a complete and efficient DWT. The scaling function represents the low frequency components of the signal. It is orthogonal to its own discrete translations and to all wavelet functions. The wavelet and the scaling functions with the discrete scaling and translation parameters build a complete orthogonal basis of the Hilbert space. The DWT is thus another representation of the time signal. As an example, Fig. 5.1 shows the form of the third order Daubechies scaling and wavelet functions and their Fourier transforms [22]. From the Fourier transforms it can be seen that the scaling function covers lower frequency range while the wavelet function stretches in a higher frequency range. From this point of view, DWT is actually the division of the time signal into different frequency bands. Thus, it is straightforward to understand that the calculation of DWT is realized using filter banks. In inverse DWT the calculation is similar. This process is illustrated in Fig. 5.2. DWT transforms the original

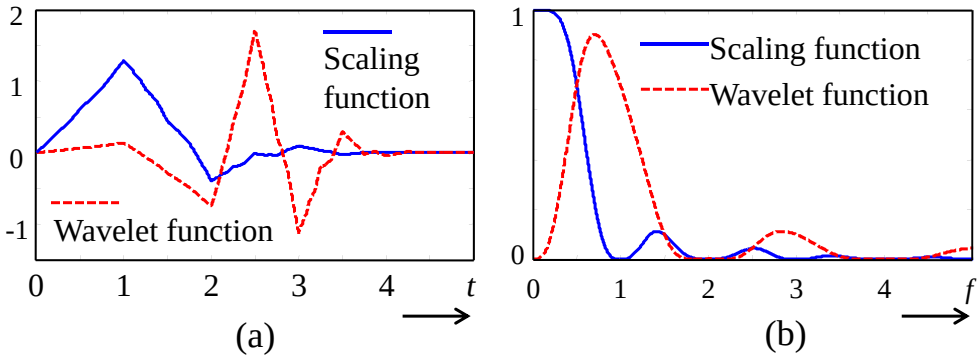

Figure 5.1.: The third order Daubechies scaling and wavelet function (a) and their Fourier transforms (b)

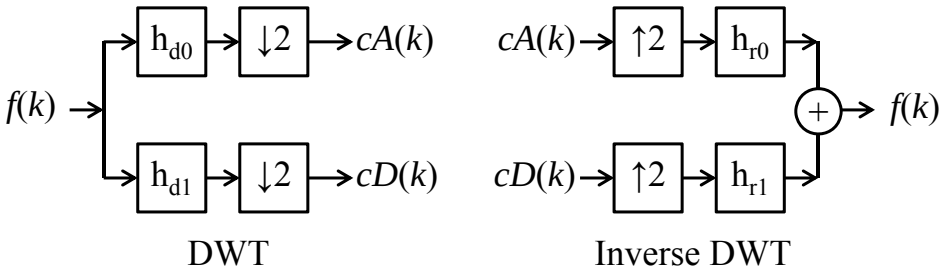

Figure 5.2.: DWT and inverse DWT calculation using filter banks

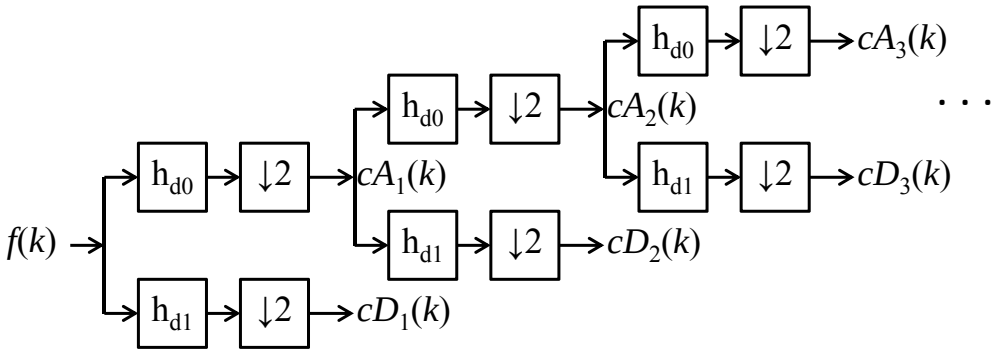

Figure 5.3.: Multi-resolution Analysis using DWT

sequence in two new series:

- the approximation coefficients, cA(k), representing the low frequency components, obtained using the low pass filter for decomposition, h_{d0}
- the detail coefficients, cD(k), representing the high frequency components, obtained using the high pass filter for decomposition, h_{d1}

The symbol ↓2 means down sampling. The operation is to delete one from every two adjacent coefficients, in order to remove the redundant information. The inverse DWT carries out the reversed operation. The operator, ↑2, expands a coefficient series by inserting a zero between every two adjacent elements. After that the two series pass through the filter bank, and added together to get the original signal.

Considering the DWT process shown in Fig. 5.2, sequence, cA(k), which represents the low frequency components can be further divided into a lower frequency part and a higher frequency part inside the frequency range of cA(k). This process is repeated and a series of coefficient sequences representing different frequency ranges is obtained, as shown in Fig. 5.3. This is the wavelet Multi-resolution Analysis (MRA). The outputs of this operation, cD1, cD2, . . . , cDn and cAn, are different levels of DWT coefficients, representing the signal components from higher to lower frequencies. Here the original signal is treated as the lowest level of approximation coefficients. This analysis provides a convenient tool to observe different frequency components of the signal depending on time.

Wavelet transform is a powerful tool in signal processing for the detection of changing events. This feature is suitable for fault detection since a fault in a system can be treated as a deviation compared to the normal state. When a fault occurs, specific changes will appear in the sensor signal. Usually, it is known that the fault signal is located in a certain frequency range, but the exact frequency is often unknown or not constant. This problem can be handled with wavelet MRA. For that, the signal containing fault information is firstly decomposed in several levels. And in one or more levels, where the fault signal frequency is located, faults features will be observed.

Modelica simulation and wavelet transform were selected for the quick design of a fault detection strategy for the power system in the MEA. Since wavelet transform is not available in the standard Modelica libraries, a wavelet toolbox was developed in [34]. It is expected to be a general Modelica library with wavelet transform and some related functionality for different signal processing purposes.

5.1.1. Description of fault analysis problem

The buck converter in Fig. 3.1 operates in constant load power mode by keeping a constant output voltage, which is adjusted through the duty cycle of the PWM switching signal, which operates with a constant frequency. Based on the converter property the system is sensible to the value changes of the components on the input side, where the input capacitor, C_{in}, is especially critical in industrial drives because it is usually an electrolytic type, which has significantly lower feasibility and shorter life time compared to other components. Based on this reason, the early fault detection is focused on C_{in}. If an electrolytic capacitor approaches it life end, its capacity would reduce slowly within a certain time. However, sharp reduction or changing of capacitance might also occur. For fault detection, especially for early stage fault diagnosis, both the stepping type and the slow changing of capacitor fault should be considered.

5.1.2. Extraction of fault information

The first step is the extraction of the fault information from the sensor signals. Supposing the measured signal is $f(k) = x(k) + g(k)$, where $x(k)$ is the signal in normal operation state, and $g(k)$ the additional signal in fault condition. Using the wavelet technology, the sensor signal $f(k)$ is decomposed with MRA using wavelet function, to obtain wavelet coefficients in n levels:

$$\begin{aligned} \mathrm{DWT}_\psi\{f\} &= A_n\{f\} + \textstyle\sum_{i=1}^{n} D_i\{f\} \\ &= A_n\{x\} + A_n\{g\} + \textstyle\sum_{i=1}^{n}(D_i\{x\} + D_i\{g\}) \end{aligned} \tag{5.3}$$

where $D_i\{\}$ represents the detail coefficients, and $A_i\{\}$ stands for approximation coefficients. The term $D_i\{\}$ with smaller index i, represents higher frequency components, namely faster changing signals. The signal x in the normal operation condition is composed of the average value of the input current, which changes very slowly, and the ripples caused by the PWM controlling, which have a constant frequency defined by the controller. The slower components are transformed to the approximation coefficients, $A_n\{x\}$; and the components with PWM frequency, which are higher frequency components, are transformed to the very low level of $D_i\{x\}$. On the other hand, the fault signal, i.e. the information of the reduction of C_{in}, is reflected by the fluctuation of the input current. As it is known that the fluctuation frequency is actually the PWM frequency, most of the fault information is contained in the PWM components, which means the lower levels of detail coefficients, $D_i\{g\}$. Depending on the fault occurrence rate, complex fluctuations could take place. This

information will be carried by the PWM frequency, too, but its own frequency components are visible in other levels of $D_i\{g\}$. In any circumstance few information will be present in the low frequency range, i.e. in $A_n\{g\}$. Therefore, we can extract the fault information from the input current signal simply by isolating some levels of detail coefficients, $D_i\{f\}$. Of course, the PWM information will also be involved. It has to be removed before the faults can be identified. Since this frequency is known and it always has a very high value, these components can be easily suppressed with low pass filter or band stop filter. After all irrelevant information is excluded the final fault information is represented with a single value, changing according to the failure rate. The fault can be simply identified by comparing it with a known threshold.

5.1.3. Process for simulation and fault detection

As mentioned in the problem description the input current signal is used for fault detection. At first the model will be simulated with different reduction rates of the C_{in} capacitance. The reduction rates were selected between 1 and 100 ms with a capacitance drop from 10 to 8 μF, corresponding to 20% capacitance loss. With this fault level the system can still operate normally. However, a 20% reduction indicates a high possibility of a complete failure of the capacitor in the near future. The reduction is applied at 0.1 s after the startup of the simulation so that the system can achieve a stable state before the faults could occur. After simulation, the data segment containing the fault event will be read out from the simulation result data file. It is converted to equidistant time series with a sampling rate of 200 kHz. Equidistant sampling is the requirement of wavelet transform and most other signal processing methods. The fault detection process is illustrated in Fig. 5.4 .

To simulate the real world, a white noise signal with normal distribution is added on the input current signal. After that, MRA is applied on the data. The wavelet function used here was the third order Daubechies function shown in Fig. 5.1. The detail coefficients in the DWT result are extracted and their absolute values are calculated since only the magnitude of the DWT coefficients contains fault information. To remove the high frequency PWM component, a second order Butterworth low pass filter is used. The filter cut off frequency is set as 0.5 kHz, much lower than that of the PWM frequency, in order to suppress a large part of the noise signal, too. After this step, different fault features can be visually identified and suitable fault detection methods can be established.

5.1.4. Results of wavelet analysis

Tests with different values were carried out. Fig. 5.5 and Fig. 5.6 give two examples with fast and slow changing faults, respectively. Since all fault features are mainly present in the first three levels of the wavelet decomposition, only these coefficients are shown in the figures. It was noticed that the fault features differed significantly between fast and slow changing rates. For the changing rates faster than 5 ms, a pulse feature appeared in almost every level of the wavelet detail coefficients. This

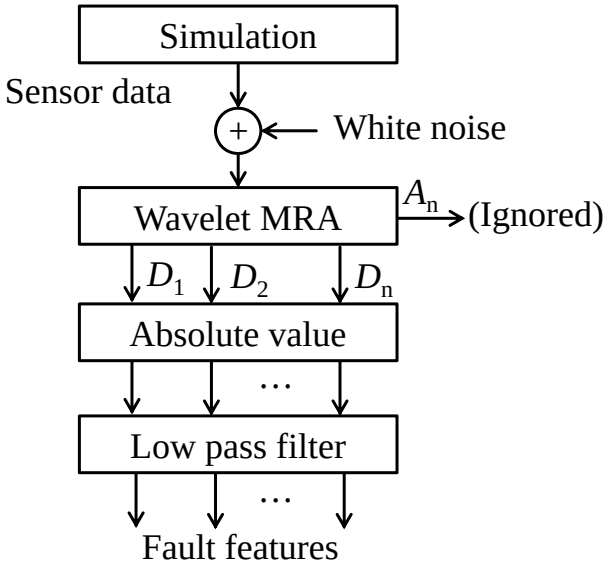

Figure 5.4.: Process for simulation and fault detection using wavelet transform

is well seen in Fig. 5.5, where 20% capacitance drop took place within 1 ms and the plotted signals in subfigures are, a: capacitance value C_{in}; b: input current I_{in}; c-e: wavelet coefficients in MRA from Level 3 to 1; f-h: fault features contained in detail wavelet coefficients of level 3 to 1. In the first MRA level the feature magnitude changed from 55 to 70 mA with the fault. In the other two higher levels the fault event was extra present with pulses. The magnitude of the pulses increased with the changing rate. The pulses appeared in other higher decomposition level, too. However, in level three it was significantly higher than those in other levels. For the fault with 1 ms dropping time, as shown in Fig. 5.5, the pulse peak reached almost 100 mA in level 3. The simulation showed that for the dropping time up to 5 ms, the peak height reduced linearly to about 20 mA. For the changing rates slower than 5 ms, the fault features were only significant in the lowest level of the wavelet MRA coefficients. Fig. 5.6 shows an example, where the 20% capacitance drop took 100 ms and the plotted signals in subfigures are, a: capacitance value C_{in}; b: input current I_{in}; c-e: wavelet coefficients in MRA from Level 3 to 1; f-h: fault features contained in detail wavelet coefficients of level 3 to 1. Now, only the first wavelet decomposition level contained a fault feature: the feature magnitude changed from about 55 to 70 mA linearly with the reduction of the capacitance. This was the same as the level 1 feature in fast changing faults. For even lower changing rates this linear relationship was always present. Not like in the case of fast changing fault, no significant features were observed in other decomposition levels. Based on the simulation study, the following fault detection strategy can be defined for early stage fault detection of the input capacitor C_{in}:

- In wavelet decomposition level one, if the feature magnitude exceeds 70 mA, a capacitance reduction of 20% of C_{in} is detected.

- In wavelet decomposition level three, if the pulse value exceeds 20 mA, the event implies a fast drop of the C_{in} capacitance. The pulse peak value could be used to estimate the capacitance changing rate.

5.2. Multi-model based fault detection technique

As demonstrated in Sec. 5.1, the signal based approach for fault detection has several drawbacks, e.g. difficult to deal with slow fault process and unsuitable for multi-fault cases. In contrast, a model based fault detection approach can give more possibilities. Reviewing the considerable development of fault diagnosis techniques and many successful applications attached to them in the last time [35, 20], power systems seem to be a real hard challenge for the available fault diagnosis techniques. In spite of a few applications of neural networks for fault detection in power systems [105], the application of analytical model-based fault detection for power systems is just in the beginning phase. With the help of more accurate modeling of power systems and embedded microprocessors in digital controllers of power distribution systems within the MEA, an unprecedented affordable opportunity can be provided for health monitoring and fault diagnosis using model-based fault diagnosis techniques. To the best knowledge of the author, few studies for health monitoring of power systems using multi-model based approach have been given before in literature.

A model based fault diagnosis system, as the one presented in Fig. 5.7 processes the measurable signals $Y(t)$, $U(t)$ and produces information on the fault occurrence and localization. The main component of the fault diagnosis system is the residual generator, which produces the residual signals $R(t)$ using the available measurements $Y(t)$ and the known values of control inputs $U(t)$ in the form

$$R(t) = Q(t) \begin{bmatrix} Y(t) \\ U(t) \end{bmatrix} \tag{5.4}$$

The residual generator is implemented on-line and generates the values of residuals in real time, which are then used to decide on the absence or presence of faults. For decision making, the residuals are further processed to obtain the evaluation signal.

Traditional fault detection as well as isolation technologies, unknown-input observers, parity space, principle component analysis, $\mathcal{H}_2$ and $\mathcal{H}_\infty$ optimal filter synthesis techniques are mentioned in [20, 47]. Among them the model based fault detection technique including diagnostic observer and parity space can be concluded to a unifying paradigm - nullspace based approach [109, 111]. A general framework of fault detection and isolation is depicted in Fig. 5.7, where actuator input and sensor output are required by a residual generator for the faults occurring on actuators, sensors defined as additive fault and parametric faults defined as multiplicative fault on plant.

5.2.1. Modeling of faults

A main non-trivial task to be fulfilled before solving various fault detection problems is the development of adequate models, which fit into the available design method-

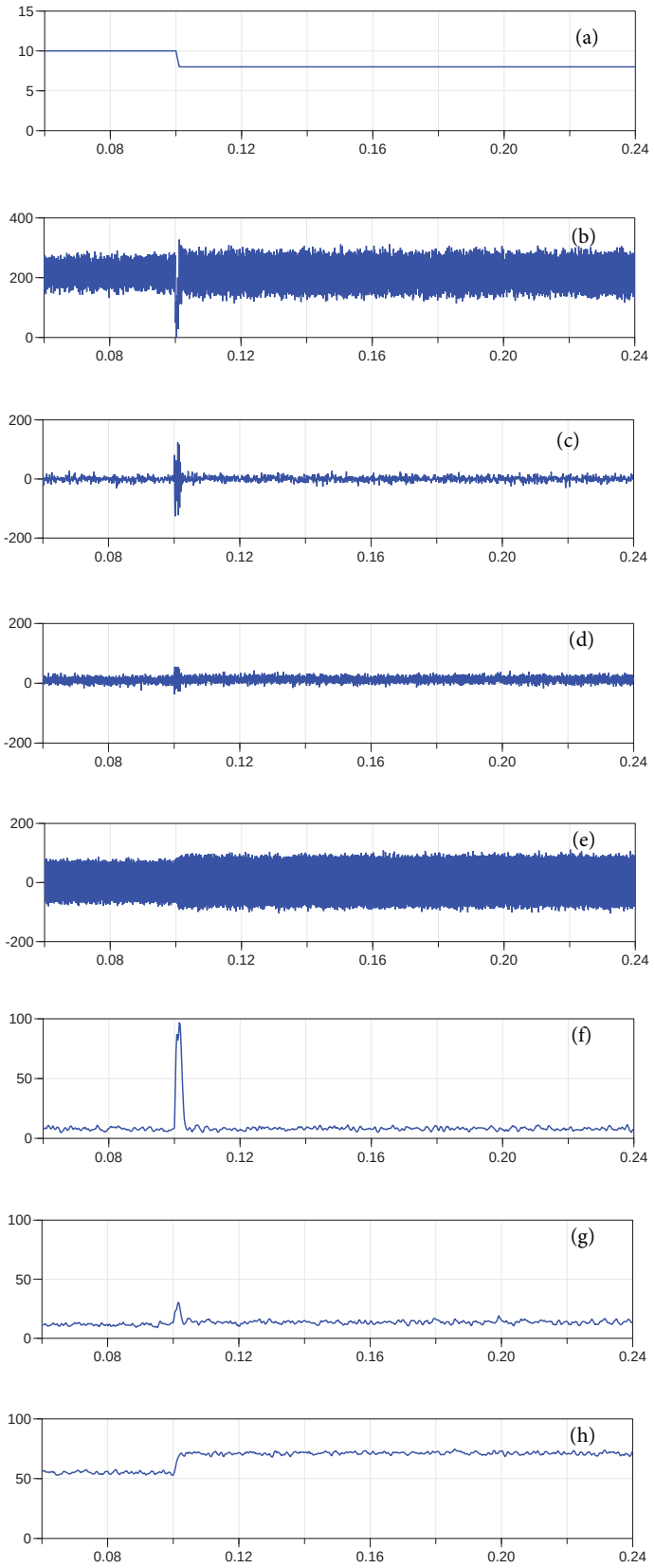

Figure 5.5.: The wavelet analysis result of a fast capacitance drop within 1 ms (time unit is [s])

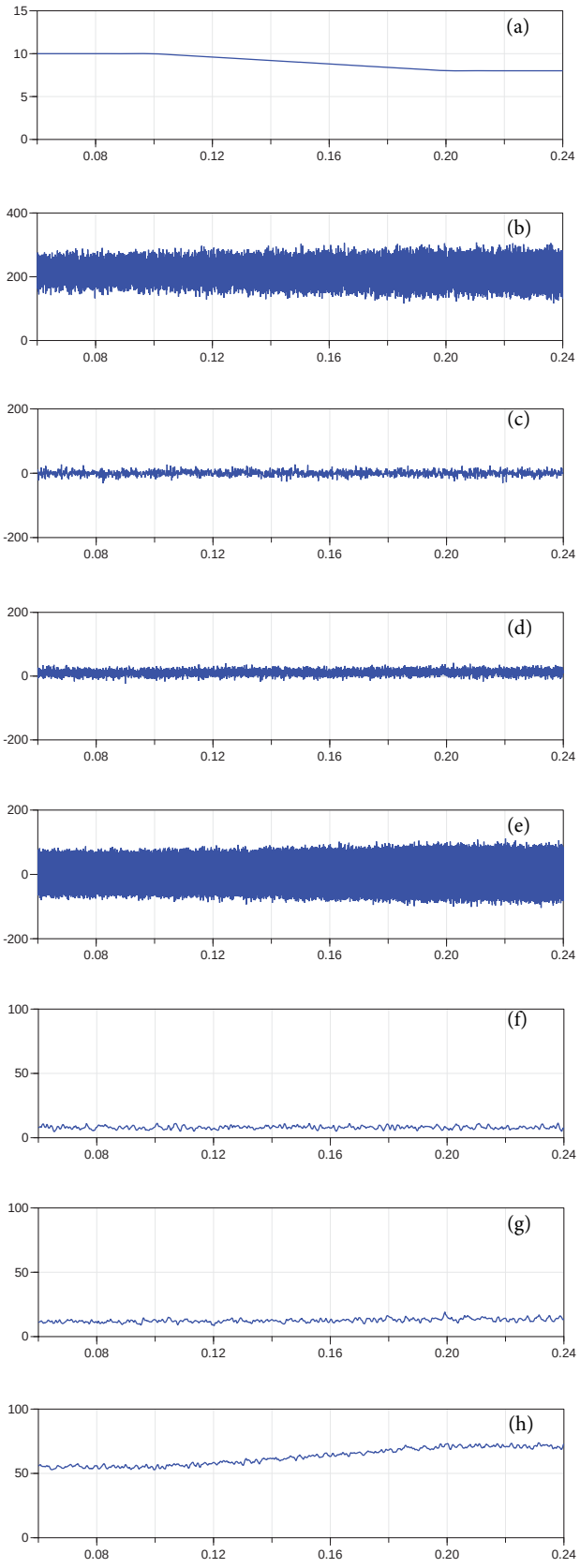

Figure 5.6.: The wavelet analysis result of a slow capacitance drop within 100 ms (time unit is [s])

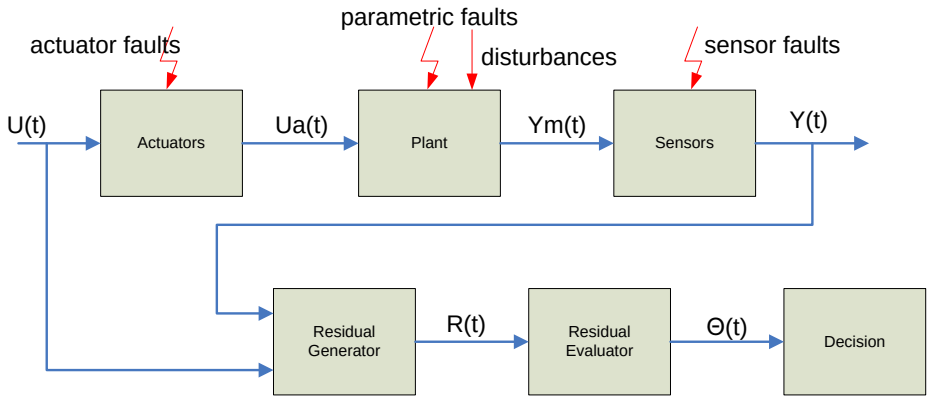

Figure 5.7.: General framework of fault detection and isolation according to [111]

ologies. The multi-model based approach associates to each fault a corresponding model, which is derived by adjusting appropriately the non-faulty system model to a particular fault situation. For example, this can involve setting the model parameters to some particular values, removing some of the system control inputs or measured outputs, defining new disturbance inputs to account for the potential effects of the respective fault, or combinations. The result of this approach is a so-called multi-model, a collection of individual models, where each model corresponds to a specific fault situation. The fault detection is becoming a model detection problem. The multi-model based approach for fault modeling has certain popularity in addressing fault tolerant control applications, where the detection of the right fault model automatically triggers the reconfigurations of the controller. Considering the multi-model linear time-invariant systems described by input-output transfer functions

$$y^{(i)}(\lambda) = G_u^{(i)}(\lambda)u(\lambda) + G_d^{(i)}(\lambda)d(\lambda) \quad i \in [0, N] \tag{5.5}$$

where the vector $y^{(i)}(\lambda)$, $u^{(i)}(\lambda)$, $d^{(i)}(\lambda)$ are Laplace or Z-Transformed vectors of i^{th} system output $y(t)$, control input vector $u(t)$, and disturbance vector $d(t)$. $G_u^{(i)}(\lambda)$ and $G_d^{(i)}(\lambda)$ are the transfer function matrices from the corresponding plant inputs to outputs. Assuming that all models are controlled with the same control inputs, the disturbance inputs can be different for each component model. The state-space realizations corresponding to the multi-model in Eq. 5.5 are in the form:

$$\begin{aligned} \lambda x^{(i)}(t) &= A^{(i)}x^{(i)}(t) + B_u^{(i)}u(t) + B_d^{(i)}d(t) \\ y^{(i)}(t) &= C^{(i)}x^{(i)}(t) + D_u^{(i)}u(t) + D_d^{(i)}d(t) \end{aligned} \tag{5.6}$$

where $x^{(i)}(t)$ is the state vector of the i^{th} system. $x^{(i)}(t)$ and $x^{(j)}(t)$ have generally different dimensions for $i \neq j$. The fault-free system can be defined by the model with index $i = 0$. The above description of the faults is a very general way to account for all categories of parametric faults. Let θ be a parameter vector, whose components are model parameter which characterize different fault situations, the system model depending on θ can be described with

$$y(\lambda) = G_u(\lambda, \theta)u(\lambda) + G_d(\lambda, \theta)d(\lambda) \tag{5.7}$$

Let $\theta^{(i)}$, $i \in [0, N]$ be a set of values, which characterize the normal operation without fault for $\theta^{(0)}$ and the i^{th} fault situation for $\theta = \theta^{(i)}$. The multi-model defined in Eq. 5.5 can be represented as

$$\begin{aligned} G_u^{(i)}(\lambda) &= G_u(\lambda, \theta^{(i)}) \\ G_d^{(i)}(\lambda) &= G_u(\lambda, \theta^{(i)}) \end{aligned} \tag{5.8}$$

Assuming that the state-space realization corresponding to Eq. 5.6 has the form:

$$\begin{aligned} \lambda x(t) &= A(\theta)x(t) + B_u(\theta)u(t) + B_d(\theta)d(t) \\ y(t) &= C(\theta)x(t) + D_u(\theta)u(t) + D_d(\theta)d(t) \end{aligned} \tag{5.9}$$

Eq. 5.6 can be defined by setting $A^{(i)} = A(\theta^{(i)})$, $B_u^{(i)} = B_u(\theta^{(i)})$, $C^{(i)} = C(\theta^{(i)})$,$D^{(i)} = C(\theta^{(i)}), \cdots$. In practical applications, e.g. an electrical network, the underlying system model is a nonlinear state-space model, which depends explicitly on the parameters. A linearized parametric model of the form in Eq. 5.9 is usually not available. A multi-model with matrices defined in Eq. 5.10 can be easily achieved using repeated linearization of the underlying nonlinear model for the selected values of the parameter $\theta^{(i)}$ on the corresponding operating point in steady state.

5.2.2. Algorithm for solving the multi-model based fault detection problem

Assuming that $N + 1$ models describe the normal and faulty systems. i^{th} model with $i \in [0, N]$ is specified in the input-output form Eq. 5.5, where the model with index 0 represents the model without faults. The model detection problem can be formulated as follows: determine a bank of $N + 1$ stable and proper scalar output residual generators

$$r^{(i)}(\lambda) = Q(\lambda) \begin{bmatrix} z(\lambda) \\ u(\lambda) \end{bmatrix} \quad i \in [0, N] \tag{5.10}$$

such that

- $r^{(i)}(t) = 0$ when $z(t) = y^{(i)}(t)$
- $r^{(i)}(t) \neq 0$ when $z(t) = y^{(j)}(t)$ for $i \neq j$
- all residual signals $r^{(i)}(t)$ are asymptotically bounded

The formulation of the model detection problem allows an easy detection of the actual model by simply looking for the residual signal with the smallest magnitude. The requirements formulated for the model detection problem can be easily expressed in equivalent algebraic design conditions for each of the $N + 1$ residual generators. The first condition is equivalent to determine each detector $Q^{(i)}(\lambda)$ so that

$$Q(\lambda) \begin{bmatrix} G_u^{(i)}(\lambda) & G_d^{(i)}(\lambda) \\ \mathbf{I} & \mathbf{0} \end{bmatrix} = 0 \tag{5.11}$$

The second condition enforces the unambiguous detection of the i^{th} model by additionally requiring that

$$R_f^{(i,j)}(\lambda) := Q(\lambda) \begin{bmatrix} G_u^{(j)}(\lambda) & G_d^{(j)}(\lambda) \\ \mathbf{I} & \mathbf{0} \end{bmatrix} \neq 0, when\ i \neq j \tag{5.12}$$

Subtracting Eq. 5.11 from Eq. 5.12, $R_f^{(i,j)}(\lambda)$ can be interpreted as a weighted measure of the distance between the i^{th} and j^{th} model. It follows that the i^{th} detector will produce a residual signal whose amplitude depends on the difference between the outputs of the actual model and those of the i^{th} model. To fulfill the third requirement, each detector $Q^{(i)}(\lambda)$ must ensure that all $R_f^{(i,j)}(\lambda)$ are stable transfer function matrices. If the model detection problem is solvable, each residual generation filter $Q^{(i)}(\lambda)$ can be computed as a scalar output filter lying in the left nullspace of the transfer function matrix $G^{(i)}\lambda$ with

$$G^{(i)}\lambda := \begin{bmatrix} G_u^{(i)}(\lambda) & G_d^{(i)}(\lambda) \\ \mathbf{I} & \mathbf{0} \end{bmatrix} \tag{5.13}$$

A global detector band can be built by stacking the N+1 scalar output residual generators as

$$\mathbf{Q}(\lambda) := \begin{bmatrix} Q^{(0)}(\lambda) & Q^{(1)}(\lambda) & \cdots & Q^{(N)}(\lambda) \end{bmatrix}^T \tag{5.14}$$

Let $\mathbf{Q}(\lambda)$ be a given detector and let $R_f(\lambda)$ be the corresponding transfer matrix from i^{th} model to j^{th} residual signal. Denoting the (i,j) entry of $R_f(\lambda)$ as $R_{f,ij}(\lambda)$, the fault signature matrix S can be defined with the (i,j) entry - S_{ij} given by

- $S_{ij} = 1$ if $R_{f,ij}(\lambda_s) \neq 0$
- $S_{ij} = -1$ if $R_{f,ij}(\lambda_s) = 0$ and $R_{f,ij}(\lambda) \neq 0$
- $S_{ij} = 0$ if $R_{f,ij}(\lambda_s) = 0$

where $\lambda_s = 0$ for a continuous-time system and $\lambda_s \neq 0$ for a discrete-time system. If $S_{ij} = 1$, the model j is strongly detectable in residual i. If $S_{ij} \neq 1$ the model j is weakly detectable in residual i. The model j is decoupled and not detectable from residual i , if $S_{ij} = 0$. Therefore, considering the conditions of residual filter, only entries in the diagonal of the signature matrix are desired to be zero.

5.2.3. Residual evaluation and decision making

When the residual signal is just weakly detectable, a correct fault detection will become difficult or not possible alone with the information of the residual signal. In such a case, the residual evaluator is usually needed to generate an evaluation signal $\Theta(t)$ in Fig. 5.7 , which is an approximate measure of the residual signal energy (e.g. of the 2-norm). The evaluation signal can be generated by

$$\Theta(t) = \alpha r^2(t) + \beta \int_{t-T}^{t} r^2(\tau) d\tau \tag{5.15}$$

Where the parameters α and β allow a desired weighting between instantaneous and long-term measures, T defines the duration of observation windows [41]. The decision making function has a binary output $d = 0$ or $d = 1$, which is computed with the residual evaluation signal in such manner that

$$\begin{aligned} \Theta^{(i)}(t) \geq J_{th} &\Rightarrow d_{(i)}(t) = 1 \\ \Theta^{(i)}(t) < J_{th} &\Rightarrow d_{(i)}(t) = 0 \end{aligned} \tag{5.16}$$

where J_{th} is a threshold value. In the case of model detection, the signal $d_{(i)}(t)$ is called model index, which indicates the best fitting model to the plant, i.e. the present fault situation.

5.2.4. Design process of residual generator

A main task to solve the fault detection and isolation problem using a multi-model based approach is the design of a residual generator. The design process contains typically following procedures:

- appropriately modelling of the system with faults
- linearization of the original nonlinear systems after trimming
- synthesis of the residual filter bank
- design of the residual evaluator, if required
- design of the decision maker, i.e. setting threshold, if required

The tool chain for the design of residual generator in the presented work is depicted in Fig. 5.8

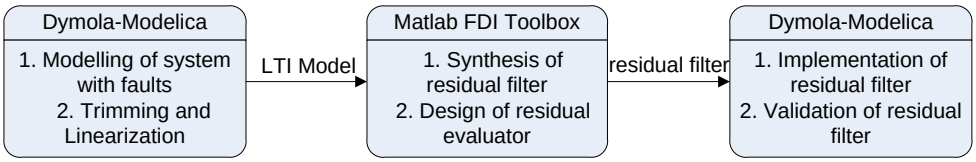

Figure 5.8.: Road map and tool chain for Fault Detection using nullspace approach

5.2.5. Toolbox for design of fault detection residual generator

The fault detection and isolation toolbox for MATLAB (FDI) developed by DLR provides a comprehensive set of high level m functions to support the design of residual generation filters using reliable numerical algorithms [110]. In the toolbox, a fairly complete collection of methods, solving various fault detection problem have several common appealing properties: applicable to both standard and descriptor

system, appropriate filter dynamics specification and least-order filter design. The reason for the interest in the low and least order property of the residual generator is primarily that the dependency of a residual generator on the model should be as little as possible. A low order usually implies that only a small part of the model is utilized for the residual generator design. This means that few model errors will affect the residual signal, since all parts of the model have errors such as modeling error and linearization error. The further advantages of low order residual generators are easier implementation and less on-line computational burden [32].

5.3. Applying the multi-model based approach for the health monitoring design[1]

In the present HVDC architecture, electro-mechanical actuators are connected with DC link network, where DC/AC inverter are used to tightly regulate the motor current waveforms. Besides the benefits on this architecture such as full decoupling between turbine speed and load speed and increased motor robustness preventing over currents, mostly perfect regulation has also the disadvantage that it makes the motor drive appear to be a constant power load which has a negative impedance at low frequencies [65]. Considering the highly simplified model of the motor drive with an input filter in Fig. 5.9, where L_f, R_f, C_f are inductor, resistor and capacitor of the input filter and P^* is the motor load power at steady state, the impedance Z_{inv} of the motor by linearizing the input current i_{dc} regarding the input voltage V_{dc} can be described by

$$Z_{inv} = -\frac{P^*}{V_{dc}^{*2}}\Delta V_{dc} \tag{5.17}$$

Due to the negative impedance, the system can become unstable with an inadequate or degraded input filter. Using the eigenvalue of the linearized model of the electro-mechanical actuator, the necessary condition Eq. 5.18 for the stability of the system can be easily derived:

$$\frac{R_f}{L_f} > \frac{P^*}{C_f V_{dc}^{*2}} \tag{5.18}$$

When the motor power P^* keeps being constant, a degraded capacitor with decreased value can destabilize the system, the motor and power supply. Therefore, the function of the input filter in front of the DC/AC inverter within the EMA is twofold:

- power quality guarantee of HVDC main bus with regards to voltage and current harmonics
- stabilization of DC link network

Considering the significant cost benefit, an aluminum electrolytic capacitor is proposed to be used for the input filter. However, using an aluminum capacitor for the

[1] This section is an extended and improved version of [51]

input filter has an inherent disadvantage, that the DC network becomes more fragile concerning the possible capacitor failure due to aging, manufacturing defect, ware-out faults and so on [45]. The health monitoring of the capacitor in the input filter is therefore a new important task when designing the HVDC network architecture of the MEA in spite of an optimal pre-design regarding the system stability [64]. Early detection of this incipient type fault on the capacitor used in the input filter would allow preventive fail and maintenance to be performed, and provide sufficient time for the controlled shutdown of the process, thereby reduce the costs of outage-time and repairs.

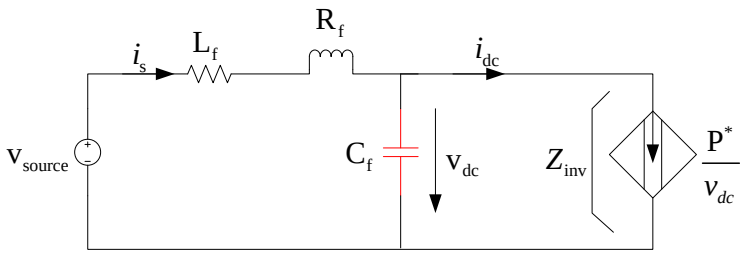

Figure 5.9.: A highly simplified DC motor model with input filter

5.3.1. Modeling of the health status

To undertake the health monitoring for the input filter of an EMA, a 2^{nd} order Butter-worth type filter and a DC motor drive are modeled in Dymola (Fig. 5.10). At steady state, the EMA can be seen as a constant power load with power P^*. Since a degraded capacitor usually exhibits a decreased capacitance value, the health

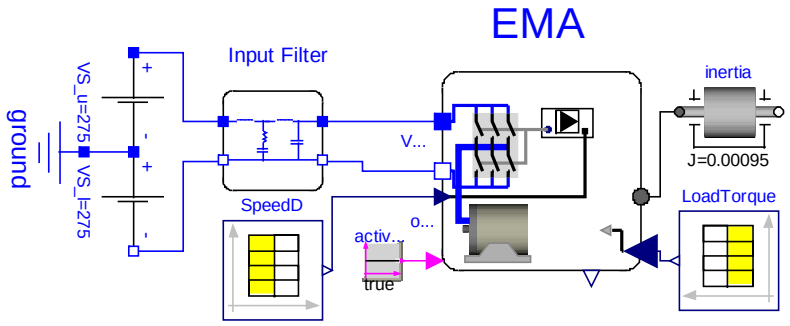

Figure 5.10.: The EMA Modell with the input filter in Dymola

status of the input filter can be modeled by assigning the capacitor with different capacitance values. For the sake of simple illustration, three health statuses $h_i, i \in (1, 2, 3)$ of the input filter have been defined by setting the capacitor in input filter such as

Table 5.1.: Parameters in the input filter of the EMA

Parameter	Description	Value
L_f	filter inductance	$3.24e^{-6}$ Henry
R_f	filter resistance	$2e^{-3}$ Ohm
C_f	filter capacitance	$420e^{-6}$ Farad
P^*	steady state motor power	4028 Watt

- h_1: $C_f = 5e^{-2}$ Farad, nominal system
- h_2: $C_f = 5e^{-3}$ Farad, degraded degree I
- h_3: $C_f = 5e^{-4}$ Farad, degraded degree II

Certainly, the proposed health monitoring scheme is also capable to deal with more degraded degrees. The capacitor in the input filter with degraded degree II is considered as a very critical situation, i.e. the stability boundary of the system. The capacitor in the input filter shall be immediately exchanged when degrade degree II arises. Denoting the DC main bus voltage V_{source} as the input u_r and the output current i_{dc} of the input filter as the output y_r of a LTI system, which are assumed as accessible, with the parameters in Tab. 5.1, the different health statuses defined above can be described by the following three LTI systems G_1, G_2, G_3 in Eq. 5.19-5.21.

$$\begin{aligned} \frac{d}{dt}\begin{pmatrix}\Delta i_s \\ \Delta V_{dc}\end{pmatrix} &= \begin{bmatrix}-616.3 & -2407 \\ 2560 & .276\end{bmatrix}\begin{pmatrix}\Delta i_s \\ \Delta v_{dc}\end{pmatrix} + \begin{pmatrix}4.7 \\ 0\end{pmatrix} u_{r1} \\ y_{r1} &= \begin{bmatrix}0 & -7.1\end{bmatrix}\begin{pmatrix}\Delta i_s \\ \Delta V_{dc}\end{pmatrix} \end{aligned} \tag{5.19}$$

$$\begin{aligned} \frac{d}{dt}\begin{pmatrix}\Delta i_s \\ \Delta V_{dc}\end{pmatrix} &= \begin{bmatrix}-616.3 & -9629 \\ 6400 & 2.76\end{bmatrix}\begin{pmatrix}\Delta i_s \\ \Delta v_{dc}\end{pmatrix} + \begin{pmatrix}9.4 \\ 0\end{pmatrix} u_{r2} \\ y_{r2} &= \begin{bmatrix}0 & -14.2\end{bmatrix}\begin{pmatrix}\Delta i_s \\ \Delta V_{dc}\end{pmatrix} \end{aligned} \tag{5.20}$$

$$\begin{aligned} \frac{d}{dt}\begin{pmatrix}\Delta i_s \\ \Delta V_{dc}\end{pmatrix} &= \begin{bmatrix}-616.3 & -1.9e^4 \\ 3.2e^4 & 27.6\end{bmatrix}\begin{pmatrix}\Delta i_s \\ \Delta v_{dc}\end{pmatrix} + \begin{pmatrix}18.8 \\ 0\end{pmatrix} u_{r3} \\ y_{r3} &= \begin{bmatrix}0 & -14.2\end{bmatrix}\begin{pmatrix}\Delta i_s \\ \Delta V_{dc}\end{pmatrix} \end{aligned} \tag{5.21}$$

5.3.2. Simulation results

The residual generator filter $\mathbf{Q}(s)$ for the multi-models in Eq. 5.19-5.21 is derived with the FDI toolbox, which is written as

$$\mathbf{Q}(s) = \begin{pmatrix} -\frac{5.65s^2+3.48e3s+3.48e7}{s^2+6.16e^2s+6.16e^6} & -\frac{4.8e5}{s^2+6.16e^2s+6.16e^6} \\ -\frac{5.65s^2+3.46e3s+3.48e7}{s^2+6.13e^2s+6.16e^6} & -\frac{1.13e-13s+4.8e5}{s^2+6.13e^2s+6.16e^6} \\ -\frac{1.72s^2+1e3s+1.05e9}{s^2+5.88e2s+6.16e8} & -\frac{1.46e5}{s^2+5.88e2s+6.16e6} \end{pmatrix} \tag{5.22}$$

The conducted signature matrix

$$S = \begin{pmatrix} 0 & -1 & -1 \\ -1 & 0 & -1 \\ -1 & -1 & 0 \end{pmatrix} \tag{5.23}$$

indicates, that the LTI models $G_1,\ G_2,\ G_3$ describing the predefined health statuses of the capacitor in the input filter, are only weakly detectable with the residual generators in Eq. 5.22. It means, that the residual signal will disappear at steady state. To solve this weakly detectable problem, a virtual test signal such as

$$\epsilon(t) = 0.01sin(20000\pi t) \tag{5.24}$$

has been introduced, which is added to the input u_r of the residual generator. The simulation results of the residual signals are plotted in Fig. 5.11. In order to explicitly perform a decision-making, a residual evaluator defined in Eq. 5.15 is applied, where $\alpha = 0$, $\beta = 2$ and $T = 0.05$. The residual evaluator signals are shown in Fig. 5.12. Setting the threshold $J_{th} = 1$, the decision-making signals $d_{(i)}(t)$ defined in Eq. 5.16 are shown in Fig. 5.13. Finally, the actual health status of the capacitor in the input filter of the EMA denoted with h^* can be determined by

$$h^* = h_i,\ \forall d_i(t) = 0,\ i \in 1, 2, 3 \tag{5.25}$$

As validation scenario, the degraded degree I and the degraded degree II of the capacitor have been activated at 3 second and 4.5 second, respectively. Fig. 5.13 shows, that the decision-making signals has correctly determined the present health status with a time delay of about 0.1 second, which will be allowed for a long-term health monitoring process.

5.4. Discussion

From the conducted studies in this chapter, the multi-model based approach is suitable for fault detection and long-term health monitoring. The wavelet technique provide an alternative way to solve the abrupt failure issue. The signal based approaches are easily applicable, fast and efficient and very robust against model uncertainty. Compared to the signal based approach, the model based approach has much more information of the plant to be monitored. As result, the system performance in the fault-free status would be always known for the health management

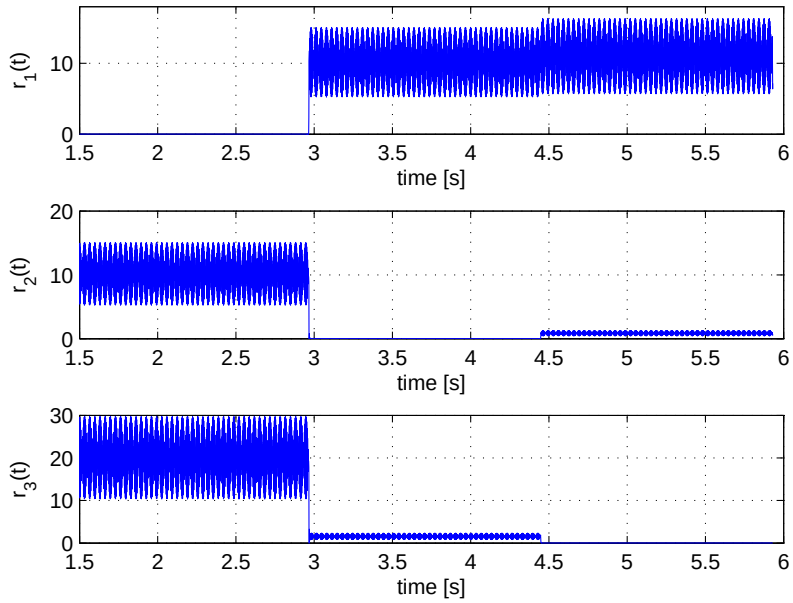

Figure 5.11.: Simulation results of the residual generators $\mathbf{r}(t)$ (time unit is [s])

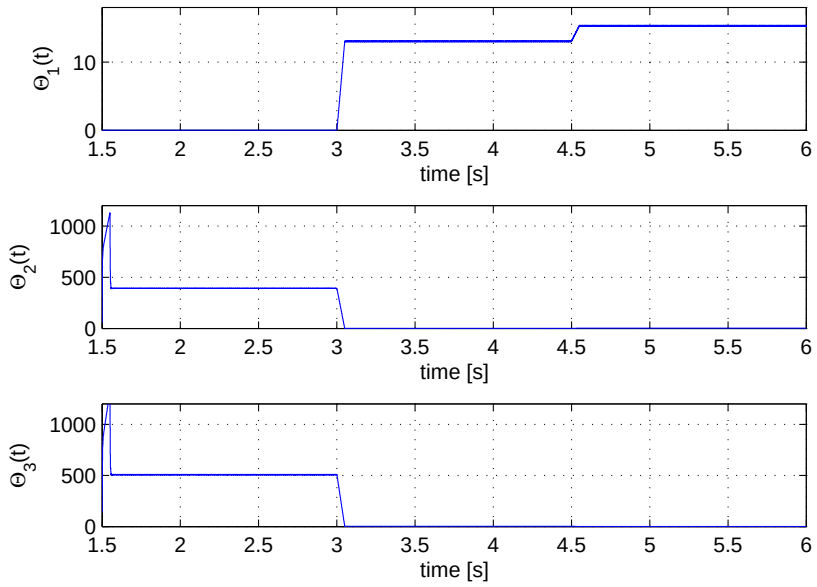

Figure 5.12.: Simulation results of the residual evaluators $\Theta(t)$ (time unit is [s])

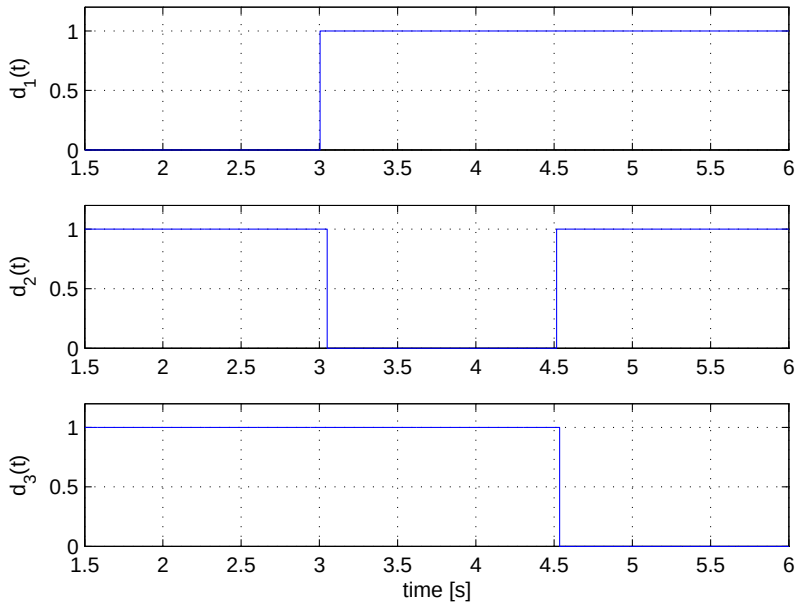

Figure 5.13.: Simulation results of the decision-making d(t) (time unit is [s])

system. The main disadvantage of the model based approach is the system uncertainty, which might lead to incorrect mathematical models during the operation. The main advantage of the hardware redundancy based fault diagnosis is simplicity and the ability for direct fault isolation. However, the hardware redundancy can only be applied to a number of key components due to the high costs. Furthermore, this scheme can not guarantee a successful fault detection, since a hardware redundancy based approach does not exactly know the fault-free performance of the process component and can fail if the majority of process components have faults.

6. Virtual testing for system verification and validation

While the previously proposed methods to test stability, power quality and failure performance can be successfully applied for component and even sub-system level, today the simulation based virtual testing is still the most efficient and proven method to validate the performance of integrated aircraft systems. For the MEA, the system integration testbed is a engineering tool used to incorporate, optimize and validate vital aircraft systems, such as electrical generation, distribution and flight control systems. There is a virtual integration of these systems, with each laid out in relation to the actual configuration of the aircraft, and all components installed at the same place as they would be on the real airframe. The virtual testing is becoming an indispensable method during the aircraft development process to confirm the characteristics of all system components, or to discover an incompatibility that may require modifications during early development stages. Additionally, the effects and subsequent treatments of failures introduced in the systems can be studied in full detail and recorded for analysis by using the virtual testing method. As result, the virtual integration platform for energy systems allows addressing integration issues prior to their physical integration on the test rigs and also extends test coverage.

6.1. General requirement

In the MEA, even more equipments and sub-systems including power electronic system, i.e. switching components have to be considered. Therefore, the advanced modeling and simulation approaches are the key factors for successfully building the virtual system integration platform and performing the virtual testing tasks, especially for large scale complex system such as the electrical power network in the MEA. There are some typical tasks, which shall be performed with virtual system integration platform during the system verification and validation design phase. Some typical tasks are

- frequency analysis
- steady state analysis
- parameter studies
- coherency analysis between simulation and hardware test
- special issues such as inrush current simulation

Obviously, the virtual testing that covers all electric power systems in MEA is very challenging. To deal with this job, special requirements in terms of methods and tools have to be fulfilled. First of all, component and system models shall be build at both functional and behavioral levels. Furthermore, to simulate complete aircraft power systems which are usually very stiff and suffering from huge amount of event handling actions due to switching components, the performances and robustness of solver have to be ensured. Since various analysis tasks such as harmonic analysis in frequency domain and stability analysis in time domain have to be done, tools for analysis and post-processing [52] are required. Finally, it should be possible to customize different test scenarios by scripting tools.

6.2. General test process

The total virtual testing process can be briefly divided into two steps. Before performing various simulations and tests of the total integrated system model, each subsystem or component model shall firstly be evaluated by a so-called component standalone test. A standalone test for one component usually consists of a bunch of tests such as power connection, power disconnection, power consumption at steady state, current harmonic analysis and so on. Standalone tests are required for both functional and behavioral models. Various virtual tests for the integrated systems can begin, once standalone tests for all components and subsystems are successful finished. Finally, based on the simulation results of the integrated models, specific analysis and post-treatment tasks can be performed .

6.3. Case studies

To present the virtual testing activities, four case studies are demonstrated here. The process of a component standalone test is presented by the ATU, where various tests and post-treatments are conducted. The second case study deals with modeling and simulation of the integrated power network, namely a large scale complex system. The inrush current and sympathetic effect analysis for auto-transformers are addressed in the third case study. Finally, the model validation process, i.e. the coherency tests, are described by means of the DCCU and the VFG.

6.3.1. Standalone tests for the ATU

A 230VAC/115VAC auto-transformer model depicted in Fig. 2.18 is used to demonstrate standalone tests for components. The tests considered here are harmonic current test, inrush current test, power connection and power disconnection test. The harmonic current analysis aims to determine pollution due to the equipment on different frequency levels. The fast Fourier transformation is performed when the simulation of the ATU model reaches steady state. The results for harmonic current analysis with system setup of 230V and 720Hz input voltage is depicted in Fig. 6.1. The result of an inrush current test which studies if the ATU may cause an

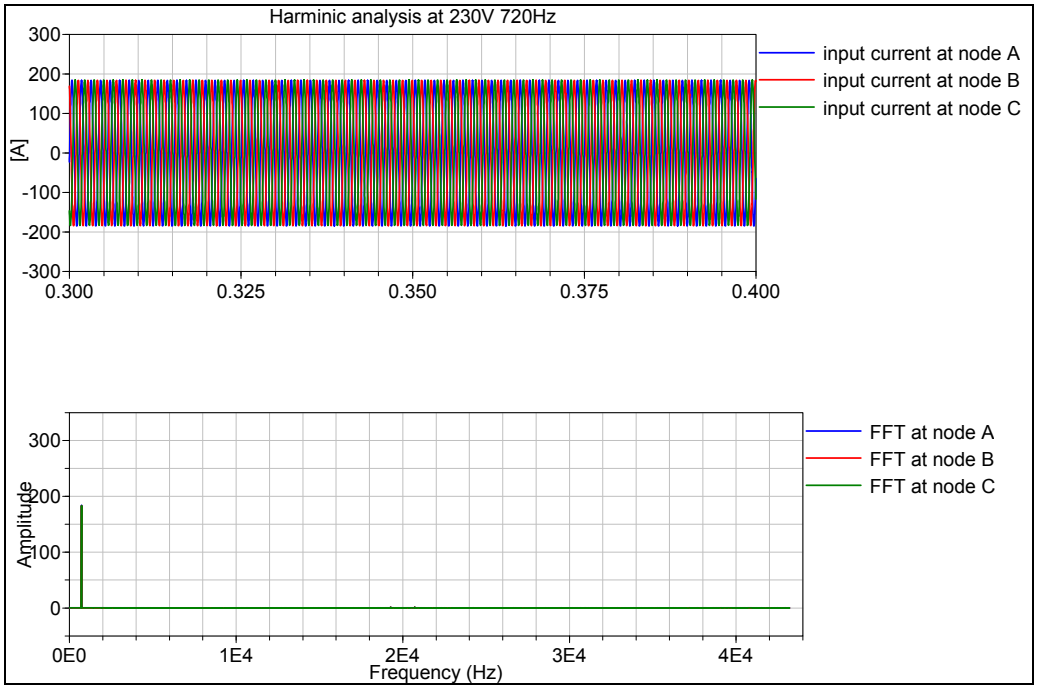

Figure 6.1.: Simulation results of input currents (time unit is [s]) and their FFT spectra in the current harmonic analysis of the behavioral ATU model with 230V and 720Hz input voltage

inadvertent trip at power up is presented by Fig. 6.2. Power load connection and disconnection tests whose results are depicted in Fig. 6.3 and 6.4 aim at checking if the ATU behavior at load connection and disconnection is compliant with the associated requirement.

6.3.2. Simulation of a large scale power network

After successful stand-alone tests for all components, various scenarios for testing the complete electric power network can be started. To demonstrate the capability of Modelica/Dymola to deal with large scale power systems, the proposed electric power network depicted in Fig. 6.5 has been simulated in Dymola. For the successful simulation of such a complex system, which is normally very stiff due to high frequency switching actions of the semi-conductor components, a proper initialization can be the key factor. Moreover, the event handling issue of the integrator has to be carefully solved. The integrated electric power network model including behavioral models of a VFG, an ATRU, an ATU, a DCCU, a PMSM and a 115V AC constant power load (CPL) is depicted in Fig. 6.5. In this electric power network, the ATRU is connect to grid at 0.0025 second. After the precharging ATRU with 25e-3 second, the DC output of the ATRU is connected with the HVDC power network. The PMSM which has a 20e-3 second precharging time is connected with the HVDC power network at 0.055 second. After the power inverter in the PMSM

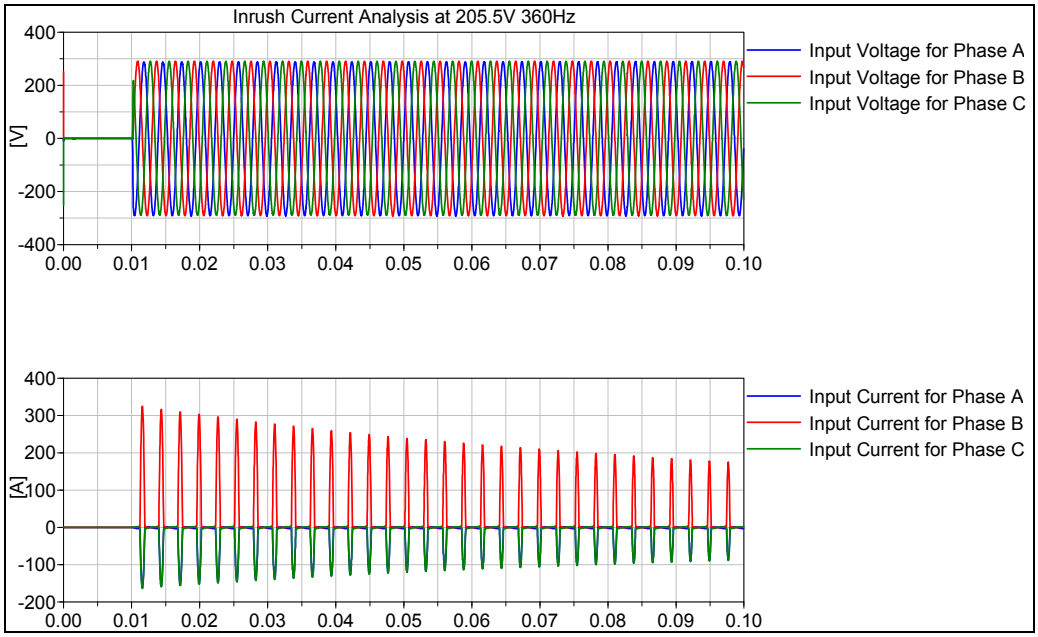

Figure 6.2.: Simulation results of output currents and POR voltages in the power load connection test of the behavioral ATU model with 205.V and 360Hz (time unit is [s])

is activated, a constant speed command is given for the PMSM under a constant load. The speed-up process of the PMSM presented by the input currents of PMSM, the output voltage from ATRU, the output AC currents and voltages of the VFG is recorded in Fig. 6.6 and Fig. 6.7 for the behavioral model and in Fig. 6.8 and Fig. 6.9 for the functional model. In the simulation results, the inrush currents are clearly seen at the moment of switching on ATRU and DC ripple at the ATRU output. These values are very important indicators for the electric power network in the MEA [65]. The result of this case study proves the capability of the Modelica based tool to perform simulation tasks of very complex large scale power systems.

6.3.3. Modeling and simulation of inrush current in power transformers

A typical power network architecture in the MEA contains an 18-pulses ATRU which transfers 230V AC voltage to 540V DC voltage supplying DC loads such as the electric environmental system, 230V/115V AC auto-transformers and electric actuators. It is well know, that a potentially disruptive transient condition may occur when an unloaded transformer, e.g. ATRU or ATU unit, is connected to the power systems. Under certain conditions, a transient inrush current, several times the rated value, may result in the mal-operation of overload/fault relays with the consequence of disconnecting the transformer from the power system. This phenomenon has to be comprehensively understood to ensure and determine the system reliability in

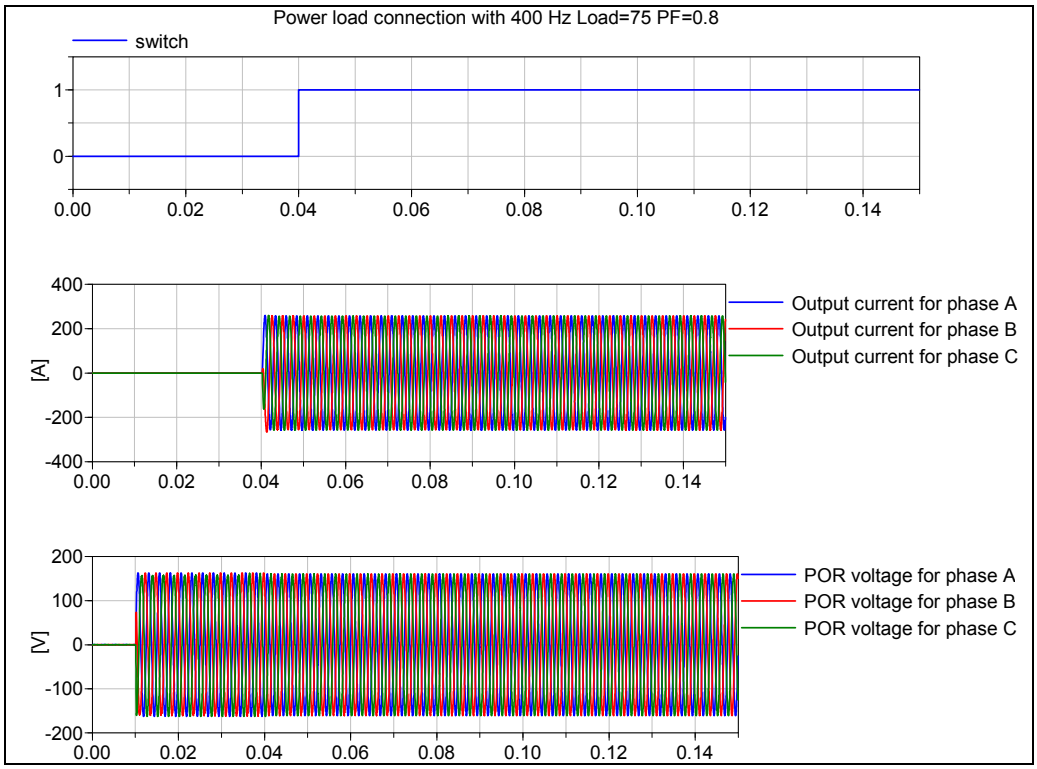

Figure 6.3.: Simulation results of output currents and POR voltages in the power load connection test of the behavioral ATU model with 75% load and 0.8 power factor (time unit is [s])

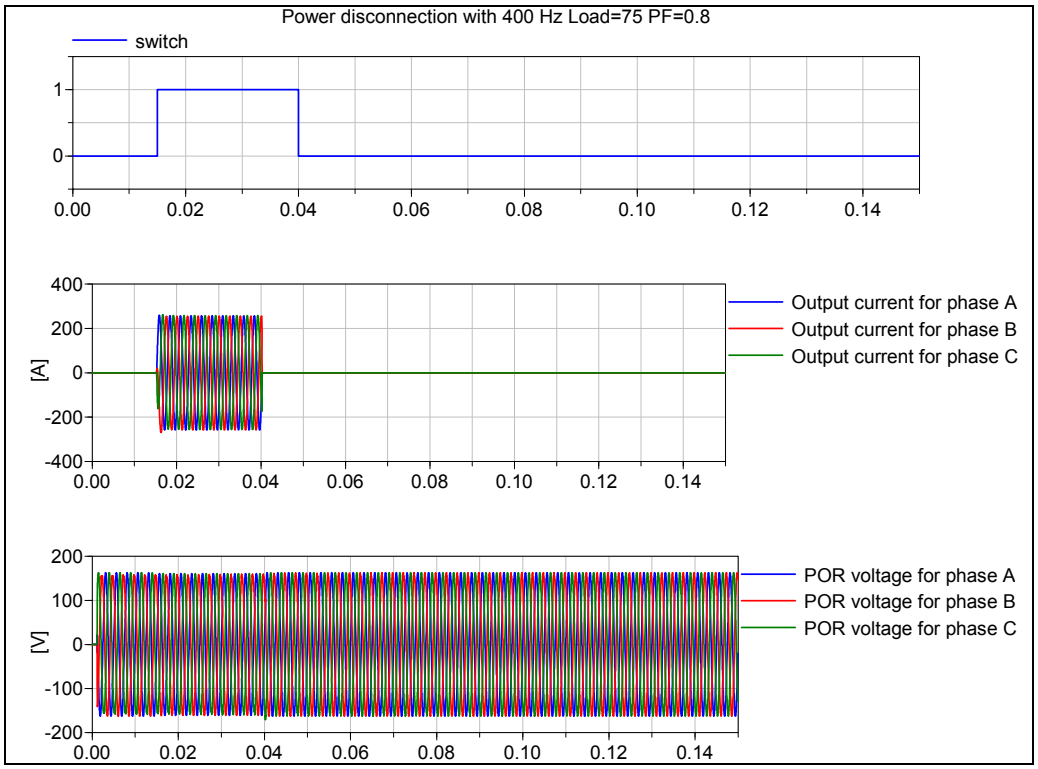

Figure 6.4.: Simulation results of output currents and POR voltages in the power dis-connection test of the behavioral ATU model with 75% load and 0.8 power factor (time unit is [s])

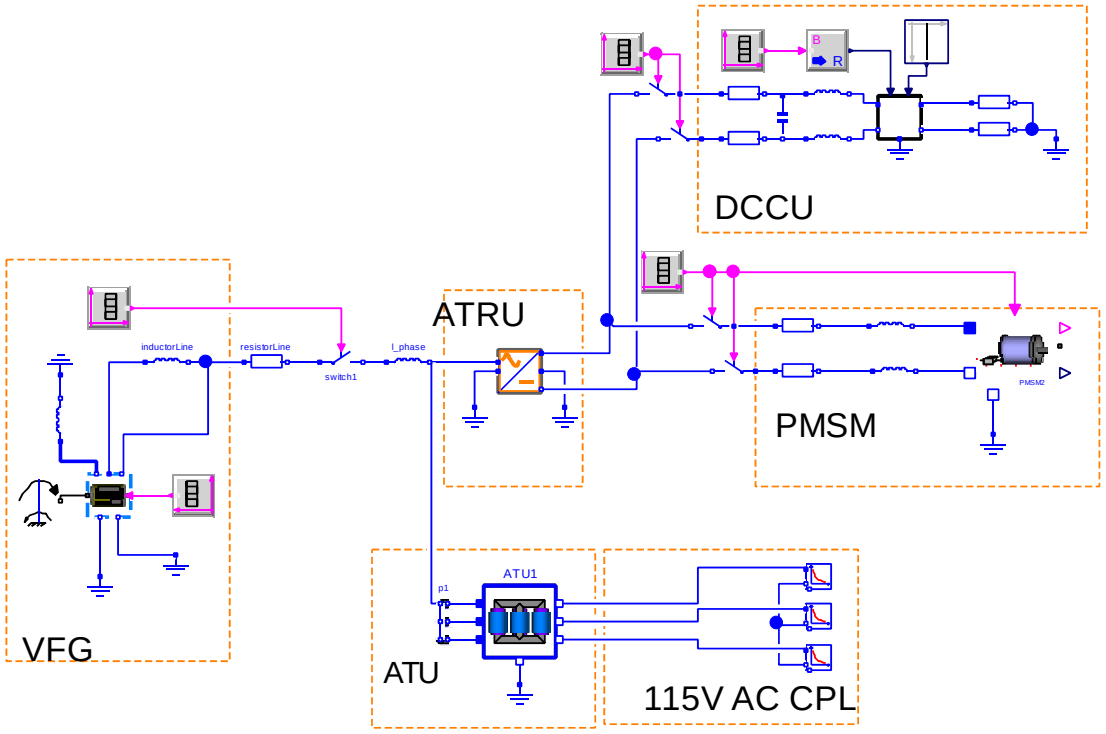

Figure 6.5.: An integrated electric power network for the MEA

the MEA energy system. This case study utilizes the Modelica language to build physical models of power transformers in the MEA to perform a thorough analysis for the inrush current effects in the power transformers. Concretely, the power on test of a single unloaded auto-transformer and the sympathetic effect of parallel connected auto-transformers have been treated.

Inrush current test for auto-transformer

When doing inrush current studies for power transformers, attention traditionally has been paid on overload and short-circuit operations only. However, the connection of unloaded transformers to a power system also may result in a transient inrush current several times of the rated value. Concerning the design and test of such a complex electrical network for the MEA, the inrush current effects e.g. the magnitude and the interactive behaviors have to be comprehensively studied. Those kinds of challenging tasks now can be easily done by the advanced magnetic circuit models together with a complete aircraft power system virtual testbed [57]. To check out the inrush current performance when connecting an unloaded 3 phase auto-transformer to a power network, the ATU model depicted in 2.18 has been used. An AC power source can be modeled by a sinusoidal voltage model from the Modelica standard library. The complete test bench is depicted in Fig. 6.10. The geometric parameters for the ATU can be seen in Fig. 2.17. The simulation results with AC source voltage 360Hz and 205V is presented in Fig. 6.11, where 3 phase input voltages and input

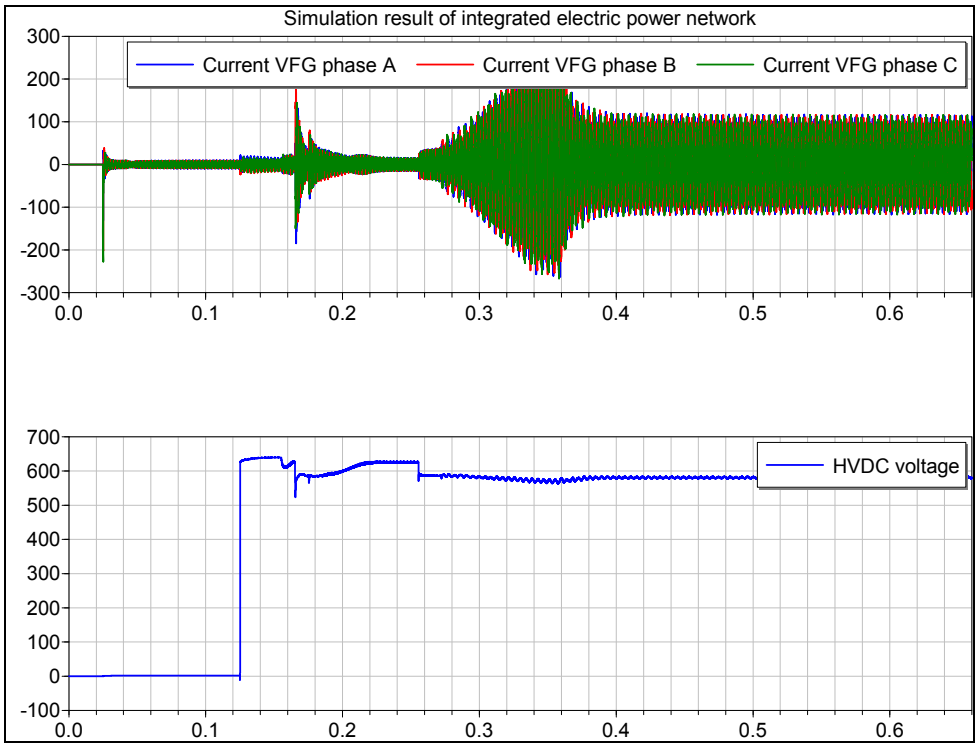

Figure 6.6.: Simulation results of VFG phase currents and HVDC net voltage in the integrated electric power network test at behavioral level (time unit is [s])

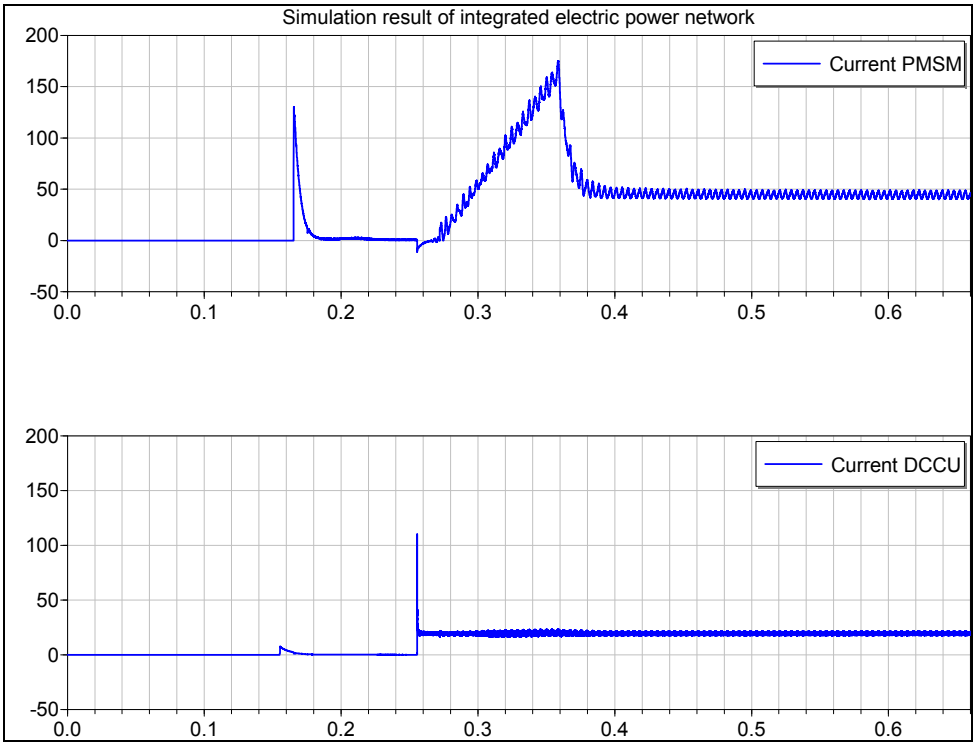

Figure 6.7.: Simulation results of PMSM current and DCCU current in the integrated electric power network test at behavioral level (time unit is [s])

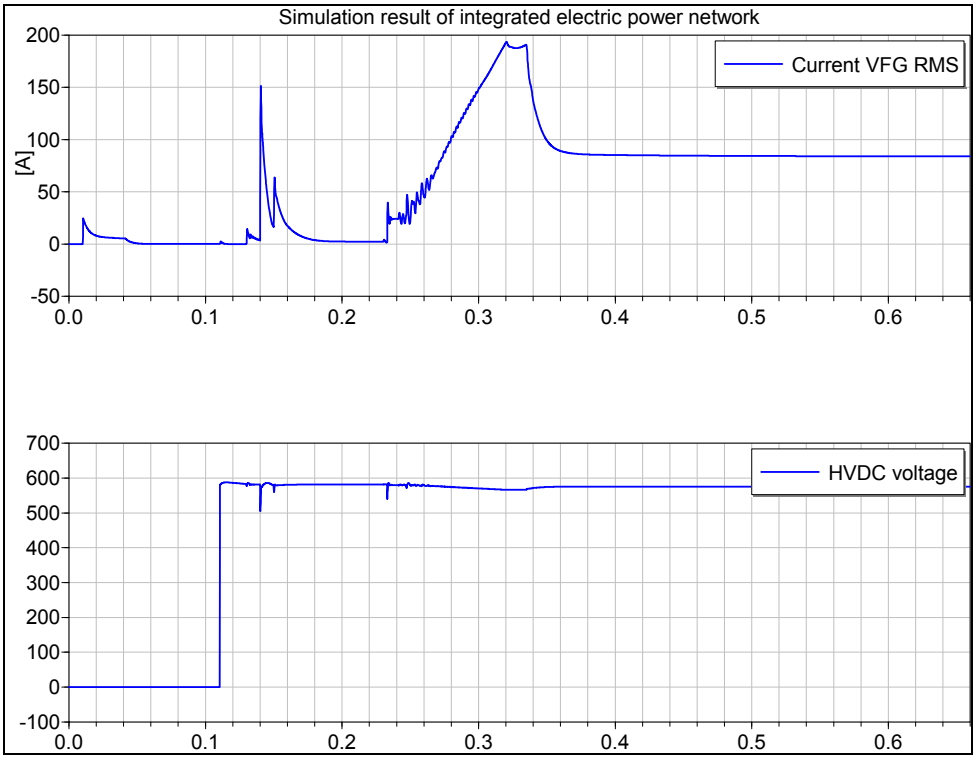

Figure 6.8.: Simulation results of VFG phase currents and HVDC net voltage in the integrated electric power network test at functional level (time unit is [s])

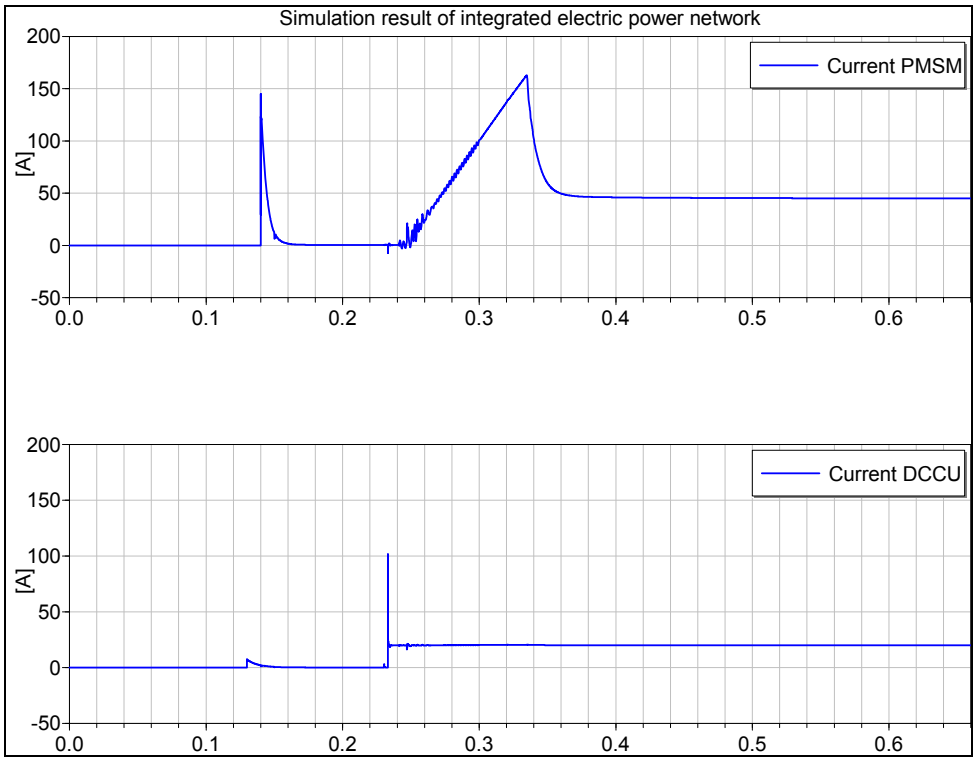

Figure 6.9.: Simulation results of PMSM current and DCCU current in the integrated electric power network test at functional level (time unit is [s])

currents are plotted.

Study of sympathetic effects

In aircraft power systems, voltage drops across the system impedance, i.e. series resistance in long transmission lines, can be caused by the inrush current when connecting extra transformers. This voltage drop may produce an unexpected magnetic saturation in the transformers, which are already connected to power grid. As a consequence, magnetizing currents of high magnitude are produced in those transformers. This interactive behavior between the incoming and the already connected transformers can significantly affect the magnitude of the inrush currents and therefore may cause critical issues such as false operation of transformer relays and temporary harmonic over-voltages. Compared with an inrush current study for the single auto-transformer, the simulation and analysis of the sympathetic effect is much more complicated. It is very important to find the instance of connecting the incoming transformers, where the maximum inrush currents will occur. In order to present the simulation based approach for the worst case study of sympathetic effect, two ATUs and power sources have been modeled in the behavioral level. This test bench contains a VFG and two unloaded ATUs is depicted in Fig. 6.12 .

The worst case test aims at defining the connection time of the ATU2 to achieve the maximum inrush current level, due to the previously mentioned sympathetic

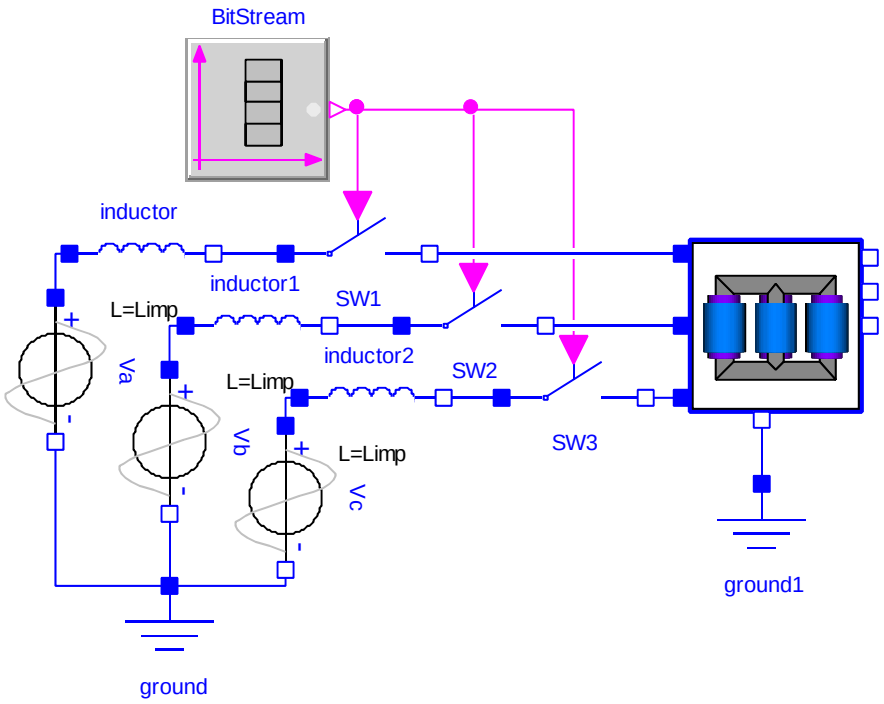

Figure 6.10.: Test for connecting single unloaded auto-transformer

effect. The total test procedure has the following three essential steps

- start simulation from $t = 0$, then connect ATU1 to power network, stop simulation once the state variables, such as magnetic flux and input current of ATU1, reach the steady-state at $t = t_{steady}$
- re-start simulation with the initial condition from the simulation result at t_{steady}, connect the ATU2 at $t = t_{steady} + N \cdot \epsilon \quad N \in [1 : 20]$, stop simulation at a predefined time
- post-treatment of the simulation results

Since the initial value of the remanent magnetic field in ATUs can significantly affect the inrush currents, the test bench should be able to set the initial value of magnetic flux in the ATU2 at the beginning of step 2.

Although the idea of the worst case test seems to be simple, it is usually a very challenging task for a simulation environment. Since the first step may take very long time till all the state variables in ATU1 reach the steady state, this step should just be run for once. The simulation platform must be able to re-initialize a simulation with a previously generated result file. Moreover, scripting features have to be supported to automatically repeat a number of simulations with different setups for step 2. Finally, the simulator should be able to initialize the magnetic characters such as remanent magnetization in power transformers.

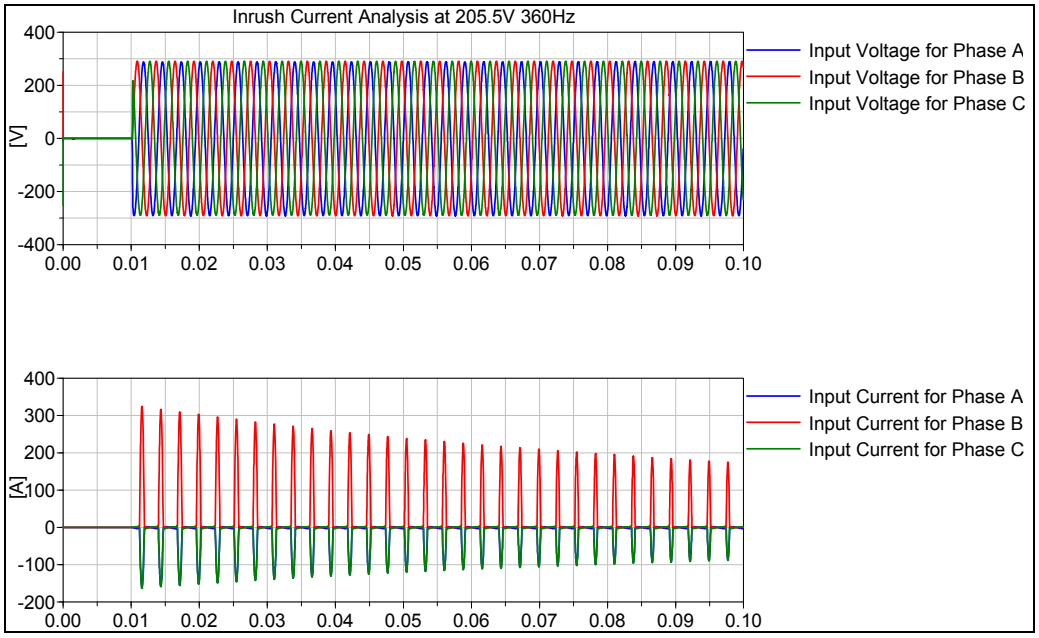

Figure 6.11.: Simulation results of input voltages and input currents in the inrush current analysis of the behavioral ATU model with 205V/360Hz (time unit is [s])

Two test cases considered here in principle have the same test procedure like previously defined. They only differ in the initial conditions of the remanent magnetic field in the ATU2 core. While the remanent magnetic field is set by half of the nominal flux in the first test case, the second test case uses nominal flux as initial condition.

Most simulation tools provide basic post processing functions but with a limited converge. Thus, specific analysis functions usually have to be developed for the simulation platform using a post treatment language. Also systematic design and test automation often demands user specific scripts. When performing simple/single simulations, it is sufficient to select menu commands or to type commands in the command input line of the command window. However, to perform more complex actions (e.g. automatically repeating more complicated parameter studies a number of times), it is much more convenient to use the scripting facility. The goal is often to fully automate the simulation. Just to name some features, the script facility makes it possible to load model libraries, set parameters, set start values, simulate and plot variables.

Dymola supports easy handling of scripting, both with functions and script files (.mos files). Considering the test procedure, the Dymola script for the worst case study of the sympathetic effect is presented in Fig. 6.13. This script function simulates the test bench first till 5.791 seconds and records the simulation result in a “end.txt” file. This result will be always defined as initial condition for the following 20 simulations with different connecting time for ATU2. A real variable Tatu2 is defined to vary the connecting time of ATU2 and has a time step $\epsilon =$

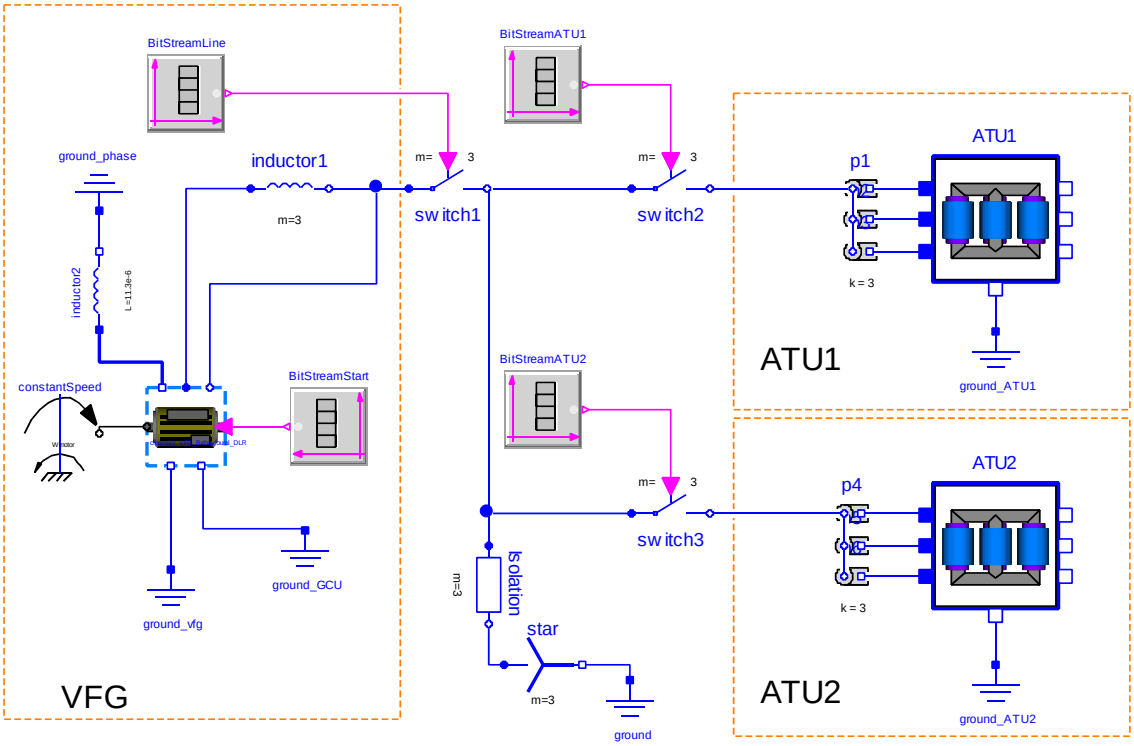

Figure 6.12.: Test bench for sympathetic effect

0.000125 second for each simulation loop. Simulation setups such as used integrator, simulation time are also defined in the script function. Additional scripts have been made for post-processing. It is a big advantage for users, that a complex test like analysis of sympathetic effect can be easily formulated with the Dymola scripting language in a very compact manner. Simulations have been performed at a behavioral modeling level with the VFG model being set to 230Vac/400Hz. Once the first ATU reaches its steady-state (here 5.79 seconds), the second ATU is connected at different times to cover one period. The automatic process with 20 simulations to capture a maximum ATU2 inrush current has been implemented by the Dymola script language as previously explained.

Results to be recorded for the two test cases are inrush currents in the VFG, the ATU1 and the ATU2. As shown in Fig. 6.14, the maximum inrush currents of the VFG and the ATU2 reached 164.1A and 155.5A during the 8th simulation when the second ATU is connected at 5.7935 seconds. The maximum reached current of the ATU1 at 5.793125 seconds is 9.4A. For the test case 2, Fig. 6.15 shows, the maximum inrush currents of the VFG and the ATU2 have reached 276.9A and 266A during the 8th simulation when the second ATU is connected at 5.7935 seconds. The maximum reached current of the ATU1 at 5.793125 seconds is 13.4A. The magnetic flux through the leg A in the ATU2 core in the worst case is depicted in sub-Fig. 6.16 for test case 1 and sub-Fig. 6.17 for the second test case.

```
function Script_Case1_with_simulation_paper
  import Modelica.Utilities.Flies.*;

protected
  Real Tatu2 = 5.791;

algorithm

  //performe simulation till steady-state
  translateModel("Case1");
  simulateModel("Case1",
   stopTime=5.79,
   numberOfIntervals=0,
   method="Radau",
   resultFile="Case1");

  //backup dsfinal
   copy("dsfinal.txt","end.txt",true);

  //do parameter studies about
  //switch on time of ATU2 with
  //time step 0.000125s

for i in 1:1:20 loop

  Tatu2 :=5.791 + i*0.000125;
  importInitial();
  simulateExtendedModel("Case1",
    startTime=5.79,
    stopTime=5.8,
    numberOfIntervals=0,
    method="Radau",
    resultFile="dres_"+String(i),
    initialNames={"Tatu2"},
    initialValues={Tatu2},
    finalNames={"Tatu2"});

  //re-initialization
  Files.copy("end.txt","dsfinal.txt",true);

end for;
end Script_Case1_with_simulation_paper;
```

Figure 6.13.: Scripting for the worst case study of sympathetic effect

6.3.4. Coherency test

The coherency test is required to test and ensure the model quality, for the functional models as well as the behavioral models. In order to evaluate the coherency between two temporal curves, defined $X_1(t)$ and $X_2(t)$, with $X_1(t)$ the reference curve, the criterion function $C_{err}(t)$ based on the average of the relative error versus the time between the curves is used and defined by Eq. 6.1

$$C_{err}(t) = \frac{1}{T_c} \int_{t}^{t+T_c} \frac{|X_1(u) - X_2(u)|}{|X_1(u)| + 0.01X_n} du \tag{6.1}$$

The criterion can be separated into two different functions such as the relative error between $X_1(t)$ and $X_2(t)$ as

$$rel_{err}(t) = \frac{|X_1(t) - X_2(t)|}{|X_1(t)|} \tag{6.2}$$

and the average of the relative error given by Eq. 6.1. T_c is the period used to calculated the average of the weighted relative error and X_n is the nominal value of the reference curve. The coherency test is normally accepted if the average of the relative error is lower then 5% at any time.

Functional model vs. behavioral model

The coherency between a functional model and a behavioral model of the rectifier unit in Fig. 6.18 is evaluated by using the model RMS values $X_{beh_{rms}}(t)$ of the behavioral data $X_{beh}(t)$ as reference and the functional model data $X_{func}(t)$ for the comparison. The criterion is defined by Eq. 6.3

$$C_{err-bf}(t) = \frac{1}{T_c} \int_{t}^{t+T_c} \frac{|X_{beh_{rms}}(u) - X_{func}(u)|}{|X_{beh_{rms}}(u)| + 0.01X_n} du \leq 0.05 \, \forall t \tag{6.3}$$

The period T_c used for average calculation is around 25 ms for allowing the functional models to be representative of the commutation test. The criterion $C_{err-bf}(t)$ shall be lower then 5% at any time. The output voltages of the behavioral and functional model, when connecting with DC load are depicted in Fig. 6.19 and the evaluation result for the coherency test is presented in Fig. 6.20. This result shows, that the functional model of the rectifier unit matches the behavioral model quite well.

Behavioral model vs test data of the VFG

The quality of the behavioral model has to be checked and evaluated before the applications. The usual way to evaluate the behavioral model is to perform the coherency test between the measurement data from the hardware and the corresponding behavioral model. To demonstrate this process, the VFG defined in Fig. 2.5 is evaluated by using the measurement data $X_{meas}(t)$ as the reference and the simulation data

$X_{simulation}(t)$. In the considered test, the VFG is disconnected to a fixed load. The measurement data have been taken from the test rig at the Airbus France[1]. This test rig is the hardware implementation related to the electrical network architecture depicted in Fig. 6.5. The criteria of the coherency test is given by Eq. 6.4

$$C_{err-mb}(t) = \frac{1}{T_c} \int_{t}^{t+T_c} \frac{|X_{meas}(u) - X_{simulation}(u)|}{|X_{meas}(u)| + 0.01X_n} du \leq 0.05 \, \forall t \tag{6.4}$$

The period T_c used for the average calculation is equal to $5\mu s$ as the maximum time step at which the behavioral model shall be able to run. The criterion $C_{err-mb}(t)$ shall be lower then 5% at any time. The normalized values of phase currents and voltage in the VFG model and measurement data are depicted in Fig. 6.22 and 6.23. The criterion of the coherency test has been fulfilled by the result in Fig. 6.24.

[1] www.airbus.com

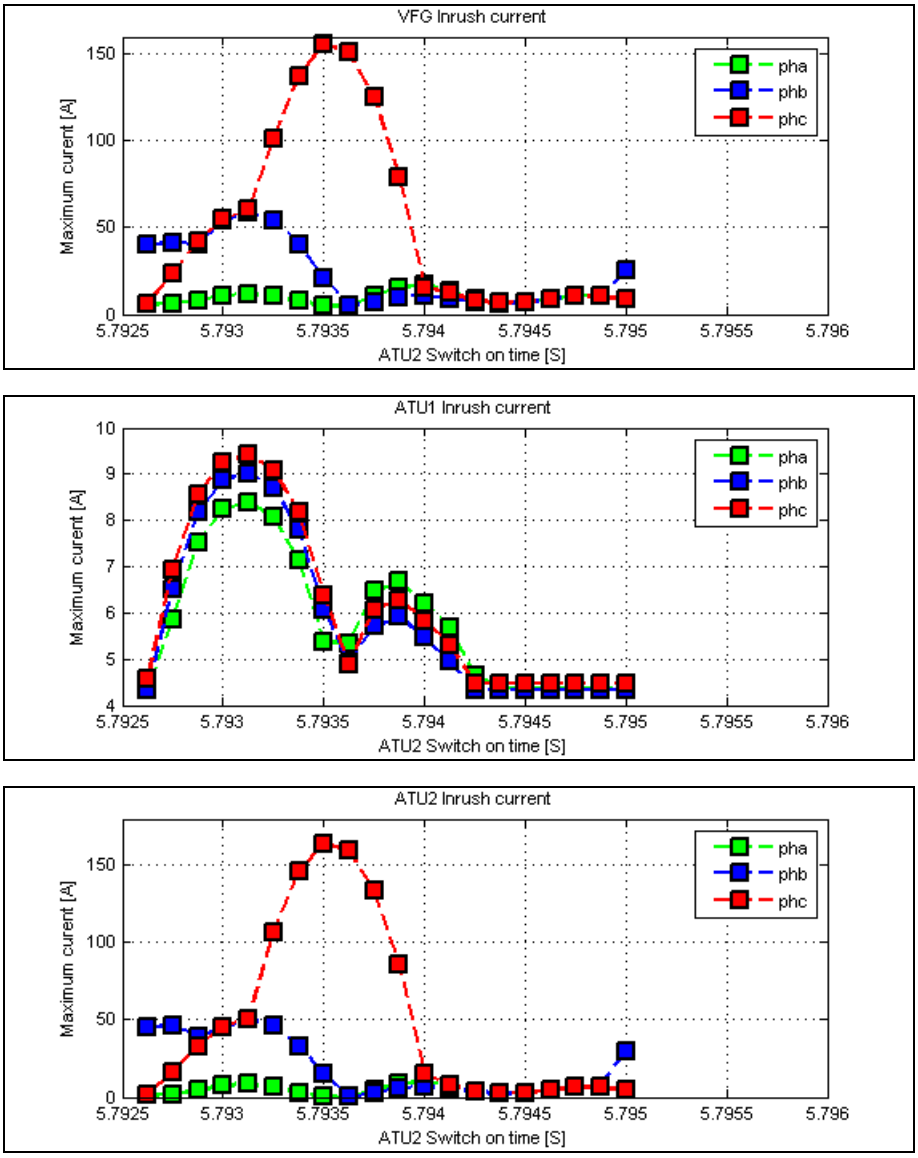

Figure 6.14.: Test result of case 1 (initial remanent magnetic field in ATU2 is set by half of the nominal flux) for sympathetic effect study

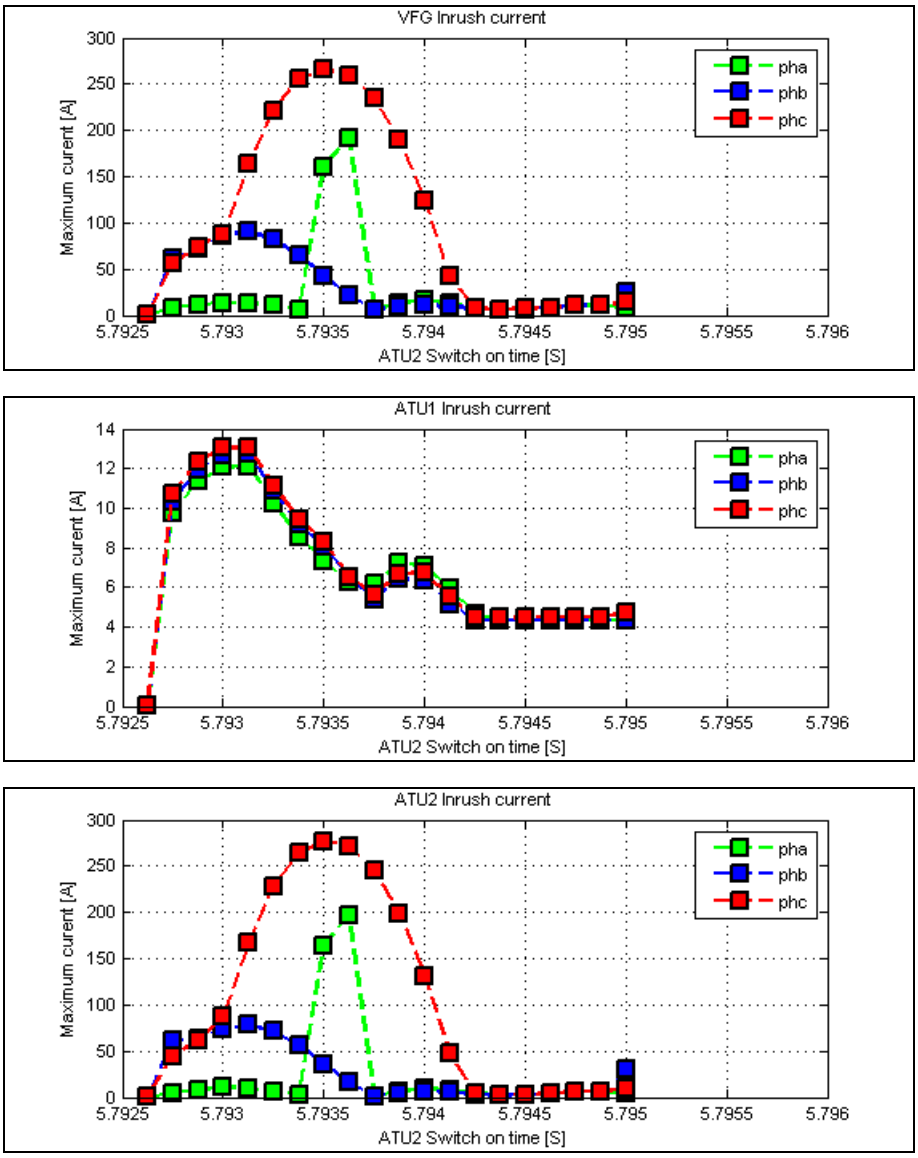

Figure 6.15.: Test result of case 2 (initial remanent magnetic field in ATU2 is set by the nominal flux) for sympathetic effect study

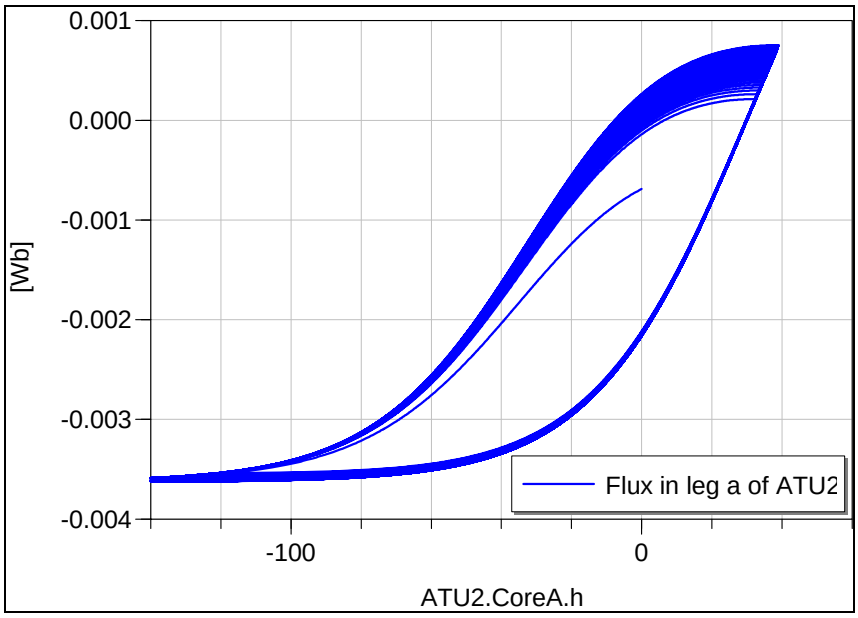

Figure 6.16.: Magnetic flux in ATU2 core for case 1 (initial remanent magnetic field in ATU2 is set by half of the nominal flux)

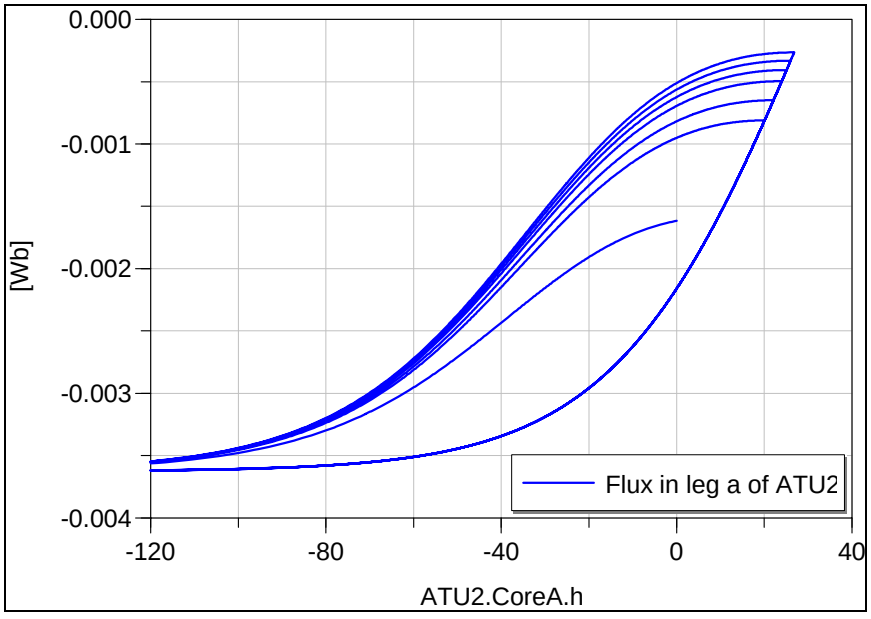

Figure 6.17.: Magnetic flux in ATU2 core for case 2 (initial remanent magnetic field in ATU2 is set by the nominal flux)

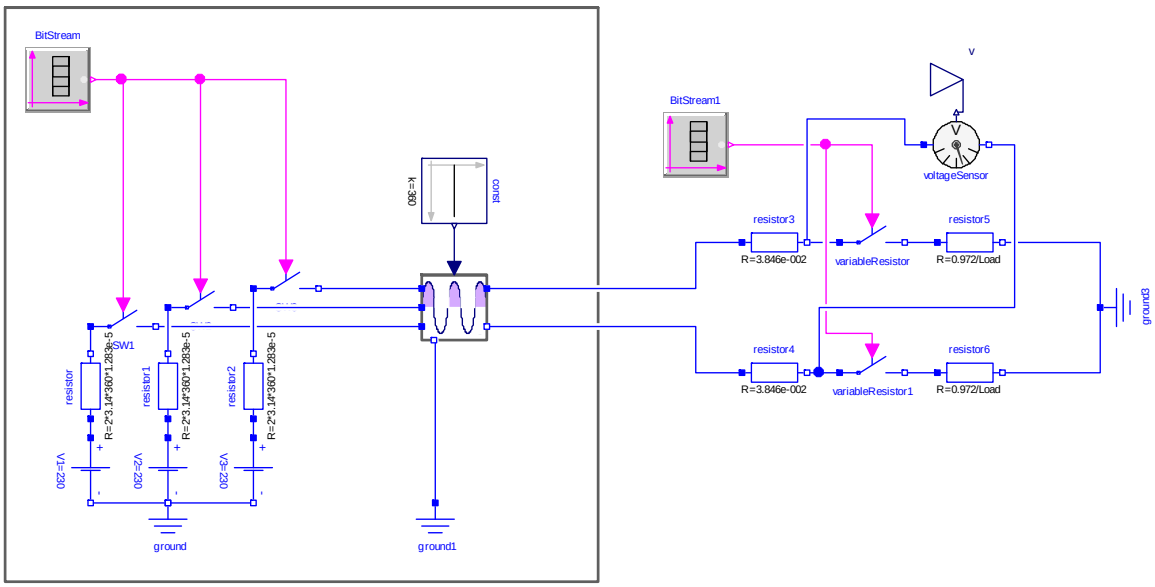

Figure 6.18.: Coherency test of a rectifier unit between behavioral and functional models

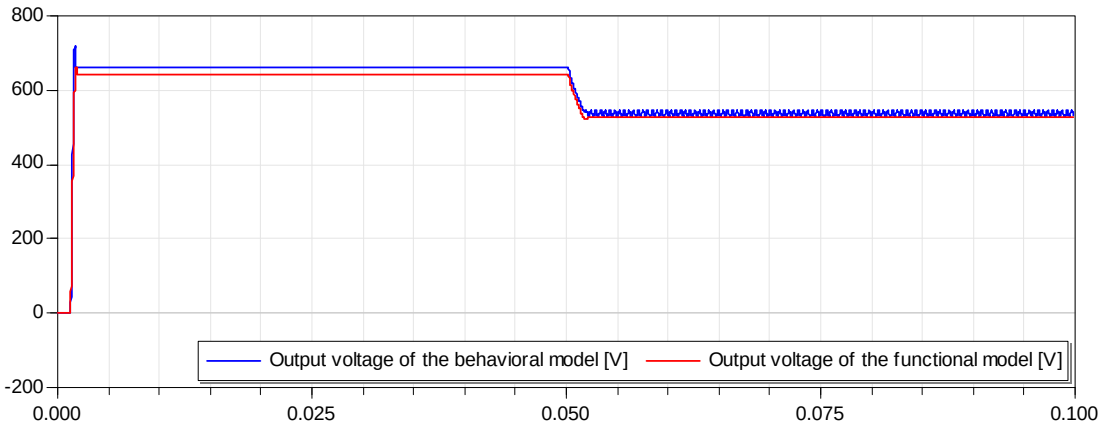

Figure 6.19.: Coherency test by the output voltages of the rectifier unit in Fig. 6.18between behavioral and functional models (time unit is [s])

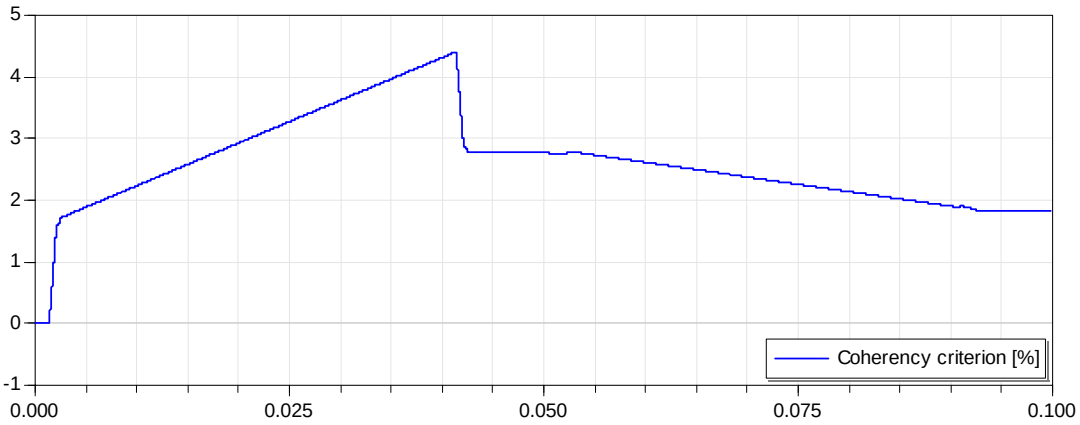

Figure 6.20.: Coherency test of rectifier unit between behavioral and functional models (criterion)

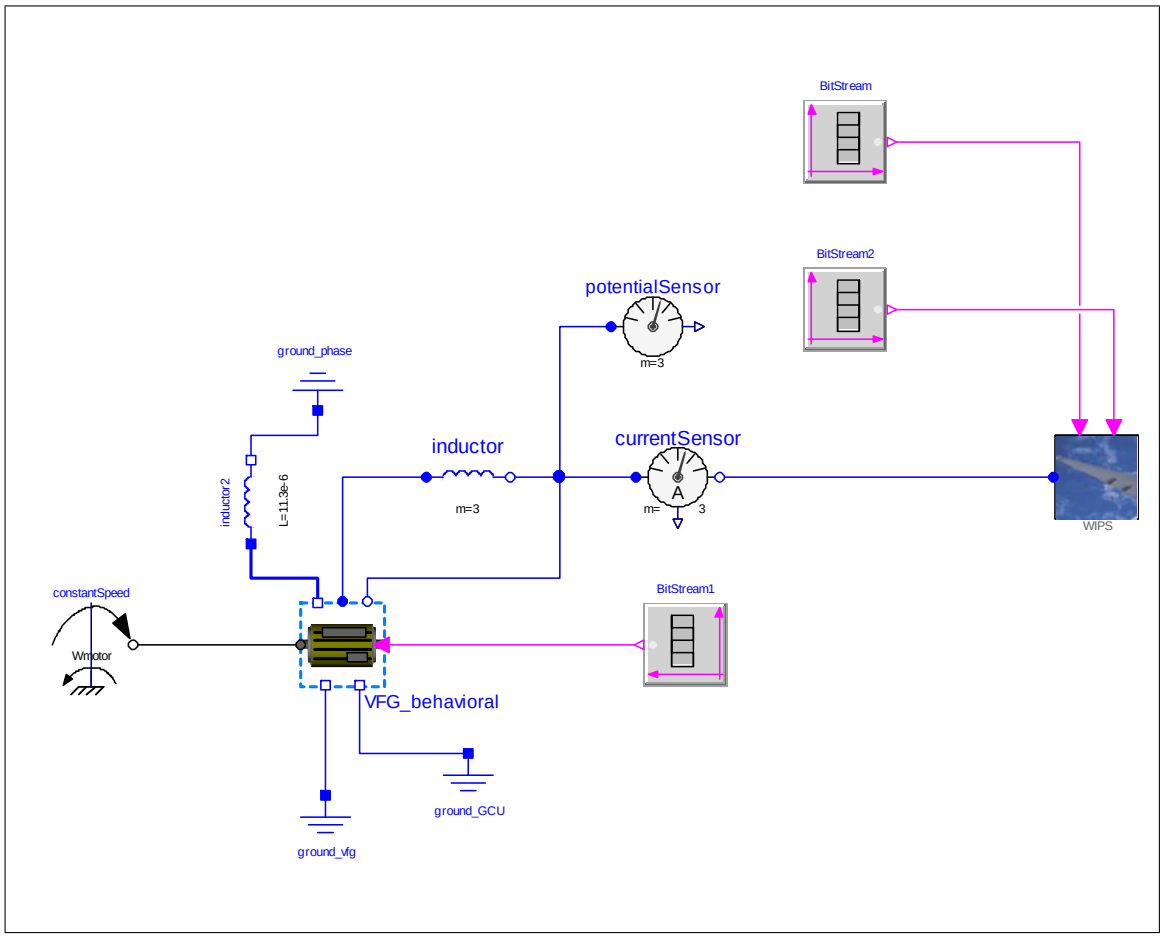

Figure 6.21.: Coherency test of VFG between measurement data and behavioral model

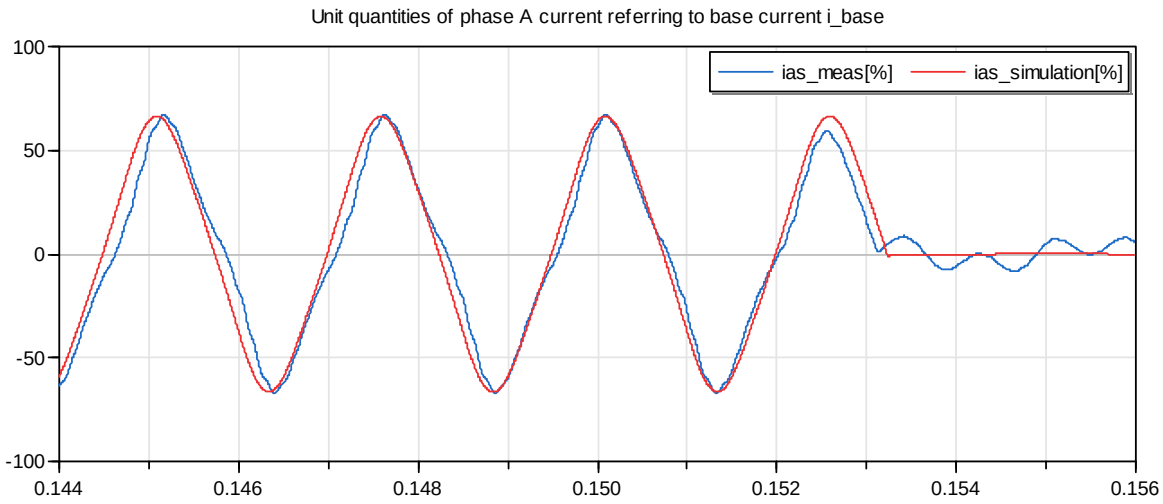

Figure 6.22.: Current in phase A of the coherency test between measurement data and simulation (time unit is [s])

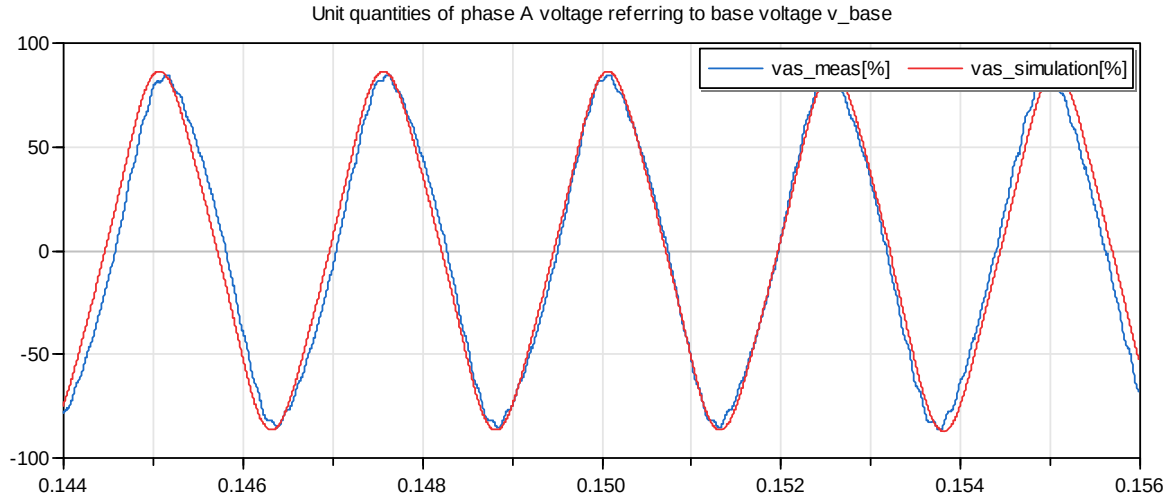

Figure 6.23.: Voltage in phase A of the coherency test between measurement data and simulation (time unit is [s])

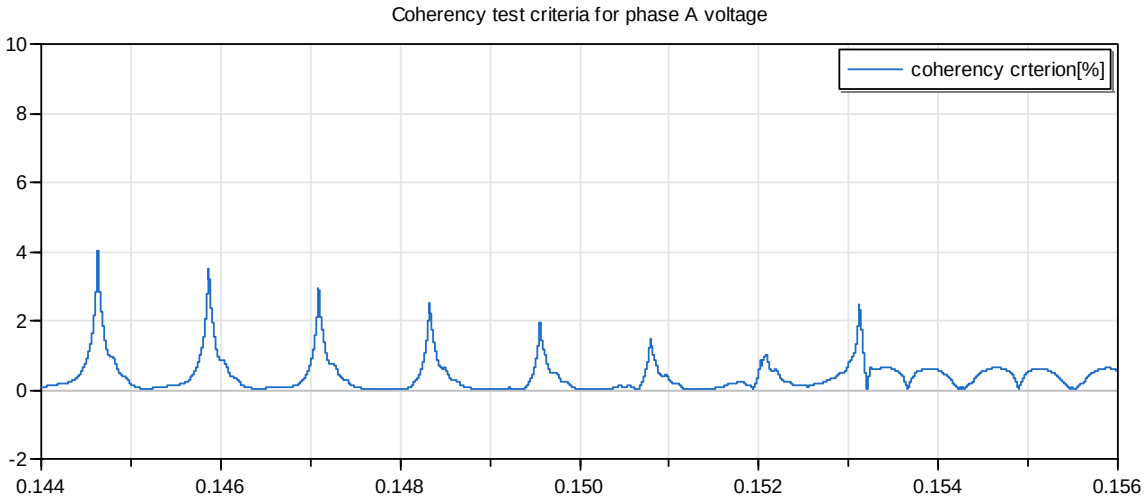

Figure 6.24.: Criterion of the coherency test between measurement data and simulation (time unit is [s])

7. Summary and future work

7.1. Summary

In this thesis, new modeling and simulation methods and tools for the different tasks of the design process of the electric network in the MEA are presented. Concretely, it is shown, that the lift technique traditionally used for periodic systems is very suitable to conduct a generalized averaged model from a topological model of a wide class of power electric systems. In this way, the traditional multi-level modeling approach currently utilized in the aircraft industry is extended. Using the derived generalized averaged model, it becomes possible to acquire the improved LTI description in level 2 models including high frequency effects in the original power electric system. This can significantly ease the work to deal with the previously mentioned issues concerning the electric network of the MEA.

Various specific model based methods for the network stability, health monitoring and power quality analysis have been developed during the work on this thesis. For the stability analysis, comprehensive comparisons among traditional small signal based stability approaches such as Modal analysis, Middlebrook criteria and the recently proposed robust μ analysis approach are performed. Moreover, the simulation based anti-optimization approach has been applied to conduct large signal stability studies, which are required for the stability assessment specified by industrial requirements.

Reviewing the considerable development of fault diagnosis techniques and many successful applications attached to them in the last time, power systems seem to be a real hard challenge for the available fault diagnosis techniques. With the help of more accurate modeling of power systems and embedded microprocessors in digital controllers of power distribution systems within the MEA, an unprecedented affordable opportunity can be provided for health monitoring and fault diagnosis using model based fault diagnosis techniques. In this thesis, the multi-model based health monitoring and fault detection for the power system in the MEA are demonstrated.

The other issue addressed in this thesis is about advanced power quality assessment, which is an important task within the large scale virtual test in the validation and verification design phase of the aircraft development. The virtual test will quickly allow to check the overall performance, anticipating any problem on the hardware and extrapolating results with a real hardware test. One big issue is the steady-state analysis of an integrated power electric system before conducting power quality analysis e.g. Fourier analysis. The conventional brute force simulation to yield the steady-state waveforms of a complex power system with a large amount of switchers is very expensive and is suffering from numerical instabilities. In this

thesis, a new optimization based method to compute the steady-state waveforms is introduced. The convergence performance of the steady-state computation is significantly improved by utilizing start values calculated from simulations of a set of generalized averaged models of the original power systems. Finally, Modelica based modeling simulation techniques successfully have been applied to conduct the virtual testing for system verification and validation

7.2. Future work

Concerning the future work of the model based design for the MEA system, a central topic is how to get the highly efficient models with adequate details, which can be simulated by real time system hardware. For this purpose, the modeling and simulation technologies should be further improved. The MEA power network whose dynamic models exhibit a hybrid and very complex manner, i.e. with continuous and discrete sub-components, like power semi-conductors, typically with several thousand Hertz switching frequency. As result, the model of such a system often is very stiff, event intensive and normally cannot be simulated efficiently by means of any explicit integration method, since very small time steps are needed to keep the numerical stability.

Also implicit numerical integration methods, such as DASSL [91] cannot efficiently simulate these systems especially when the size grows to the order of hundreds, thousands, or even more interconnected units, due to the many events. Instead of the traditional state-of-the-art hybrid Differential Algebraic Equation (DAE) solvers, the Quantized State System (QSS) methods [62], which replace the time discretization of the classic numerical integration algorithms by the quantization of the state variables, could be ideally suited to solve models of such systems like a MEA power network [31]. The QSS methods can scale up better than the traditional integration methods and provide time savings without loss of the numerical precision. A potential and meaningful work in the future will be the utilization of the QSS methods to simulate the integrated aircraft system models, which has been implemented and presented in this thesis.

However, when concerning the real time simulation issue, where usually explicit integration methods with fixed step size are utilized, new modeling approaches will be needed to reduce the stiffness and the effects from high frequency switching events. The simulation tool PLECS [5] has proposed a piece-wise linear electrical circuit simulation method [9], which uses ideal instantaneous switches by ignoring the processes during switching. It means that the model is purely linear before and after the instant of switching and therefore has a piece-wise linear behavior. This method leads to so-called variable-structural systems and a considerable speedup for the simulation. Variable-structure systems form a collective term for models, where equations change during the time of simulation. This class of models is generally not supported in M&S frameworks. The work in [118] explores the modeling of variable-structure systems for equation-based languages in full generality. More works should be done in the future, in order to make the Modelica based tools capable to handle

variable-structural systems. This will greatly improve the simulation efficiency when dealing with complex power electronic systems like the MEA power network.

Finally, as the real time platform of the simulation for the MEA power network, whose iteration rate has to be in the order of one microsecond, extreme computational power in terms of speed and resource is required. Considering the state-of-the-art computer technique, the Field-programmable Gate Array (FPGA) based platform could be suitable for the simulation of large scale power networks. Some commercial FPGA based simulation platforms for power electronic systems, e.g. from Typhoon HIL [6], are already available. From the perspective of Modelica system engineers, the simulation tools should provide a seamless interface between the Modelica models and FPGA compatible code, in order to efficiently conduct hardware-in-the-loop tests as well as rapid control prototyping design. For this purpose, some work for Modelica based simulation environments have already been done, for instance, a Modelica package for fixed-point arithmetic for automatic code generation for FPGA target is described in [86] and an integrated methodology for compiling Modelica models to an FGPA implementation has been proposed in [61]. Due to the immaturity of the present technologies with respect to code generation features, a lot of work and research need to be done in the future to achieve a full mapping between Modelica models and FPGA code. Furthermore, customized FPGA platforms with user-specific I/Os and computation power could be a key factor for a successful model based design process for the MEA.

A. Modelica based design platform for switched reluctance drives

A switched reluctance machine is a doubly salient pole machine fed by a unipolar power converter. Concerning its simplicity, robustness, low cost and high efficiency, the switched reluctance machine becomes a good competitor to conventional AC machines in the aircraft and automobile industry [63]. Some new research works have presented the possibility to use the switched reluctance machine as generator in the MEA [38] and as major actuator in the upcoming electric vehicle. However, the design of SRD systems is a very challenging job, especially due to its special converter topology and the inherent high torque ripple. The whole design process for the machine, the power converter and the control system has to be considered in a very integrated manner. For better applying the model based design approach, it is crucial to have a design platform, which can incorporate most of the design activities such as the modeling, the simulation, the machine design and hardware-in-the-loop tests. By replacing the hardware prototypes by accurate mathematical models, the design process for SRD drive systems can be greatly improved. The so-called model based design approach has many advantages such as low costs, short time to market and better control performance. A Modelica based design platform dedicated to apply a model based design approach for SRD drive systems typically have the features such as modeling, simulation, integration and real time capability.

A.1. Modeling of switched reluctance machine

In contrast to a conventional DC-machine, synchronous and induction machines whose output torque can be presented by the vector product between current and magnetic field, switched reluctance machines work on the principle of reluctance force. The torque is developed from the physical nature of magnetic paths, which always attempt to minimize the magnetic resistance in the magnetic loop [84]. For the modeling purpose, a Modelica SRM library has been recently developed. The other present modeling tools supporting switched reluctance machines e.g. Simpower by Mathworks [70] do not provide full flexibility to build models. In [54], a switched reluctance drive library has been created using Modelica, to achieve the maximum flexibility, motor type converge and model re-usability. There are two major parts addressed in the Modelica SRM library. The first one is for building a phase model of the SRM. Subject to the SRM dynamic model described in Eq. A.1 and Eq. A.2,

$$v(t) = Ri(t) + \frac{d\Psi(i,\theta)}{dt} \tag{A.1}$$

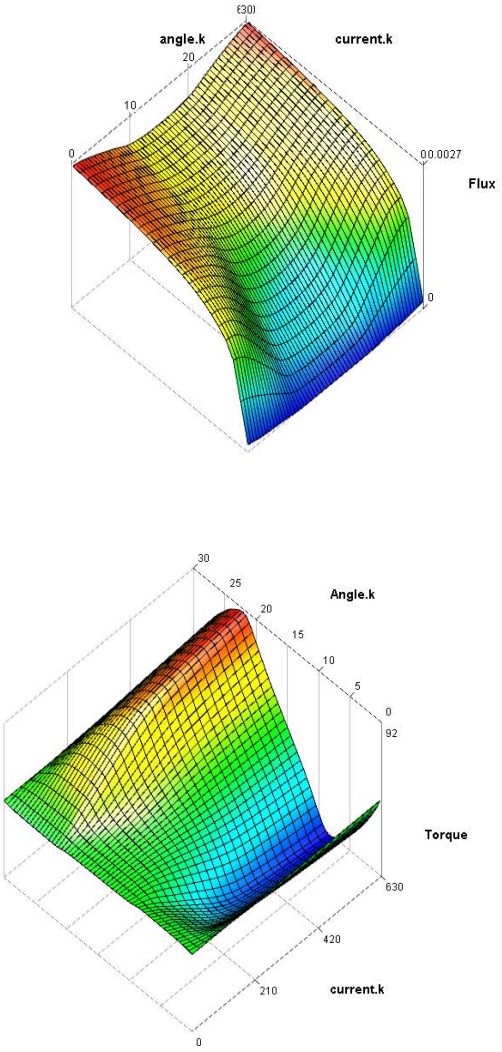

Figure A.1.: Magnetic flux and torque functions of current and rotor position

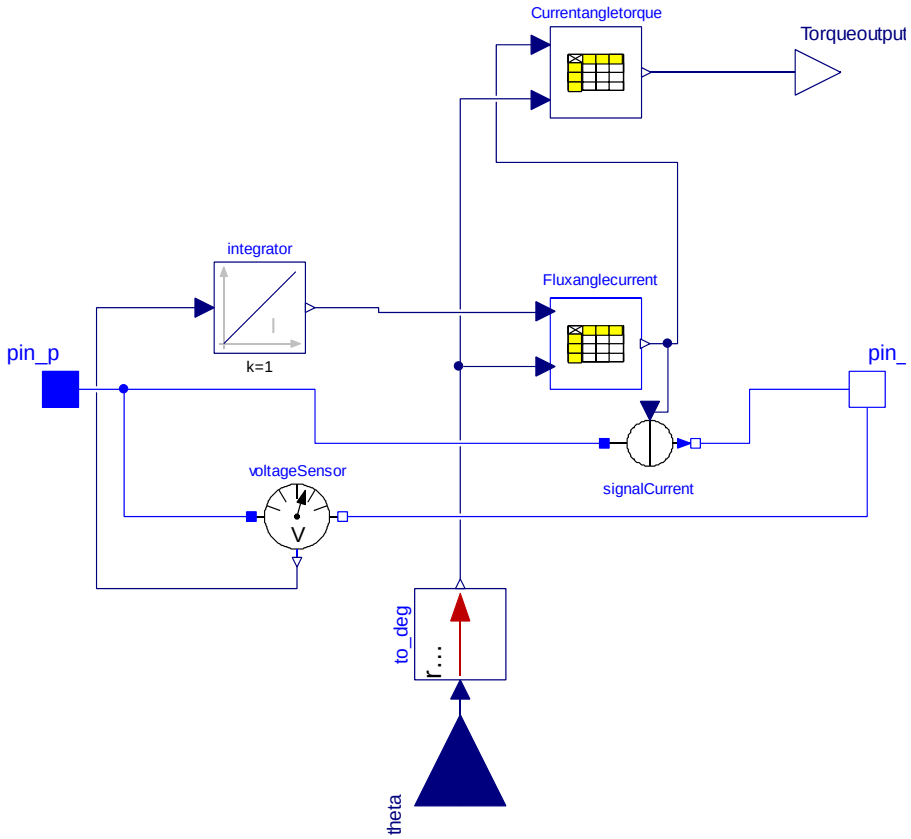

Figure A.2.: FEM data based model for one SRM phase

$$T = T(i, \theta) \tag{A.2}$$

the FEM data table based one phase model by ignoring the phase resistance is depicted in Fig. A.1, where $v(t)$, T and Ψ denote the phase voltage, mechanical torque and magnetic flux, respectively. The power converter for controlling SRMs such as an asymmetric bridge power converter has been implemented by using the Modelica standard library. Normally, idealized models of semiconductor e.g. power MOSFET and IGBT are sufficient for control design task. For some detailed investigation of switching performance and loss, the Spice semiconductor models can be incorporated into Modelica. In Fig. A.1, typical FEM data tables for magnetic flux and torque functions $\Psi(i, \theta)$, $T(i, \theta)$ depending on phase current and rotor position are illustrated.

The output torque of switched reluctance machines is commanded by two variables, i.e. the excitation level represented by current or flux-linkage and rotor position. Therefore, a high-grade torque controller must possess two feedback signals, for either the current or the flux-linkage and for the rotor position, to obtain a full access on the output torque. There are two major control strategies e.g the current based torque control and the direct torque control [21, 46]. The major difference

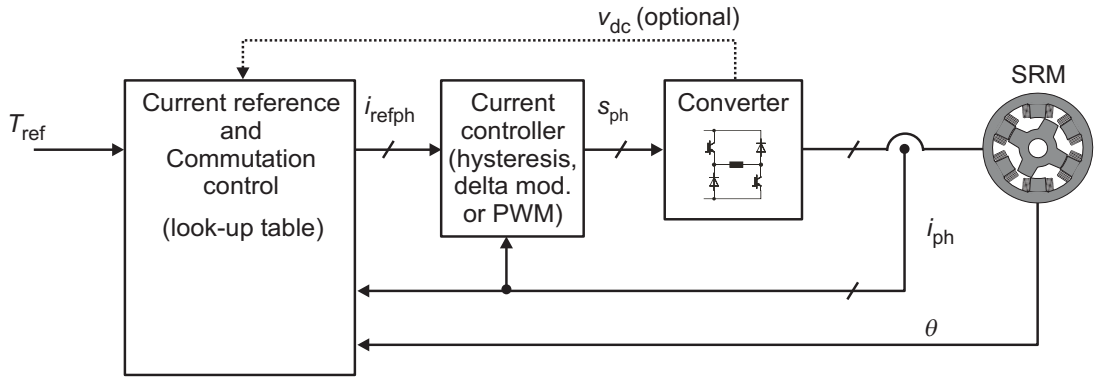

Figure A.3.: Schematic current based torque control

between two control strategies is that the output torque is directly managed as a control variable and there is no inner current control loop any more.

A.1.1. Current based torque control

The schematic diagram of the current based torque control is depicted in Fig. A.3. Besides analytical modeling approach [70], the result of the Finite Element Method (FEM) for modeling the magnetic and mechanic characteristics in Eq. A.1 and A.2 can also be imported into the library by look-up tables. Based on there look-up tables, the switched reluctance machine can also be modeled. However, those kinds of models are not quite suitable for the control design due to high computational cost. The major components in a current based torque control unit are power converter, current controller and signal sensors for current as well as rotor angle. The asymmetric bridge type power converter is addressed in the Modelica switched reluctance machine library. Using the Modelica standard library, a power converter depicted in Fig. A.4 can be easily implemented. Even more detailed models with thermal effects and power loss can also be treated. Since the turn on/off angles of each phase in the rotor play a crucial role for torque control, the actual angle θ_{mi} in relation to each phase/rotor pair has to be conducted by the measured rotor rotation angle. Taking the example of a 16 stators 12 rotor poles switched reluctance machine, the angle between ith rotor and phase can be described in Eq. A.3, assuming that the rotor starts from angle zero,

$$\theta_{mi} = \Theta \bmod 30 - (i-1) \times 7.5 \tag{A.3}$$

where Θ is the measured rotor rotation angle. Besides basic components to build a switched reluctance machine, the infrastructure models of the current controller provide the user a convenient way to implement the own control unit. The hysteresis current regulator offers a very fast dynamic response by keeping the output current in a given hysteresis band. Its switching frequency varies considerably with torque speed operating points and rotor positions [15]. The hysteresis based approach for

current control is incorporated in the Modelica library. The hysteresis band of the current control is made by the Hysteresis block from the Modelica standard library. Furthermore, some algorithms of direct torque control are also included in the library.

A.1.2. Modeling of direct torque controller

Among several new proposed methods to suppress the high torque ripple of switched reluctance machines, the direct torque control approach seems to be a promising one. Using the direct torque control approach, the instantaneous output torque is treated as a control variable. There is no inner current control loop anymore. The details of the direct torque control approach is described in [46]. The implementation of the direct torque controller is much more complicated than the current based torque control. The asymmetric bridge type power converter is also used for the direct torque control approach to excite a machine phase with three voltage levels. Since the power converter of direct torque control has three working modes, i.e. magnetization, demagnetization and freewheeling, the logic inputs for power converter are required for the individual turning of both IGBT switchers within the asymmetrical half bridge converter. Component models for the direct torque control approach have three major parts. The first part is made for detecting which phases are currently for turning on and in which working status the phases are being. Three possible status of a active machine phase with direct torque control are incoming, single active and outgoing respectively. For a 16/12 type switched reluctance machine, the present communication status of a machine phase i can be decided by the current angle in Eq. A.3

- incoming phase when $\theta_{on} < \theta_{mi} < \theta_{off} - 7.5$
- outgoing phase when $\theta_{on} + 7.5 < \theta_{mi} < \theta_{off}$
- single active phase when $\theta_{off} < \theta_{mi} < \theta_{on} + 7.5$

In the second part, hysteresis torque controllers for three different phase working statuses are included. In the last part of the direct torque controller, the logic control signals for IGBT switchers inside the converter are generated. More details about the implementation of the direct torque controller in the Modelica SRM library are addressed in [54].

A.1.3. Demonstration

A 22KW SRD design example is used to demonstrate the proposed approaches for optimal control design of SRDs. The complete virtual test rig implemented with Dymola is shown in Fig. A.5. The control parameters in two PI controllers (speed and current control) have been optimized by MOPS. The piecewise approximated inverse FEM torque function has been derived by the approach introduced in [49] for the feed forward current control. The torque contour function introduced in [44] is applied. The simulation results including speed performance, phase currents

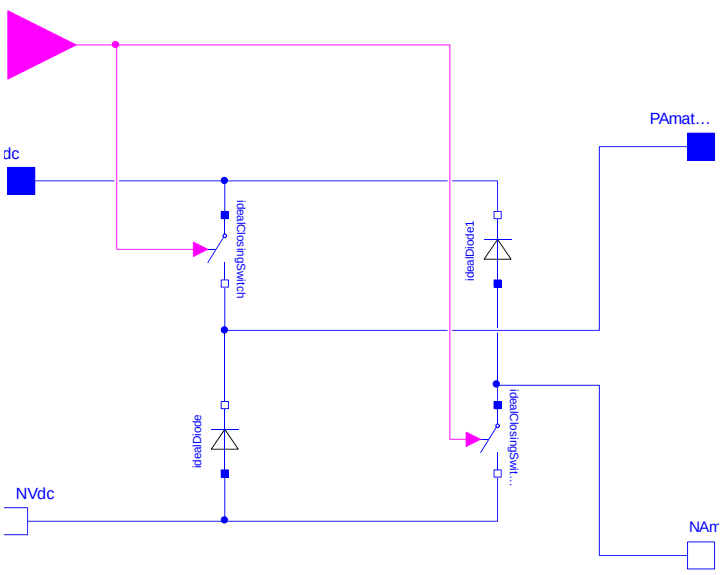

Figure A.4.: Asymmetric bridge power converter

and motor torque at 1/4 quadrants operation with external load (positive speed, acceleration/braking) are depicted in Fig. A.6. The simulation results reveal a very good performance regarding dynamic response, control accuracy and torque ripple.

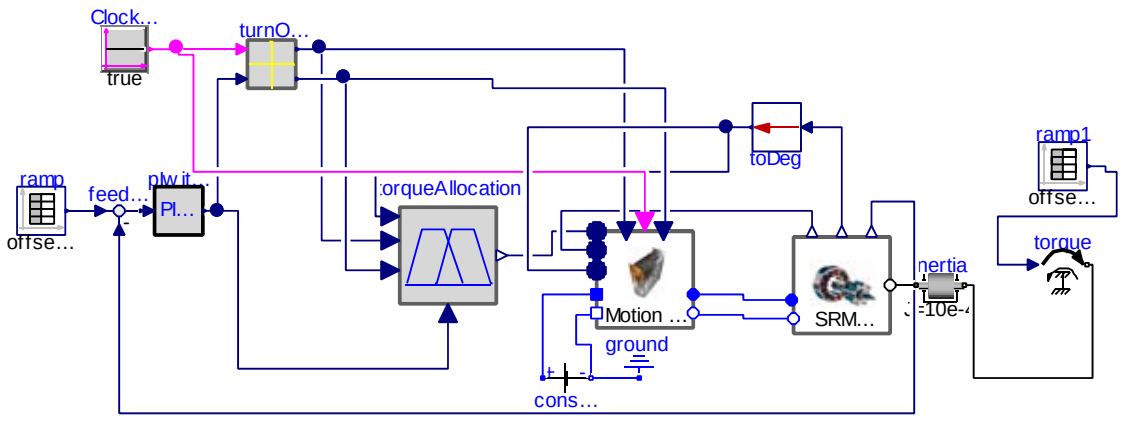

Figure A.5.: 16/12 4 phases SRM with control

A.2. Interoperability with other design tools

While the analysis and synthesis of motor control can conveniently be done using system level models of SRD drives, some design activities such as structure design of the machine and the hardware-in-the-loop test for the controller are also very important for a successful design process. The proposed Modelica based design

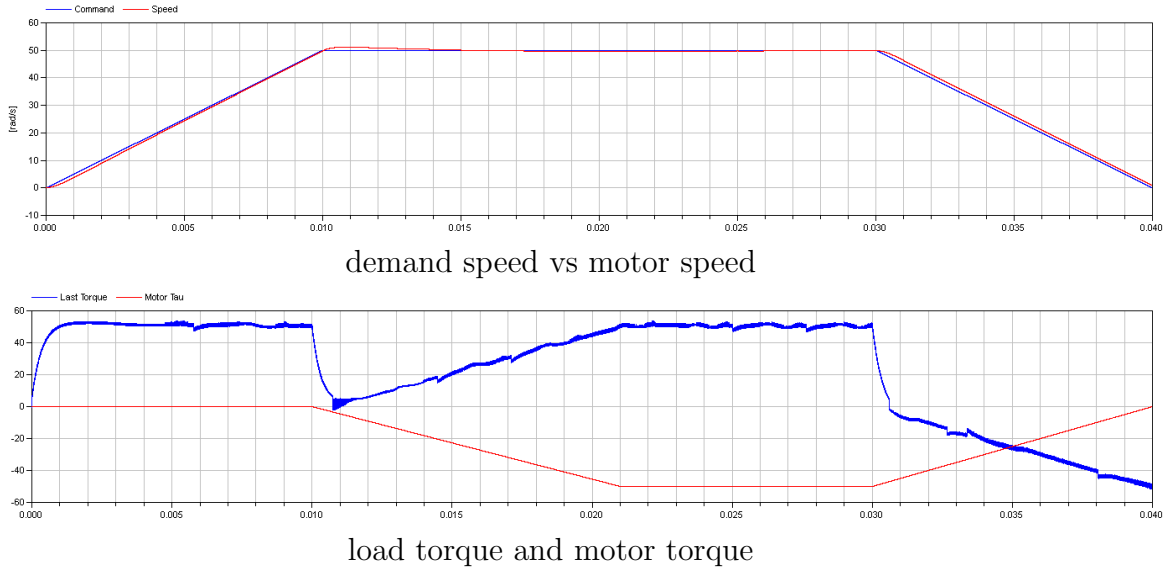

Figure A.6.: Simulation results of speed, phase currents and torque in the controlled SRD (time unit is [s])

platform easily incorporate those kinds of design tasks by the interfaces to FEM programs and hardware-in-the-loop tools.

Two approaches are typically applied when making the structure design of the switched reluctance machine in cooperation with the Modelica based design platform for SRD drive systems. Using the first approach, there is no limit for the FEM programs, only the data of magnetic characters for magnetic flux and torque in relation to rotor angle and current should be saved in a Modelica compatible table format to accomplish the modeling of the switched reluctance motor in the design platform. The typical data in the table for magnetic characters is illustrated in Fig. A.1. The second approach uses a special Modelica environment like MapleSim[1] and the Maplesim Connector for JMAG-RT[2], which is a high-speed, high-fidelity plant model based on the JMAG FEM program. The MapleSim Connector for JMAG®-RT allows one to combine the powerful finite element analysis (FEA) abilities of JMAG with the advanced physical modeling approach of MapleSim to produce high-fidelity system models that seamlessly incorporate components from each system.

[1]MapleSim is a registered trademarks of Waterloo Maple Inc.
[2]https://www.jmag-international.com/products/jmag-rt/index.html

B. Aircraft power system library

The aircraft electrical network validation and verification process strongly relies on software for modeling, simulation and analysis of network components and systems. To ease the design process for the future MEA, a dedicated Modelica based model library has been made to incorporate the major electrical components and systems for the MEA, as well as the typical tests frequently to be performed.

B.1. Introduction

A proper platform for the aircraft electrical network validation and verification process should fulfill the basic requirements in aspects of modeling, simulation and post processing. Concerning the modeling features, a highly compact and integrated model library aircraft is crucial to significantly ease aircraft manufactures to undertake model based design, system integration as well as system verification and validation. For this purpose, a Modelica aircraft power system library has been developed by combining the powerful simulation and post-processing capabilities of Dymola. The library has some major advanced features such as

- Easily modeling for most components and systems in the flight electrical system
- Automated testing and documentation
- Capability for various post-treatments

B.2. Description of the library

The aircraft power system library has been hierarchically built, where the library structure has been arranged by the frequently used electrical equipment such as VFG, ATRU, ATU, RU, DCCU, PMSMs and electrical loads. For each equipment, a sub-folder is made to include the component models, basic modeling utilities, test model at behavioral and functional levels and a list of standalone tests. Some typical standalone tests already have been prepared and can be individually used just by slightly modifications. For instance, the standalone tests such as the steady state test, the power load connection/disconnection tests and short circuit tests are implemented in the sub-folder "StandalAlone_tests". Parallel to the electrical equipment models, some demonstrations for simple tests of components are collected in the folder "CommonTests" and the examples for the integrated test cases are addressed in the "Testbench". An overview of the aircraft power system library is

presented in Fig. B.1. Besides a number of available ready-to-use equipment models, there is a special feature of the library to greatly ease the automated testing process. Namely, the tests frequently to be performed for verification and validation process have been implemented by Modelica functions as test scripts, which are saved in the same folder with the related models. The test scripts were customized from existing commands of the Modelica language and Dymola application programming interface (API) functions. The built in functions and model management tools of Dymola were found to be sufficient for the study. Among others, the following scripts and tools were found to be necessary repeatedly for the V&V study:

- Transformation of input data: From input files data are converted into a Modelica compatible type. This function is of major relevance in an industrial process since input data might not be Modelica compatible and the use of additional software is undesirable in standardized processes. By the help of some Dymola built in functions conversions from text files, Microsoft Excel sheets and more was performed. MATLAB's matrix data format .mat is already supported by Dymola.

- Transformation of output data: Same as for the import, the output features are important. Typical outputs programmed in functions were time domain results (.mat result files), tables (Excel) and generic data (.txt). For generation of frequency domain data, it was necessary to have the fast Fourier transformation function executable by a script. Thanks to the co-funding by the JTI project this function is now provided in Dymola. The application of the FFT function includes parameter studies with tabulated output of total harmonic distortion or harmonic content at specified harmonics.

- Coherency test models: Test of linear dependency of signals in time domain by convolution. Coherency is an important criterion in verification tests to analyze the validity of models and model abstraction levels. It is applied for the verification of models versus hardware test data or between different models. The script calculates coherency by the application of the coherency function to two simulation or measurement waveforms.

- AC modulation envelope: The AC envelope function is the smooth curve outlining the extreme positions of a distinctive alternating wave with a fixed frequency. The modulation envelope shows its amplitude variation in the frequency domain. The AC amplitude is an important measure for the voltage quality which must be stabilized by the generator control. The developed function relies on peak finding and transformation of data to frequency domain by FFT.

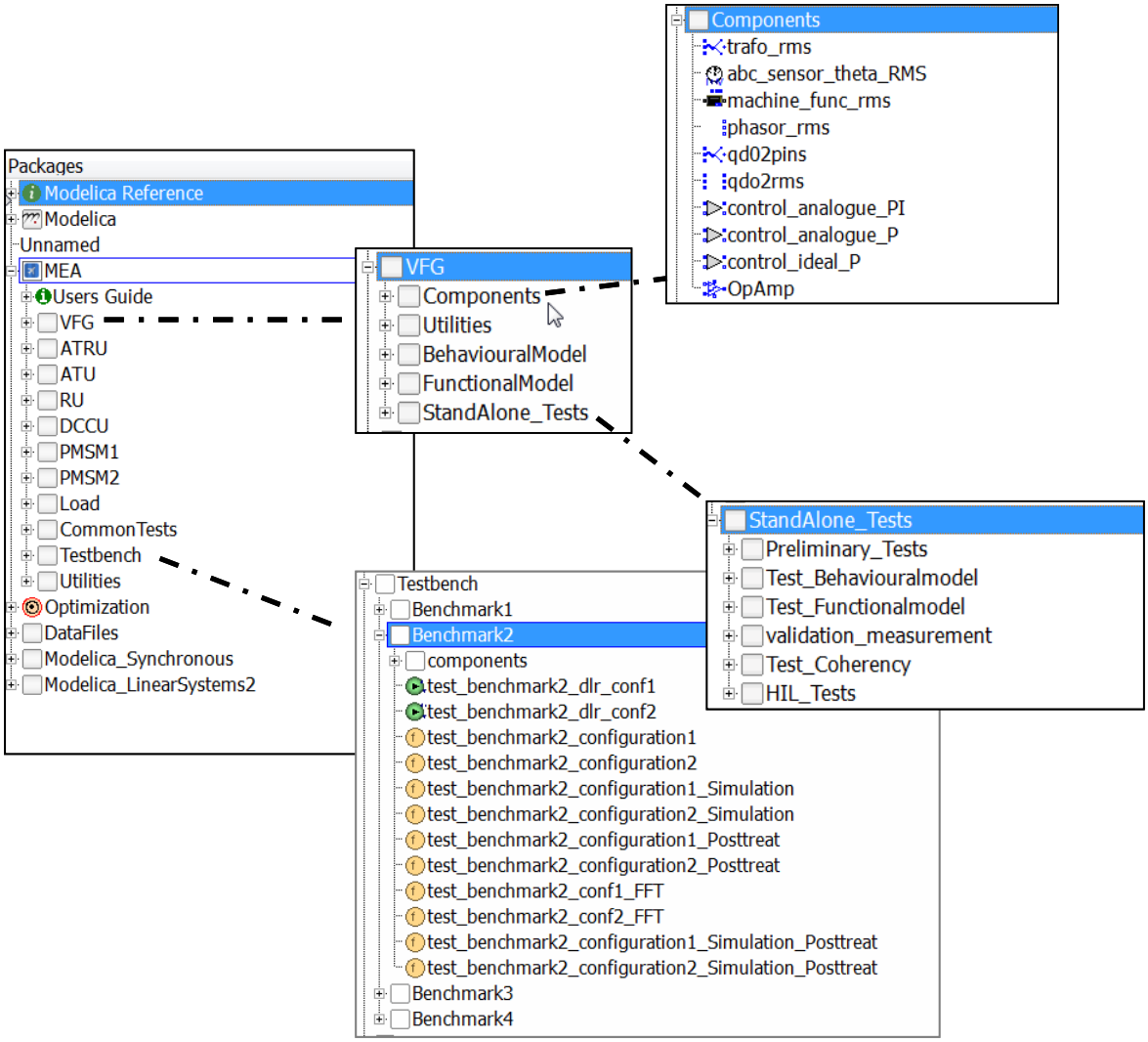

Figure B.1.: The MEA Modelica library

Bibliography

[1] Website of cleansky: http://www.cleansky.eu/.

[2] Website of fmi: http://www.fmi-standard.org.

[3] Website of Modelica association: http://www.modelica.org.

[4] Website of more open electrical technologies: http://www.eurtd.com/moet/.

[5] Website of plexim: http://www.plexim.com/de/plecs.

[6] Website of typhoon hil: https://www.typhoon-hil.com/.

[7] Pulse width modulation, June 12 1951. US Patent 2,556,457.

[8] A. Abel and T. Nähring. Frequency-domain analysis methods for Modelica models. In *Proc. 6th Int. Modelica Conference, Bielefeld, Germany*, 2008.

[9] J. H. Alimeling and Wolfgang H. Plecs-piece-wise linear electrical circuit simulation for simulink. In *Power Electronics and Drive Systems, 1999. PEDS'99. Proceedings of the IEEE 1999 International Conference on*, volume 1, pages 355–360. IEEE, 1999.

[10] G. J. Balas, J. C. Doyle, K. Glover, A. Park, and A. Simith. μ analysis and synthesis toolbox. 1998.

[11] J. Bals, W. Fichter, and M. Surauer. Optimization of magnetic attitude and angular momentum control for low earth orbit satellites. In *Spacecraft Guidance, Navigation and Control Systems*, volume 381, page 559, 1997.

[12] J. Bals, Y. Ji, M. Kuhn, and C. Schallert. Model based design and integration of more electric aircraft system using Modelica. *Moet Forum at European Power Electronics Conference and Exhibition*, 2009.

[13] F. Bar and H. Galperin. Harnessing the swarm communications policy in an era of ubiquitous networks and disruptive technologies. 2004.

[14] F. Barruel, N. Retire, Schanen J. L, and A. Caisley. Stability approach for vehicle dc power networks: Application to aircraft on-board system. power electronics specialists. *IEEE 36th Power Electronics Specialists Conference*, 2005.

[15] F. Blaabjerg, P. C. Kjaer, P. O. Rasmussen, and C. Cossar. Improved digital current control methods in switched reluctance motor drives. *IEEE Transactions on Power Electronics*, 1999.

[16] T. Bödrich and T. Roschke. A magnetic library for Modelica. In *Paper presented at the 4th International Modelica Conference*, 2005.

[17] T. Buente, A. Sahin, and N. Bajcinac. Inversion of vehicle streering dynamics with Modelica/Dymola. *Proceedings of the 4th international Modelica conference*, 2005.

[18] V. A. Caliskan, O. C. Verghese, and A. M. Stankovic. Multifrequency averaging of dc/dc converters. *IEEE Transactions on Power Electronics*, 14(1):124–133, 1999.

[19] W. P. Cao, B. C. Mecrow, G. J. Atkinson, J. W. Bennett, and D. J. Atkinson. Overview of electric motor technologies used for more electric aircraft (mea). *Industrial Electronics, IEEE Transactions on*, 59(9):3523 –3531, sept. 2012.

[20] J. Chen and P. Patton. *Robust Model-based Fault Diagnosis for Dynamic Systems*. Kluwer Academic Publishers, 1999.

[21] A. D. Cheok and Y. Fukuda. A new torque and flux control method for switched reluctance motor drives. *IEEE Transactions on power electronics*, 2002.

[22] I. Daubechies. *Ten lectures on Wavelets*. SIAM, 1992.

[23] M. Elbuluk and M. Kankam. Potential starter/generator technologies for future aerospace application. *IEEE AES System Magazine*, pages 24–31, 1997.

[24] A. Emadi and M. Ehsani. Electrical system architecture for future aircraft. *Proceeding of the 34th Intersociety Energy Conversion Engineering Conference*, 1999.

[25] J. Faucher. Simulation study of new aircraft electrical power network performances. In *Proc. More Electric Aircraft Forum, Barcelona, Spain*, pages 8–11, 2009.

[26] X. G. Feng, J. J. Liu, and F. C. Lee. Impedance specifications for stable dc distributed power systems. *Power Electronics, IEEE Transactions on*, 17(2):157–162, 2002.

[27] G. Ferreres. *Practical Approach to Robustness Analysis with Aeronautical Applications*. Kluwer Academic/Plenum Press, 1999.

[28] G. Ferreres. *A practical approach to robustness analysis with aeronautical applications*. Springer Science & Business Media, 1999.

[29] C. Fielding and A. Varga. *Advanced techniques for clearance of flight control laws*, volume 283. Springer Science & Business Media, 2002.

[30] M. Fleischer. Foundations of swarm intelligence: From principles to practice. *arXiv preprint nlin/0502003*, 2005.

[31] X. Floros, F. Bergero, N. Ceriani, F. Casella, E. Kofman, and F. E. Cellier. Simulation of smart-grid models using quantization-based integration methods. *Proceeding of the 10th International Modelica Conference*, 2014.

[32] E. Frisk and M. Nyberg. A minimal polynomial basis solution to residual generation for fault diagnosis in linear systems. *Automatica*, 37(9):1417 – 1424, 2001.

[33] B. Fritchman. Easy5 and integrating boeing's systems design environment. *Easy5 2000 user conference*, 2000.

[34] J. B. Gao, Y. Ji, J. Bals, and R. Kennel. Wavelet library for Modelica. *Proceeding of the 10th International Modelica Conference*, 2014.

[35] J. J. Gertler. *Fault Detection and Diagnosis in Engineering Systems*. Marcel Dekker, 1998.

[36] T. Giese, D. Schlabe, R. Slate, M. Crespo, F. Tichy, and C. Baumann. Extended design office concept definition. *Cleansky WP2.1.1 deliverable*, 2010.

[37] A. Griffo and J. B. Wang. *State-space average modelling of synchronous generator fed 18-pulse diode rectifier*, pages 2386–2395. IEEE Computing, 2009.

[38] L. Q. Han, J. B. Wang, and D. Howe. Small-signal stability studies of a 270v dc more-electric aircraft power system. In *Proc. 3rd IET Int Power Electronics, Machines and Drives Conf*, pages 162–166, 2006.

[39] S. Hecker. *Generation of low order LFT Representations for Robust Control Applications*. Fortschrittberichte VDI, 2006.

[40] S. Hecker and A. Varga. Symbolic techniques for low order lft modelling. *Proceedings of IFAC World Congress*, 2005.

[41] S. Hecker, A. Varga, and G. Looye. A desktop environment for assessment of fault diagnosis based fault tolerant flight control laws. In *IEEE International Symposium on Computer Aided Control System Design*, volume 9, 2008.

[42] S. Hecker, A. Varga, and Jean-Francois Magni. Enhanced lfr toolbox for matlab. *Aerospace Science and Technology*, 2005.

[43] V. L. L. Huang, P. N. Suganthan, and J. J. Liang. Comprehensive learning particle swarm optimizer for solving multiobjective optimization problems. *International Journal of Intelligent Systems*, 21(2):209–226, 2006.

[44] I. Husain and M. Ehsani. Torque ripple minimization in switched reluctance motor drives by pwm current control. 11(1):83–88, 1996.

[45] A. M. Imam. *Condition monitoring of electrolytic capacitors for power electronics applications*. PhD thesis, Georgia Institute of Technology, 2007.

[46] R. B. Inderka and R. W. Doncker. Ditc-direct instantaneous torque control of switched reluctance drives. *IEEE Transactions on Industrial Applications*, 39, 2003.

[47] R. Isermann. *Fault-diagnosis systems: an introduction from fault detection to fault tolerance*. Springer Science & Business Media, 2006.

[48] E. Jacobsen and R. Lyons. The sliding dft. *Signal Processing Magzine*, 20:74–80, 2003.

[49] Y. Ji. A novel Modelica based design platform for switched reluctance drive systems. In *Electrical Machines and Systems (ICEMS), 2014 17th International Conference on*, pages 3302–3308. IEEE, 2014.

[50] Y. Ji and J. Bals. Multi-model based fault detection for the power system of more electric aircraft. In *Asian Control Conference, 2009. ASCC 2009. 7th*, pages 93–98. IEEE, 2009.

[51] Y. Ji and J. Bals. Health monitoring for the electrical network of more electric aircraft. In *IAENG TRANSACTIONS ON ENGINEERING TECHNOLOGIES: Volume 4: Special Edition of the World Congress on Engineering and Computer Science-2009*, volume 1247, pages 86–99. AIP Publishing, 2010.

[52] Y. Ji and J. Bals. A novel Modelica signal analysis tool towards design of more electric aircraft. In *Computer Science and Information Technology (ICCSIT), 2010 3rd IEEE International Conference on*, volume 5, pages 152–156, 2010.

[53] Y. Ji and J. Bals. Modeling and control design of switched reluctance machine using Modelica. *The 19th IASTED International Conference on Applied Simulation and Modeling*, 2011.

[54] Y. Ji and J. Bals. Physical modelling of switched reluctance machine using Modelica. In *IAENG International Conference on Control and Automation*, 2011.

[55] Y. Ji, J. Bals, M. Kuhn, and M. Otter. Technical report on Modelica benchmark models. 2013.

[56] Y. Ji, J. Bals, Kuhn M, and M. Otter. Technical report on Modelica criteria & tool performance evaluation. 2013.

[57] Y. Ji and M. Kuhn. Virtual testing for large scale power systems of more-electric aircraft with Modelica. *14th IEEE Workshop on Control and Modeling for Power Electronics*, 2013.

[58] Y. Ji, A. Pfeiffer, and J. Bals. Optimization based steady-state analysis of switched power electronic systems. In *Control and Modeling for Power Electronics (COMPEL), 2010 IEEE 12th Workshop on*, pages 1–6, 2010.

[59] H. D. Joos. A multiobjective optimisation-based software environment for control systems design. In *Computer Aided Control System Design, 2002. Proceedings. 2002 IEEE International Symposium on*, pages 7–14. IEEE, 2002.

[60] J. Kennedy. Particle swarm optimization. In *Encyclopedia of Machine Learning*, pages 760–766. Springer, 2010.

[61] C. Koellner, T. Blochwitz, and T. Hodrius. Translating Modelica to hdl: An automated design flow for fgpa-based real-time hardware-in-the-loo simulations. *Proceeding of the 9th International Modelica Conference.*

[62] E. Kofman and S. Junco. Quantized state sytem. a devs approach for continuous system simulation. *Transactions of SCS*, 2001.

[63] R. Krishnan. *Switched Reluctance Motor Drives.* CRC Press, 2001.

[64] M. R. Kuhn, Y. Ji, H. D. Joos, and J. Bals. An approach for stability analysis of nonlinear electrical network using antioptimization. In *Power Electronics Specialists Conference, 2008. PESC 2008. IEEE*, pages 3873–3879, 2008.

[65] M. R. Kuhn, Y. Ji, and D. Schröder. Stability studies of critical dc power system component for more electric aircraft using μ sensitivity. In *Control Automation, 2007. MED '07. Mediterranean Conference on*, pages 1–6, 2007.

[66] M. R. Kuhn and M. Otter. Right sized multi domain simulation for electrical system. *VIVACE Forum 2*, 2006.

[67] M. R. Kuhn and M. Otter. A multi level approach for aircraft electrical systems design. *6th International Modelica Conference*, 2008.

[68] P. Kundur, N. J. Balu, and M. G. Lauby. *Power system stability and control*, volume 7. McGraw-hill New York, 1994.

[69] A. Kusko and M. T. Thompson. *Power quality in electrical systems.* McGraw-Hill, 2007.

[70] H. Le-Huy and Brunelle P. Versatile nonlinear switched reluctance motor model in simulink using realisic and analytical magnetization characteristics. *31st Annual Industrial Electronics Society Conference*, 2005.

[71] F. Lester. Beyond the More Electric Aircraft. *Aerospace Ameria*, 43:9, 2005.

[72] J. J. Liang and P. N. Suganthan. Dynamic multi-swarm particle swarm optimizer. In *Swarm Intelligence Symposium, 2005. SIS 2005. Proceedings 2005 IEEE*, pages 124–129. IEEE, 2005.

[73] M. Liu, C. K. Tse, and J. Wu. A wavelet approach to fast approximation of steady-state waveforms of power electronics circuits. *International journal of circuit theory and applications*, 31(6):591–610, 2003.

[74] X. Y. Liu, A. J. Forsyth, and A. M. Cross. Negative input-resistance compensator for a constant power load. *IEEE TRANSACTIONS ON INDUSTRIAL ELECTRONICS*, 54, 2007.

[75] N. R. Lomb. Least-squares frequency analysis of unequally spaced data. *Astrophysics and space science*, 39(2):447–462, 1976.

[76] K. P. Louganski. Modelling and analysis of a d.c. power distribution system in 21st century airlifters. Master's thesis, Virginia Polytechnic Institute and State University, Blacksburg Virginia,, 1990.

[77] K. P. Louganski. *Modeling and analysis of a DC power distribution system in 21st century airlifters*. PhD thesis, Virginia Polytechnic Institute and State University, 1999.

[78] J. Mahdavi, A. Emaadi, M. D. Bellar, and M. Ehsani. Analysis of power electronic converters using the generalized state-space averaging approach. *Circuits and Systems I: Fundamental Theory and Applications, IEEE Transactions on*, 44(8):767–770, 1997.

[79] D. Maksimović. Automated steady-state analysis of switching power converters using a general-purpose simulation tool. In *Power Electronics Specialists Conference, 1997. PESC'97 Record., 28th Annual IEEE*, volume 2, pages 1352–1358. IEEE, 1997.

[80] S. Mallat. *A wavelet tour of signal processing - the sparse way*. Amsterdam Elsevier, 2009.

[81] A. Marcos, D. Bates, and I. Postlethwaite. Control oriented uncertainty modelling using μ sensitivities and skewed μ analysis tools. In *Proceedings of the 44th IEEE Conference on Decision and Control, and the European Control Conference 2005 Seville, Spain, December 12-15*, 2005.

[82] P. P. Menon, D. G. Bates, and I. Postlethwaite. Optimisation-based flight control law clearance. In *Nonlinear Analysis and Synthesis Techniques for Aircraft Control*, pages 259–300. Springer, 2007.

[83] R. D. Middlebrook. Input flter consideration in design and application of switchung regulators. *IEEE Industry Applications Society Annual Meeting*, 1976.

[84] T. J. E. Miller. *Switched reluctance motos and their control*. Magna Phsics Publishing, 1993.

[85] J. Nocedal and S. Wright. *Numerical optimization*. Springer Science & Business Media, 2006.

[86] U. Nordström, José D. López, and H. Elmqvist. Automatic fixed-point code generation for Modelica using Dymola. *Proc. Intl. Modelica Conference*, 2006.

[87] USA Department of Defense. Mil-std 704f aircraft electric power characteristics. March 2004.

[88] M. Otter, B. Thiele, and H. Elmquvist. A library for synchronous control systems in Modelica. *9th International Modelica Conference*, 2012.

[89] D. A. Paice. Optimized 18-pulse type ac/dc, or dc/ac, converter system. June 23 1992. US Patent 5,124,904.

[90] R. H. Park. Two-reaction theory of synchronous machines generalized method of analysis-part i. *American Institute of Electrical Engineers, Transactions of the*, 48(3):716–727, July 1929.

[91] L. R. Petzold. A description of dassl: A differential/algebraic system solver. *IMACS World Congress*, 1982.

[92] A. Pfeiffer. *Numerische Sensitivitätsanalyse unstetiger multidisziplinärer Modelle mit Anwendungen in der gradientenbasierten Optimierung*. PhD thesis, Martin-Luther Universität Halle-Wittenberg, 2008.

[93] A. Pfeiffer. Tutorial of optimization library for Dymola. *Included in Optimization Library 2.2.1*, July 2015.

[94] V. Prasannamoorthy, N. Devarajan, K.N. Priya, and N. Meenu. Wavelet and fuzzy classifier based fault detection methodology for power electronic circuits. In *Process Automation, Control and Computing (PACC), 2011 International Conference on*, pages 1–6, July 2011.

[95] A. K. Qin, V. L. Huang, and P. N. Suganthan. Differential evolution algorithm with strategy adaptation for global numerical optimization. *Evolutionary Computation, IEEE Transactions on*, 13(2):398–417, 2009.

[96] R. E. J. Quigley. More electric aircraft. *Applied Power Electronics Conference and Exposition*, pages 906–911, 1993.

[97] X. Roboam. New trends and challenges of electrical networks embedded in more electrical aircraft. In *2011 IEEE International Symposium on Industrial Electronics*, pages 26–31, 2011.

[98] S. R. Sanders, J. M. Noworolski, X. J. Liu, and G. C. Verghese. Generalized averaging method for power conversion circuits. *Power Electronics, IEEE Transactions on*, 6(2):251–259, 1991.

[99] C. Sankaran. *Power quality*. CRC press, 2001.

[100] F. Saupe, Maurice J. B., F. A. King, and W. Fichter. Robustness analysis of linear time periodic systems using harmonic transfer function. *AIAA Guidance, Navigation, and Control Conference, Chicago, Illinois*, 2009.

[101] A. Schallert, C.and Pfeiffer and J. Bals. Generator power optimisation for a more-electric aircraft by use of a virtual iron bird. In *25th Internaltional Congress of the Aeronautical Sciences*, 2006.

[102] C. Schallert. Inclusion of reliability and safety analysis methods in Modelica. *8th International Modelica Conference*, 2011.

[103] C. Scherer. *Theory of Robust Control*. Delft University of Technology, 2001.

[104] H. A. Simon. *Models of bounded rationality: Empirically grounded economic reason*, volume 3. MIT press, 1982.

[105] K. Swarup and H. Chandrasekharaiah. Fault detection and diagnosis of power systems using artificial neural networks. *1st international forum on application of neural networks to powr system*, 1991.

[106] T. Thong, J. McNames, and M. Aboy. Lomb-wech periodogram for non-uniform sampling. In *Engineering in Medicine and Biology Society, 2004. IEMBS'04. 26th Annual International Conference of the IEEE*, volume 1, pages 271–274. IEEE, 2004.

[107] K. J. Timko, A. Bose, and P. M. Anderson. Monte carlo simulation of power system stability. *Power Apparatus and Systems, IEEE Transactions on*, (10):3453–3459, 1983.

[108] O. Urfalioglu. Robust estimation of camera rotation, translation and focal length at high outlier rates. In *Computer and Robot Vision, 2004. Proceedings. First Canadian Conference on*, pages 464–471. IEEE, 2004.

[109] A. Varga. On computing least order fault detectors using rational nullspace bases. *IFAC symposium safeprocess, Washington*, 2003.

[110] A. Varga. A fault detection toolbox for matlab. *CASCE 2006 Symposium*, 2006.

[111] A. Varga. On computing nullspace bases - a fault detection perspective. *17th world congress of the international federation automatic control, Seoul Korea*, 2008.

[112] A. Varga, A. Hansson, and G. Puyou. Optimization based clearance of flight control laws. *Lecture Notes in Control and Information Science. Springer*, page 121, 2012.

[113] G. C. Verghese and F. C. Schweppe. Selective modal analysis with applications to electric power systems, part i: Heuristic introduction. *Power Apparatus and Systems, IEEE Transactions on*, (9):3117–3125, 1982.

[114] N. M. Wereley. *Analysis and Control of Linear Periodically Time Varying Systems*. PhD thesis, Massachusetts Institute of Technology, 1991.

[115] P. M. Young, J. C. Doyle, R. D. Braatz, and M. Morari. Computational complexity of mu calculation. *IEEE Transactions on Automatic Control*, 39, 1994.

[116] H. T. Zhang, Q. An, Z. K. Hu, and Z. W. Chen. Fault detection wavelet fractal method of circuit of three-phase bridge rectifier. In *Intelligent System Design and Engineering Application (ISDEA), 2010 International Conference on*, volume 1, pages 725–729, Oct 2010.

[117] K. M. Zhou and J. C. Doyle. *Essentials of Robust Control*. Prentice Hall, 1998.

[118] D. Zimmer. *Equation-based modeling of variable-structure systems*. PhD thesis, Swiss Federal Institute of Technology, Zürich, 2010.

[119] J. Ziske and T. Boedrich. Magnetic hysteresis models for Modelica. *9th International Modelica Conference*, 2012.